Friction and plasticity of micro- and nano-scale metal contacts

Dikken, Robbert - Jan

DOI
10.4233/uuid:4a39e5a8-cf07-40dc-b291-126010092e69

Publication date
2017

Document Version
Final published version

Citation (APA)
Dikken, R. . J. (2017). *Friction and plasticity of micro- and nano-scale metal contacts*. [Dissertation (TU Delft), Delft University of Technology]. https://doi.org/10.4233/uuid:4a39e5a8-cf07-40dc-b291-126010092e69

FRICTION AND PLASTICITY OF MICRO- AND NANO-SCALE METAL CONTACTS

FRICTION AND PLASTICITY OF MICRO- AND NANO-SCALE METAL CONTACTS

Proefschrift

ter verkrijging van de graad van doctor
aan de Technische Universiteit Delft,
op gezag van de Rector Magnificus prof. ir. K. C. A. M. Luyben,
voorzitter van het College voor Promoties,
in het openbaar te verdedigen op
maandag 27 februari 2017 om 15:00 uur

door

Robbert-Jan DIKKEN

Master of Science in Applied Physics
Delft University of Technology
geboren te Wateringen, Nederland.

This dissertation has been approved by the
promotors: Prof. dr. B.J. Thijsse and Prof. dr. ir. L. Nicola

Composition of the doctoral committee:

Rector Magnificus	chairman
Prof. dr. B.J. Thijsse	Technische Universiteit Delft, promotor
Prof. dr. ir. L. Nicola	Technische Universiteit Delft, promotor

Independent members:

Prof. dr. G.C.A.M. Janssen	Technische Universiteit Delft
Prof. dr. I.M. Richardson	Technische Universiteit Delft
Prof. dr. V.S. Deshpande	University of Cambridge
Prof. dr. P. Pant	Indian Institute of Technology Bombay
Dr. M.H.F. Sluiter	Technische Universiteit Delft

This work is part of the research programme of the Foundation for Fundamental Research on Matter (FOM), which is part of the Netherlands Organisation for Scientific Research (NWO).

Keywords: Friction, Contact, Size effects, Discrete Dislocation Dynamics, Atomic effects, Molecular Dynamics

Printed by: ProefschriftMaken || www.proefschriftmaken.nl

Cover rationale: information (flow) is the commonality of all elements in this work: nature, dissipation, computation, cognitive processes and communication.

ISBN 978-94-6295-576-9

An electronic version of this dissertation is available at
http://repository.tudelft.nl/.

CONTENTS

SUMMARY

In this work a computational study is presented that aims at increasing the fundamental understanding of contact and friction. Friction is a physical phenomenon that is present all around in every day life. Often friction is functional, but friction is also a significant cause of energy dissipation. Mechanical energy is converted partly into heat which often can not be harvested for good use. Therefore, it is essential to fundamentally understand friction. However, since friction is not a simple phenomenon that consists of a single mechanism, but instead consists of a variety of mechanisms acting on different length and time scales, reaching a full understanding of friction is a formidable task. In this work we will follow a bottom-up approach and focus on contact and friction at the single asperity level. The simulations are carried out using discrete dislocation dynamics for friction at the meso-scale and molecular dynamics for friction at the atomic scale. Discrete dislocation dynamics simulations incorporate the intrinsic length scale of plastic flow, the Burgers vector, so that this method is capable of capturing size-effects in the plastic response.

The first two chapters of this work have a general character. Chapter 1 provides a short general introduction of the topic of this work. In Chapter 2 a brief overview of the computational methods, dislocation dynamics (DD) and molecular dynamics (MD), is presented.

In Chapter 3 the plastic shear response of micron-scale single asperities is studied for both rectangular and truncated sinusoidal shapes. A new definition of asperity strain is introduced that allows for fair comparison of the plastic response, since the elastic response of asperities of different size and scale are similar. It is found that the contact area is the length scale dominant in controlling the plastic shear response of a single asperity. Smaller contact area results in a harder shear response. This is attributed to the fact that the contact area controls the size of the stress zone in which dislocation nucleation can occur. The height, or the volume, of the asperity is only of influence at intermediate contact areas (depending on the material properties like source spacing). For intermediate contact area, a larger asperity height results in a softer response, since plasticity shifts from the sub-asperity to the asperity itself.

In Chapter 4 the ploughing response of a single asperity of sinusoidally shape is studied and compared with the shear response of a truncated sinusoidal shaped asperity. The contact area is very small, which results in large variation in the fric-

tion force due to the stochastic variation in the source's position and strength. The friction force can be predicted from a Gaussian distribution, irrespective whether the ploughing depth is known or not. The friction force of sheared asperities is clearly dependent on the height of the asperity. The comparison shows that if the asperity is small, so that basically all plasticity occurs in the sub-asperity, the friction strength for ploughing and shearing a flat contact are similar. Therefore, for small size the ploughing model can be simplified to a flat contact shearing model. For larger asperity size, where plasticity inside the asperity occurs, a difference is found in the friction strength for ploughing and shearing. Shearing is more difficult, due to limited material in which slip can occur and due to pile-ups on the contact area.

Following up on the observation made in Chapter 4 that dislocation pile-ups on the contact area can result in a significantly harder plastic response, dislocation impingement is studied using atomistic simulations in Chapter 5. A novel definition of atomic scale contact roughness is introduced to characterize the contact. For Al bi-crystals under compressive loading (without impingement), it is found that the atomic scale roughness controls the normal stress at which dislocation nucleation from the contact interface occurs, while no universal correlation between nucleation stress and interface energy (commonly used to characterize interfaces) is found. The absorption of a single impinging dislocation alters the local roughness, leading to a stress concentration at the impingement site. The stress at which nucleation occurs after impingement increases with increasing roughness, since at larger roughness the stress concentration due to the absorbed dislocation is less strong. At critical roughness the impingement of a single dislocation no longer affects the nucleation stress, since the roughness of the contact itself becomes responsible for nucleation. If multiple dislocations in a pile-up impinge on the contact, the nucleation stress lowers, but only up to a pile-up of three dislocations. At low and intermediate interface roughness, a maximum of two dislocations can be absorbed at the same time in the contact. Only at large roughness, atomic rearrangement allows for more dislocations to be absorbed in the contact. It is found that the repeated process of absorption and nucleation when multiple dislocation impinge roughens the contact locally, which is most clear when the initial contact roughness is low.

The absorption of impinging dislocations studied in Chapter 5 results in atomically stepped contacts. It is also known that crystal growth can result in atomically stepped surfaces. In Chapter 6 we study friction at room temperature of atomically stepped Al surfaces in contact and compare the friction behavior with that of atomically flat contacts. It is found that friction of nano-scale contacts has a self-organized critical state, which means that sliding occurs through stress drops with a power-law distribution. Smaller step spacing results more frequently

in large stress drops. Interestingly, during sliding of a stepped contact, the step is not localized, but moves in the contact plane. This leads to normal migration of the contact. During normal migration of the contact, it is found that vacancies are generated in the re-crystallized region, leading to a vacancy concentration near the contact of about two orders of magnitude higher than the room temperature equilibrium concentration. This finding is important since this could affect dislocation behavior near the contact at larger scales. If the contact consists of a step *pair*, i.e. two steps of opposite sign, the sliding behavior shows two sliding states, jerky and smooth, marked by a sudden transition. Starting from a relative rough contact, the steps organize in the contact during sliding resulting in a smooth topology which leads to smooth sliding. If the step pair height is large, a clear gap exists between the surfaces. The initial real contact area controls the static friction stress. It is found that atomic scale wear during sliding leads to full gap closure, and hence an increase in friction stress. The friction behavior becomes similar to that of small height step pair contacts once the contact has fully closed.

In Chapter 7 unexpected sensitivities to small changes in initial or processing conditions are reported for low temperature MD simulations of friction. These sensitivities can lead to very different friction behavior for step pair contacts at low temperature for different random realizations of the initial atomic velocities or different implementation of the parallelization scheme. It is found that at low temperature not only step motion but also twin nucleation from the contact can occur, which means that the friction response never reaches a steady state. This is not observed at room temperature, where the friction response always reaches a steady state as discussed in Chapter 6. Since it is commonly assumed that due to the absence of thermal noise at low temperature the results of low temperature MD simulations do not have a variation, this is a remarkable observation and requires careful considerations when performing low temperature MD simulations that involve dissipation.

SAMENVATTING

In dit werk wordt een computationele studie gepresenteerd met het doel het fundamentele begrip van contact en wrijving tussen oppervlakken van vaste stoffen te vergroten. Wrijving is een fysisch fenomeen dat overal aanwezig is in het allerdaagse leven. Vaak is wrijving functioneel, maar wrijving is ook een belangrijke oorzaak van energiedissipatie. Mechanische energie wordt deels omgezet in warmte, die over het algemeen niet benut kan worden. Daarom is het essentieel om wrijving fundamenteel te begrijpen. Echter, aangezien wrijving niet een simpel fenomeen is dat bestaat uit een enkel mechanisme, maar bestaat uit een verscheidenheid van mechanismes die op verschillende lengte- en tijdschalen relevant zijn, is het krijgen van een volledig begrip van wrijving een complexe taak. In dit werk volgen we een bottom-up benadering en ligt de focus op contact en wrijving op het niveau van een enkelvoudige asperity (oneffenheid van een oppervlak). De simulaties zijn uitgevoerd met discrete-dislocatie dynamica voor wrijving op de meso-schaal en moleculaire dynamica voor wrijving op de atomaire schaal. Discrete-dislocatie dynamica simulaties implementeren de intrinsieke lengteschaal van plastische deformatie, de Burgers vector, zo dat de methode in staat is om grootte-afhankelijkheid in de plastische respons te voorspellen.

De eerste twee hoofdstukken van dit werk hebben een algemeen karakter. Hoofdstuk 1 biedt een korte algemene introductie in het onderwerp van dit werk. In Hoofdstuk 2 wordt een kort overzicht gepresenteerd van de computationele methoden, dislocatie dynamica (DD) en moleculaire dynamica (MD).

In Hoofdstuk 3 wordt de plastische schuifrespons van micro-schaal enkelvoudige asperities bestudeert voor zowel rechthoekige als afgeknotte sinusoïdale vormen. Een nieuwe definitie van asperity-rek is geïntroduceerd ten behoeve van een eerlijke vergelijking van de plastische respons, aangezien dit de elastische respons van asperities van verschillende grootte vergelijkbaar maakt. De bevindingen tonen aan dat het contactoppervlak de dominante lengteschaal is in de plastische schuifrespons van een enkelvoudige asperity. Kleiner contactoppervlak resulteert in een hardere schuifrespons. Dit wordt toegeschreven aan het feit dat het contactoppervlak de grootte van het spanningsgebied controleert waarin dislocatie-nucleatie kan optreden. De hoogte, of het volume, van de asperity is alleen van belang voor contactoppervlakken die tussen de boven- en onderlimieten liggen (afhankelijk van materiaaleigenschappen zoals dislocatie-bron-

dichtheid). Voor contactoppervlakken tussen de boven- en onder-limieten resulteert een grotere asperity-hoogte in een zachtere respons, aangezien plasticiteit zich verplaatst van het sub-asperity-gebied naar de asperity zelf.

In Hoofdstuk 4 wordt de ploegrespons van enkelvoudige asperities van sinusoïdale vorm bestudeerd en vergeleken met de schuifrespons van een afgeknotte sinusvormige asperity. Het contactoppervlak is zeer klein, wat resulteert in een grote variatie in de wrijvingkracht veroorzaakt door de stochastische variatie in dislocatiebron-posities en -sterkte. De wrijvingskracht kan worden voorspeld op basis van een Gaussische distributie, ongeacht of de ploegdiepte bekend is of niet. De wrijvingskracht voor het schuiven van asperities is afhankelijk van de hoogte van de asperity. De vergelijking tussen de ploegrespons en de schuifrespons toont aan dat wanneer de asperity klein is, zodat praktisch alle plasticiteit in de sub-asperity optreedt, de wrijvingssterktes voor ploegen of schuiven van een vlak contact vergelijkbaar zijn. Hierom kan voor een kleine asperity het ploegmodel gesimplificeerd worden tot een vlak-contact-schuif-model. Voor grotere asperities, wanneer plasticiteit in de asperity zelf optreedt, wordt een verschil in de wrijvingssterkte voor ploegen en schuiven gevonden. De schuifrespons is harder doordat er minder materiaal beschikbaar is waarin dislocaties kunnen glijden en door dislocaties die opeenstapelen tegen het contact.

Volgend op de observatie in Hoofdstuk 4 dat dislocatie-opeenstapelingen tegen het contact kan resulteren in een significant hardere plastische respons, wordt het botsen van dislocaties met een contact bestudeerd in Hoofdstuk 5 middels atomistische simulaties. Een nieuwe definitie van atomaire contactruwheid wordt geïntroduceerd ten behoeve van de karakterisatie van het contact. De studie toont dat voor Al bi-kristallen onder compressiebelasting de atomaire ruwheid de normale spanning waarbij dislocatienucleatie van het contact plaatsvindt bepaalt, terwijl er geen universele correlatie tussen de nucleatie-spanning en de interfaceenergie (gewoonlijk gebruikt om interfaces te karakteriseren) wordt gevonden. De absorptie van een enkele botsende dislocatie verandert de lokale ruwheid, waardoor een spanningsconcentratie ontstaat. De spanning waarbij nucleatie na botsen plaatsvindt neemt toe met toenemende ruwheid, doordat voor grotere ruwheid de spanningsconcentratie door de geabsorbeerde dislocatie minder sterk is. Bij kritische ruwheid is er niet langer een effect in de nucleatiespanning gevonden van het botsen van dislocaties, aangezien hier de ruwheid van het contact zelf verantwoordelijk is voor nucleatie. Wanneer meerdere dislocaties in een opeenstapeling op het contact botsen, neemt de nucleatiespanning af, maar slechts tot drie dislocaties. Bij lage en gemiddelde interfaceruwheid, kunnen er maximaal twee dislocaties tergelijkertijd in het contact geabsorbeerd zijn. Alleen bij grote ruwheid staat atomaire herschikking toe dat meerdere dislocaties geabsorbeerd worden in het contact. Het blijkt dat het herhaalde proces van ab-

sorberen en nucleëren wanneer meerdere dislocaties botsen, het contact lokaal verruwt, wat het meest duidelijk is wanneer de initiële contactruwheid laag is.

De absorptie van botsende dislocaties bestudeerd in Hoofdstuk 5 resulteert in atomair gestapte contacten. Tevens is het bekend dat het groeien van kristallen kan resulteren in atomair gestapte oppervlakken. In Hoofdstuk 6 bestuderen we wrijving op kamertemperatuur van atomair gestapte Al oppervlakken in contact en vergelijken het wrijvingsgedrag met dat van atomair vlakke contacten. Het blijkt dat wrijving van nanoschaal-contacten een zelforganiserende kritische toestand heeft, wat betekent dat glijden plaatsvindt door spanningsvallen met een machtsfunctie-verdeling. Kleinere stapspatiëring resulteert vaker in grotere spanningsvallen. Interessant genoeg blijkt dat tijdens het glijden van een gestapt contact, de stap niet gelokaliseerd is maar beweegt in het contactvlak. Dit leidt tot migratie van het contact loodrecht op het contactvlak. Tijdens de migratie van het contact worden vacatures in het gerekristalliseerde gebied gegenereerd, wat leidt tot een vacatureconcentratie nabij het contact die circa twee orders van grootte hoger is dan de evenwichtsconcentratie op kamertemperatuur. Dit resultaat kan belangrijk zijn, aangezien het het dislocatiegedrag nabij contacten op grotere schaal kan beïnvloeden. Wanneer het contact bestaat uit een stappaar, d.w.z. twee stappen met een tegengesteld teken, heeft het glijgedrag twee verschillende toestanden, ongelijkmatig en vloeiend, met een plotselinge overgang. Vanuit een aanvankelijk ruw contact kunnen de stappen in het contact zich organiseren tijdens het glijden, wat resulteert in een vlakke topologie die op zijn beurt leidt tot vloeiend glijden. Bij een grote stappaarhoogte is er een duidelijke opening tussen de oppervlakken. Atomaire slijtage leidt tijdens glijden tot het sluiten van deze opening en verhoogt hierdoor de wrijvingsspanning. Zodra het contact gesloten is wordt het wrijvingsgedrag hetzelfde als dat van stappaarcontacten met kleine staphoogte.

In Hoofdstuk 7 wordt voor MD simulaties van wrijving op lage temperaturen onverwachte gevoeligheid voor kleine veranderingen in initiële of procesmatige condities gerapporteerd. Deze gevoeligheid kan voor stappaarcontacten op lage temperaturen leiden tot zeer verschillend wrijvingsgedrag voor verschillende atoombeginsnelheden of een verschillende implementatie van de parallelisatie. Het blijkt dat op lage temperaturen niet alleen stapbeweging maar tevens nucleatie van twins uit het contact kan plaatsvinden, waardoor de wrijvingsrespons nooit een stabiele toestand bereikt. Dit wordt niet waargenomen bij kamertemperatuur, waar de wrijvingsrespons altijd een stabiele toestand bereikt, zoals besproken in Hoofdstuk 6. Aangezien algemeen aangenomen wordt dat door de afwezigheid van thermische ruis de resultaten van MD simulaties bij lage temperaturen geen spreiding vertonen, is dit een zeer opmerkelijke observatie. Het geft aan dat zeer zorgvuldige overwegingen vereist zijn wanneer lagetemperatuur-MD

simulaties worden uitgevoerd waarbij dissipatieprocessen optreden.

1

INTRODUCTION

There is at present in the material world a universal tendency to the dissipation of mechanical energy.

William Thomson

1

1.1. GENERAL INTRODUCTION

Todays world population is growing at an exponential rate. The global energy consumption therefore also increases rapidly. With increasing global energy consumption, sustainability becomes more and more relevant. Sustainability can be approached from different perspectives. One aspect is for instance the focus on the use of sustainable energy sources. Another important aspect is limiting energy dissipation. One of the main sources of energy dissipation is friction. Of course friction is a physical phenomenon that is crucial in everyday life. Without friction we would for instance not be able to pick up an object or safely drive a car. However, friction inherently entails energy dissipation, i.e. mechanical work is converted into heat, which in many situations can not be harvested for good use. Hence, friction is besides beneficial, also a major obstacle for sustainability.

Regardless whether friction in a given situation is desired or detrimental, it is of great importance to fundamentally understand it. Especially with the ongoing trend of the miniaturization of mechanical devices, entailing an increase in surface-to-volume ratio, a rigorous understanding of friction is critical [1]. Friction of plastically deforming surfaces in contact provides an elaborate topic. Over the years different friction laws have been defined based on parameters as normal load, real contact area and contact shear strength [2–4]. The roughness of metal surfaces often involves different scales [5–7]. This means that asperities with different length scales are involved in the frictional behavior. Statistical contact theories of realistic rough surfaces constituting of asperities of multiple scales take into account the elastic interaction between these asperities and can accurately describe the pressure distribution of contacting surfaces [8, 9]. However, these theories predict very high local pressures, beyond the classical yield stress of the material. Since plasticity is know to be size dependent at the (sub)micron-scale, it is difficult to predict whether plasticity should have set in.

Friction is a phenomenon that consists of various physical mechanisms that act on different time and length scales [10, 11]. The roughness of metal contacts does not only involve the micro- and nano-length scales of asperities, but also the atomic scale due to, for instance, adsorbed atoms [12] and atomic steps [13]. Since on different length scales different dissipation mechanisms can occur, the frictional behavior is not described by simple scaling laws. It is seemingly impossible to derive friction laws that hold at all scales and therefore it is quite difficult to predict the overall behavior. Considering the interplay between various dissipation mechanisms, it becomes clear that reaching a full understanding of friction is a formidable task. Continuum approaches to model contact and friction certainly break down at the atomic scale [14], due to the discreteness of atoms. To extend the fundamental understanding of friction, a bottom-up approach is required. This means that friction first has to be understood at the smallest scales,

before friction of real rough surfaces in contact can be fully understood. This is the objective of the study in this thesis: to fundamentally understand contact and friction of metal surfaces at the nano- and micro-scales, where atomic and dislocation-mediated processes, respectively, are dominant. Size and scale effects in the plastic response of single asperities are studied at the micron-scale using discrete dislocation dynamics simulations [15, 16]. This method averages over atoms while accounting for the intrinsic length scale of plastic flow, the Burgers vector [17], which makes it able to capture size-effects in micro-scale systems, while still being computationally feasible. Contact and friction at the nano-scale are studied using atomistic simulations. In the formation of contact between metal surfaces, dislocations generated in the bulk can impinge on contacts. This can lead to several mechanisms, i.e. absorption, re-nucleation, transmission or stagnation by pile-up [18–20]. In this work the interactions of edge dislocations with Al contacts under compressive load is studied, which leads to the conclusion that the atomic scale contact roughness is pivotal in controlling the impingement behavior. The absorption of dislocations in a contact results in a stepped contact [21–23]. Such steps can also be formed by crystal growth [13, 24]. Hence, the contact of asperities can exhibit atomic scale roughness. The effect of such roughness on the friction behavior nano-scale contacts is also studied in this work. Friction of dry-contacts can show the characteristics of self-organized criticality [25–30]. In this work we observe also for stepped contacts that self-organization and self-organized criticality is very important in the sliding friction response. This is remarkable, since not only local slip is found to occur in such contacts, but also step motion leading to local contact migration. This work extends the existing knowledge of dissipation mechanism in sliding friction of metal contacts at the micro- and nano-scale.

1.2. OUTLINE OF THE THESIS

This thesis is roughly divided into two parts: 1) the study of friction at the micron-scale, where we use discrete dislocation (DD) plasticity simulations to understand the plastic response of a single asperity, and 2) friction and plasticity at the atomic scale. For the latter we apply molecular dynamics (MD) simulations. Both methods, discrete dislocation dynamics and molecular dynamics, will be presented in chapter 2.

In Chapter 3 the plastic shear response of a single asperity is investigated and the length scale that controls the plastic shear response is identified. Chapter 4 studies the ploughing response of a single asperity and a comparison is made with the shear response of a single asperity. This leads to the conclusion that flat contact models can be applied instead of the more elaborate ploughing model, when the asperity is small enough so that all plasticity occurs in the sub-asperity.

In Chapter 5 the impingement behavior of dislocation on metal contacts is analyzed and the contact characteristic that controls the dislocation nucleation from the contact is identified. Chapter 6 is devoted to the study of friction of atomically stepped surfaces in contact at room temperature. In Chapter 7 the observations of unexpected sensitivities to initial or processing conditions in low temperature MD simulations of friction are presented.

A general conclusion will be presented in chapter 8 and the outcome of this study will be put in broader context.

REFERENCES

[1] B. Bhushan, *Fundamentals of Tribology and Bridging the Gap Between the Macro - And Micro/Nanoscales* (Springer Netherlands, 2001).

[2] G. Amontons, *De la resistance caus'ee dans les machines,* Mem. de l'Academie Royale **A**, 257 (1699).

[3] F. P. Bowden and D. Tabor, *The Friction and Lubrication of Solids* (Oxford Univ. Press, New York, 1950).

[4] K. L. Johnson, *Adhesion and friction between a smooth elastic spherical asperity and a plane surface,* Proc. R. Soc. Lond. A **453**, 163 (1997).

[5] J. A. Greenwood and J. B. P. Williamson, *Contact of nominally flat surfaces,* Proc. R. Soc. Lond. A. **295**, 300 (1966).

[6] Y. F. Gao and A. F. Bower, *Elastic-plastic contact of a rough surface with weierstrass profile,* Proc. R. Soc. Lond. A. **462**, 319 (2006).

[7] L. Pei, S. Hyun, J. F. Molinari, and M. O. Robbins, *Finite element modeling of elasto-plastic contact between rough surfaces,* J. Mech. Phys. Solids. **53**, 2385 (2005).

[8] M. H. Müser, *Rigorous field-theoretical approach to the contact mechanics of rough elastic solids,* Phys. Rev. Lett. **100**, 055504 (2008).

[9] B. N. J. Persson, *Theory of rubber friction and contact mechanics,* J. Chem. Phys. **115**, 3840 (2001).

[10] E. Gnecco and E. Meyer, *Fundamentals of Friction and Wear* (Springer Berlin Heidelberg, 2007).

[11] J. Gao, W. D. Luedtke, D. Gourdon, M. Ruths, J. N. Israelachvili, and U. Landman, *Frictional forces and amontons' law: from the molecular to the macroscopic scale,* J. Phys. Chem. B **108**, 3410 (2004).

[12] F. Besenbacher, *Scanning tunnelling microscopy studies of metal surfaces,* Rep. Prog. Phys. **59**, 1737 (1996).

[13] E. Vlieg, A. W. Denier van der Gon, and J. F. van der Veen, *Surface x-ray scattering during crystal growth: Ge on ge(111),* Phys. Rev. Lett. **61(19)**, 2241 (1988).

[14] B. Luan and M. O. Robbins, *The breakdown of continuum models for mechanical contacts,* Nature **435**, 929 (2005).

[15] R. J. Dikken, E. Van der Giessen, and L. Nicola, *Plastic shear response of a single asperity: a discrete dislocation plasticity analysis,* Phil. Mag. **95(34)**, 3845 (2015).

[16] H. Song, R. J. Dikken, L. Nicola, and E. Van der Giessen, *Plastic ploughing of a sinusoidal asperity on a rough surface,* J. Appl. Mech. **82(7)**, 071006 (2015).

[17] E. Van Der Giessen and A. Needleman, *Discrete dislocation plasticity: a simple planar model,* Model. Simul. Mater. Sci. **3**, 689 (1995).

[18] T. C. Lee, I. M. Robertson, and H. K. Birnbaum, *Prediction of slip transfer mechanisms across grain boundaries,* Scr. Metall. **23**, 799 (1989).

[19] T. C. Lee, I. M. Robertson, and H. K. Birnbaum, *Tem in situ deformation study of the interaction of lattice dislocations with grain boundaries in metals,* Phil. Mag. A **62**, 131 (1990).

[20] T. C. Lee, I. M. Robertson, and H. K. Birnbaum, *An in situ transmission electron microscope deformation study of the slip transfer mechanisms in metals,* Metall. Trans. A **21A**, 2437 (1990).

[21] R. J. Dikken, B. J. Thijsse, and L. Nicola, *Impingement of edge dislocations on atomically rough contacts,* Comput. Mater. Sci. **128**, 310 (2017).

[22] T. Shimokawa, T. Kinari, and S. Shintaku, *Interaction mechanism between edge dislocations and asymmetrical tilt grain boundaries investigated via quasicontinuum simulations,* Phys. Rev. B **75**, 144108 (2007).

[23] S. H. Oh, M. Legros, D. Kiener, and G. Dehm, *In situ observation of dislocation nucleation and escape in a submicrometre aluminium single crystal,* Nature Materials **8(2)**, 95 (2009).

[24] J. F. Lutsko, A. E. S. Van Driessche, M. A. Durán-Olivencia, D. Maes, and M. Sleutel, *Step crowding effects dampen the stochasticity of crystal growth kinetics,* Phys. Rev. Lett. **116**, 015501 (2016).

[25] P. Bak, C. Tang, and K. Wiesenfeld, *Self-organized criticality: An explanation of the 1/f noise,* Phys. Rev. Lett. **59(4)**, 381 (1987).

[26] P. Bak, C. Tang, and K. Wiesenfeld, *Self-organized criticality,* Phys. Rev. A **38(1)**, 364 (1988).

[27] H. J. Feder and J. Feder, *Self-organized criticality in a stick-slip process,* Phys. Rev. Lett. **66(20)**, 2669 (1991).

[28] F. R. Zypman, J. Ferrante, M. Jansen, K. Scanlon, and P. Abel, *Evidence of self-organized criticality in dry sliding friction,* J. Phys.: Condens. Matter **15**, L191 (2003).

[29] S. V. Buldyrev, J. Ferrante, and F. R. Zypman, *Dry friction avalanches: Experiment and theory,* Phys. Rev. E **74**, 066110 (2006).

[30] P. Creeger and F. R. Zypman, *Entropy content during nanometric stick-slip motion,* Entropy **16(6)**, 3062 (2014).

2

COMPUTATIONAL METHODS

The purpose of computation is insight, not numbers.

Richard Hamming

Parts of this chapter have been published in Ref. [1] and Ref. [2].

In this chapter the computational methods that are used to study contact and friction at both the micro- and nano-scale are presented. For the nano-scale, molecular dynamics (MD) simulations are performed. These allow for the investigation of processes where it is essential to capture atomic interactions, like dislocation impingement on a contact and the friction response of atomically stepped surfaces in contact. For the micro-scale, discrete dislocation (DD) plasticity simulations are performed. This is a method that averages over the atoms, but accounts for the dynamics of dislocations, the carriers of plastic flow, using constitutive rules.

2.1. ATOMISTIC SIMULATIONS

2.1.1. MOLECULAR DYNAMICS

All matter is constructed from elementary particles. The behavior of these elementary particles is quantum mechanical and described by the Schrödinger equation. However, since all constituents interact with each other, it is a (near) impossible task to solve the Schrödinger equation at the nano-scale due to the vast amount of particles involved. Fortunately, at the nano-scale most processes are classical and can therefore be treated classically. Therefore, condensed matter systems can often be studied classically with atomic scale resolution by means of classical molecular dynamics (MD) simulations. In this study we are interested in the mechanical responses of metals. For fundamental processes like dislocation impingement on metal contacts and the frictional behavior of atomically stepped surfaces in contact, atomic interactions have to be considered, which are captured in MD simulations. The MD simulations are performed using LAMMPS [3]. Classical MD involves the integration of Newtons equations of motion:

$$\boldsymbol{F}_\mathrm{i} = m_\mathrm{i}\boldsymbol{a}_\mathrm{i} = m_\mathrm{i}\frac{\mathrm{d}^2\boldsymbol{r}_\mathrm{i}}{\mathrm{dt}^2}. \tag{2.1}$$

Here $\boldsymbol{F}_\mathrm{i}$ is the force acting on atom i due to all atoms in the system, m_i is the atomic mass, $\boldsymbol{a}_\mathrm{i}$ is the acceleration and $\boldsymbol{r}_\mathrm{i}$ is the atoms position. The force is related to the potential U by

$$\boldsymbol{F}_\mathrm{i} = -\boldsymbol{\nabla}_\mathrm{i}U. \tag{2.2}$$

Using a Velocity Verlet algorithm, the atomic positions at each time increment are determined. Below the Velocity Verlet scheme is given in the order in which the calculations are performed.

$$\boldsymbol{v}_\mathrm{i}(t+\Delta t/2) = \boldsymbol{v}_\mathrm{i}(t) + \frac{1}{2}\boldsymbol{a}_\mathrm{i}(t)\Delta t \tag{2.3}$$

$$\boldsymbol{r}_\mathrm{i}(t+\Delta t) = \boldsymbol{r}_\mathrm{i}(t) + \boldsymbol{v}_\mathrm{i}(t+\Delta t/2)\Delta t + \frac{1}{2}\boldsymbol{a}_\mathrm{i}(t)\Delta t^2 \tag{2.4}$$

$$\boldsymbol{a}_{\mathrm{i}}(t+\Delta t) = \frac{\boldsymbol{F}_{\mathrm{i}}(t)}{m} \tag{2.5}$$

$$\boldsymbol{v}_{\mathrm{i}}(t+\Delta t) = \boldsymbol{v}_{\mathrm{i}}(t+\Delta t/2) + \frac{1}{2}\boldsymbol{a}_{\mathrm{i}}(t+\Delta t)\Delta t \tag{2.6}$$

Here $\boldsymbol{v}_{\mathrm{i}}$ is the velocity of atom i and Δt is the time increment in each calculation step.

The MD simulations in this study are performed using the embedded atom method [4]. In the embedded atom method the total energy of the system is given by

$$U = \frac{1}{2}\sum_{i,j(j\neq i)} V_{s_i s_i}(\boldsymbol{r}_{ij}) + \sum_i F_{s_i}(\bar{\rho}_i), \tag{2.7}$$

where the first term represents pair interactions between atom i and j of species s_i and s_j, and the second term represents the embedding energies of atom i in an electron density $\bar{\rho}_i$ due to the other atoms. The electron density is given by

$$\bar{\rho}_i = \sum_{j\neq i} \rho_{s_j}(\boldsymbol{r}_{ij}), \tag{2.8}$$

representing the contributions from all neighboring atoms j. This method is especially useful for metals, as the embedding form using the electron density is capable of mimicking the metallic bond that arises from the collective wavefunction of the free electrons.

Temperature control is applied through a Nosé-Hoover thermostat. This thermostat uses one imaginary particle to mimic an infinite heat bath. Using a specific damping coefficient the velocities of the atoms are scaled at every time increment to reach or maintain a certain temperature in the system. Heat conduction in a metal is in reality dominated by free electrons. However, classical MD simulation can not account for this. To compensate for the much too low heat conduction, the whole system is thermalized to the desired temperature [5].

The material of choice in this work is aluminum. The choice for this material is mainly driven by the high stacking fault energy in Al. It is often favorable for dislocations in FCC metals to split into two partial dislocations separated by a stacking fault ribbon. Due to the high stacking fault energy, the separation distance between the partials is small in Al, which limits the necessary dimensions of the simulation box. A potential developed by Purja Pun and Mishin [6–8] is used, which has shown to give accurate stacking fault energies and which is especially suitable for studying mechanical behavior of interfaces.

2.1.2. ATOMIC STRUCTURE ANALYSIS

In the identification and analysis of dislocations and interfaces we mainly make use of the Common Neighbor Analysis (CNA) [9–11]. A cutoff distance is used to

analyze the topology of the bonds in the neighborhood of an atom. For FCC and HCP structure type this is the half distance between the first and second neighbor shell, which is for FCC structure type given by:

$$r_{\text{cut}}^{\text{fcc}} = \frac{1}{2}\left(\sqrt{1/2}+1\right) a_{\text{fcc}}. \tag{2.9}$$

Here a_{fcc} is the lattice constant of the FCC lattice structure. For BCC structure type the cutoff distance is given by:

$$r_{\text{cut}}^{\text{bcc}} = \frac{1}{2}\left(\sqrt{2}+1\right) a_{\text{bcc}}. \tag{2.10}$$

Here a_{bcc} is the lattice constant of the BCC lattice structure. For each of the neighbor bonds of the central atoms, three characteristic numbers are computed. First is the number of neighboring atoms that the central and the bonded neighbor have in common. Second is the total number of bonds between these common neighbors. The third is the number of bonds in the longest chain of bonds connecting the common neighbors. The set of these numbers is compared to the characteristic set of numbers for FCC, BCC, HCP or cubic diamond structure. If it does not match any set of these numbers, then it is unclassified.

2.2. DISCRETE DISLOCATION PLASTICITY SIMULATIONS

At the micro-meter scale it becomes computationally too expensive to apply MD simulations to analyze the mechanical response of metal systems. Therefore, DD simulations are applied, which entails a method that averages over the atoms, but accounts for the dynamics of dislocations, the carriers of plastic flow, using constitutive rules. As mentioned in the previous section, the material of interest is Al. The FCC crystal is represented in the two-dimensional model by three sets of parallel slip planes [12]. The three sets of parallel slip planes are inclined by $\phi = 60^{\text{o}}$ with respect to each other. One set of slip planes forms an angle $\theta = 15^{\text{o}}$ with the shearing direction as shown in Fig. 2.1. This choice ensures that there is no slip system with slip planes that are aligned with the loading direction, since in reality it is not very likely to encounter this. Such a loading would also lead to exaggerated preference of that slip system due to the two-dimensional problem at hand.

The mechanical response of the asperity is modelled using discrete dislocation plasticity [13]. This is a numerical method that combines the solution of a boundary value problem with the dynamics of discrete dislocations. At every time increment during the simulation, the displacement, strain and stress fields in the crystal are obtained by superposition of the fields that arise from individual dislocations (˜) and the fields that correct for the actual boundary conditions

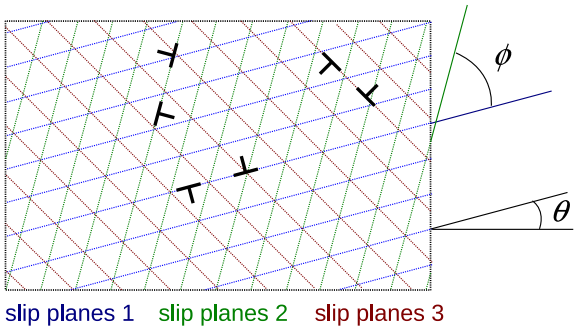

Figure 2.1: Schematic representation the slip systems.

of the problem $\hat{(\cdot)}$,

$$\boldsymbol{u} = \hat{\boldsymbol{u}} + \tilde{\boldsymbol{u}}, \quad \boldsymbol{\varepsilon} = \hat{\boldsymbol{\varepsilon}} + \tilde{\boldsymbol{\varepsilon}}, \quad \boldsymbol{\sigma} = \hat{\boldsymbol{\sigma}} + \tilde{\boldsymbol{\sigma}}. \tag{2.11}$$

The image fields $\hat{(\cdot)}$ are smooth allowing the finite element method to solve the boundary value problem.

All dislocations are of edge character, consistent with the plane strain condition imposed on the direction normal to the plane of analysis. The dynamics of the dislocations is treated in an incremental manner. At each time step, the Peach-Koehler force acting on dislocation I is calculated as

$$f^I = \boldsymbol{n}^I \cdot \left(\hat{\boldsymbol{\sigma}} + \sum_{J \neq I} \tilde{\boldsymbol{\sigma}}^J \right) \cdot \boldsymbol{b}^I, \tag{2.12}$$

where $\boldsymbol{b}^I$ is the Burgers vector of dislocation I. With this as the driving force, the dislocation structure is updated by accounting for nucleation, motion, annihilation and pinning of dislocations at point obstacles.

The nucleation criterion is based on the strength of the Frank-Read sources that are randomly distributed in the material, and on their nucleation time. When the stress on a source exceeds the source strength τ_{nuc} during a time larger than the nucleation time t_{nuc} a dislocation dipole with Burgers vector $\pm\boldsymbol{b}$ is nucleated. The dislocation dipole represents a dislocation loop in two dimensions. The distance between the two constituents of the dipole is therefore taken to be

$$L_{\text{nuc}} = \frac{\mu}{2\pi(1-\nu)} \frac{|\boldsymbol{b}|}{\tau_{\text{nuc}}}, \tag{2.13}$$

where μ is the shear modulus and ν is Poisson's ratio of the elastically isotropic crystal. Annihilation occurs when the dislocations of the dipole come very close

to each other; if their distance is smaller than $6|\boldsymbol{b}|$ they are removed from the simulation.

The Peach-Koehler force f^I causes dislocation I to move with velocity

$$v^I = \frac{f^I}{B}. \tag{2.14}$$

Here B is the drag coefficient arising from the interaction of dislocations with electrons and phonons. The motion of a dislocation is obstructed when it runs into an obstacle. These obstacles represent precipitates or forest dislocations, and are randomly distributed on potentially active slip planes. Obstacles have a shear strength τ_{obs}; when $f^I > b\tau_{\text{obs}}$ for pinned dislocation I, the dislocation is released. When the new dislocation structure is established after each time increment, the new stress and strain state in the updated dislocation structure is calculated.

We take the Burgers vector to have length 2.5 Å, typical for FCC metals. The dislocation source density and the obstacle density are chosen to be 60 μm^{-2} and 30 μm^{-2}, respectively. The source strength τ_{nuc} of each source is randomly selected from a Gaussian distribution with an average strength $\tau_{\text{s}} = 50$ MPa and a standard deviation of 20%. The obstacle strength is taken to be $\tau_{\text{obs}} = 150$ MPa (no variation). These specific material properties provide the flow strength of Al in a tensile test. A specific configuration of the system with random positions of sources and obstacles is called a realization. Each case is repeated for six realizations in order to average out statistical variations originating from the statistical nature of the source and obstacle positions and from the source strength distribution [14, 15].

As the platen that shears the crystal is assumed to be perfectly rigid, dislocations that impinge on the contact are not allowed to penetrate the platen. To establish this condition, impenetrable obstacles are placed at the end of slip planes ending in the contact just below the contact region. This means that the assumption of a rigid platen in perfect sticking contact with the crystal may lead to dislocation pile-ups below the contact.

REFERENCES

[1] R. J. Dikken, E. Van der Giessen, and L. Nicola, *Plastic shear response of a single asperity: a discrete dislocation plasticity analysis,* Phil. Mag. **95(34)**, 3845 (2015).

[2] R. J. Dikken, B. J. Thijsse, and L. Nicola, *Impingement of edge dislocations on atomically rough contacts,* Comput. Mater. Sci. **128**, 310 (2017).

[3] S. J. Plimpton, *Fast parallel algorithms for short-range molecular dynamics,* J. Comp. Phys. **117**, 1 (1995).

[4] M. S. Daw and M. I. Baskes, *Embedded-atom method: Derivation and application to impurities, surfaces, and other defects in metals,* Phys. Rev. B **29**, 6443 (1984).

[5] N. Beckmann, P. A. Romero, D. Linsler, M. Dienwiebel, U. Stolz, M. Moseler, and P. Gumbsch, *Origins of folding instabilities on polycrystalline metal surfaces,* Phys. Rev. Appl. **2**, 064004 (2014).

[6] Y. Mishin, D. Farkas, M. J. Mehl, and D. A. Papaconstantopoulos, *Interatomic potentials for monoatomic metals from experimental data and ab initio calculations,* Phys. Rev. B **59**, 3393 (1999).

[7] Y. Mishin, *Atomistic modeling of the γ and γ'-phases of the ni–al system,* Acta Mater. **52**, 1451 (2004).

[8] G. P. Purja Pun and Y. Mishin, *Development of an interatomic potential for the ni-al system,* Phil. Mag. **89**, 3245 (2009).

[9] J. D. Honeycutt and H. C. Andersen, *Molecular dynamics study of melting and freezing of small lennard-jones clusters,* J. Phys. Chem. **91**, 4950 (1987).

[10] D. Faken and H. Jonsson, *Systematic analysis of local atomic structure combined with 3d computer graphics,* Comput. Mater. Sci. **2**, 279 (1994).

[11] A. Stukowski, *Structure identification methods for atomistic simulations of crystalline materials,* Modelling Simul. Mater. Sci. Eng. **20**, 045021 (2012).

[12] J. R. Rice, *Tensile crack tip fields in elastic-ideally plastic crystals,* Mech. Mater. **6**, 317 (1987).

[13] E. Van Der Giessen and A. Needleman, *Discrete dislocation plasticity: a simple planar model,* Model. Simul. Mater. Sci. **3**, 689 (1995).

[14] A. Needleman, E. Van Der Giessen, and V. S. Deshpande, *Statistical aspects of discrete dislocation plasticity,* Scripta Mater. **54**, 729 (2006).

[15] V. S. Deshpande, A. Needleman, and E. Van Der Giessen, *Dislocation dynamics is chaotic,* Scripta Mater. **45**, 1047 (2001).

3

PLASTIC SHEAR RESPONSE OF A SINGLE ASPERITY

Many people believe that the friction to be overcome to get something started (static friction) exceeds the force required to keep it sliding (sliding friction), but with dry metals it is very hard to show any difference.

Richard P. Feynman

Parts of this chapter have been published in Ref. [1].

3.1. INTRODUCTION

As the miniaturization of mechanical devices continues, the need for a fundamental understanding of friction and plasticity increases [2] since the statistical averages that describe these phenomena at the macroscopic scale are no longer valid [3]. Over the years different friction laws have been defined based on parameters as normal load, real contact area and contact shear strength [4–6]. Nevertheless, there still is a debate about whether describing friction in a rigorous manner is possible, since the aforementioned laws do not hold at small size scales for various reasons [7]. For instance, in the case of metal surfaces with contacts at the (sub-)micron scale, classical local continuum plasticity theories cannot be applied, since they lack a length scale that is necessary to capture size effects [8]. A plasticity size effect in metals occurs when the loaded specimen, or the region subjected to a strain gradient, is comparable in size to a characteristic length associated to the discrete nature of the carriers of plasticity, the dislocations. Various non-local plasticity models [9–12] have been developed in recent years to incorporate the effect of dislocations in a continuum setting. While dislocation flow can be described through mean fields, effects caused by discreteness cannot, think of source limitation effects but also of the highly localized contact pressure profiles, characteristic of discrete dislocation plasticity. At present, statistical contact theories describing the pressure distribution of contacting surfaces with arbitrary roughness [13, 14] provide the most accurate description of contact, since they account for a statistical asperity distribution and the elastic interactions of the asperities. However, these statistical contact theories predict relatively high pressures suggesting that yield takes place locally. Because plasticity is size dependent at small scales it is difficult to predict at which contact pressure plastic deformation sets in.

Friction of real rough surfaces is the outcome of multiple asperities being flattened and sheared. Numerical analyses of multi-asperity contacts were performed, which show that interactions between neighboring asperity contacts play a critical role in determining the true area of contact between the surfaces [15–17]. The present work extends those contact studies by looking at friction. However, we will here neglect asperity interaction and focus on a unit event: the frictional behavior of a single asperity. The problem is analyzed using discrete dislocation plasticity simulations. The choice for this method is related to the scale of the single asperity under consideration which is in the micron regime. This length scale addresses an intermediate regime where molecular dynamics [18, 19] is too computationally expensive but local continuum theories are not suitable [20–22]. Dislocation dynamics fills the gap since it averages over the atoms, but accounts for the nucleation and glide of individual dislocations.

The assumption is made that an asperity protruding from a metal single crys-

tal is in static frictional contact with a rigid platen. As the rigid platen is displaced tangentially, the asperity is sheared. The displacement imposed at the top of the asperity induces a load on the underlying crystal that leads to strain gradients as well as to a geometry-dependent plastic zone. Therefore, identification of the length scale that controls a possible size dependent plastic behavior of the asperity is not trivial. Only in the absence of strain gradients, the characteristic length scale is dislocation spacing. For problems that involve strain gradients, like bending, shearing and indentation, the controlling length scale is much more difficult to identify.

In this chapter we will elucidate the plastic shear behavior of single asperities of various sizes and shapes, and search for the length scale that controls the plastic behavior. Also the occurrence of plasticity inside and underneath the asperity is analyzed. For certain asperity sizes and shapes, plastic deformation of the asperity itself can be ignored. However, if the plastic zone underneath the asperity is large, it can be of significance for real multi-asperity surfaces.

A discrete dislocation analysis of static friction between a flat single crystal and a rigid single asperity performed by Deshpande *et al.* [23] showed a clear dependence on contact size of the contact shear stress. Building on these findings, the shearing of a metallic single asperity by a rigid platen in this study introduces a higher level of complexity since the geometry of the asperity comes into play. Here, single asperities of rectangular and truncated sinusoidal shapes are investigated. For the rectangular asperity, the width is also the contact area, but for a sinusoidal asperity the initial contact area is an extra geometrical parameter which increases the level of complexity, but is more likely to occur in reality.

3.2. PROBLEM FORMULATION

Figure 3.1 shows the two dimensional model of a FCC metal single crystal with an isolated asperity protruding from the flat surface. Two asperity shapes are analyzed: (1) a rectangular shape with height h_{asp} and width w, and (2) a truncated sinusoidal shape with amplitude A, wavelength w and contact area C. For the rectangular asperity $C = w$. In case of a sinusoidal asperity, a flat contact area is artificially created by truncating its apex before loading. The height, $h = 50\mu$m, and width, $\lambda = 1000\mu$m, of the crystal are significantly larger than the dimensions of the asperity, so as not to affect the results.

The mean tangential contact shear stress is given by

$$\tau = \frac{1}{C}\int_{x_1 \in C} \sigma_{12}\, dx_1 \tag{3.1}$$

with the coordinates (x_1, x_2) being parallel and normal to the crystal, respectively. The asperity is sheared by means of a rigid platen that is displaced in the x_1-

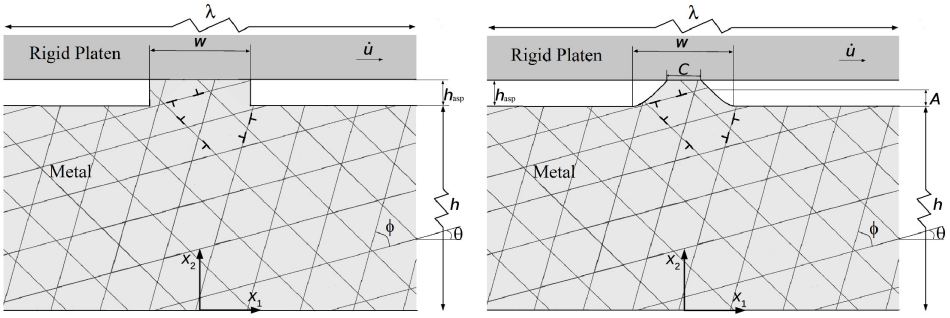

Figure 3.1: Schematic representation of the shearing problem with (a) a rectangular shaped single asperity, and (b) a truncated sinusoidal shaped single asperity.

direction by applying the following boundary conditions at the contact area:

$$u_1^{\mathrm{c}} = \int \dot{u}\,dt, \quad u_2^{\mathrm{c}} = 0 \quad x_1 \in C. \tag{3.2}$$

The surface not in contact is traction free, i.e. $T_1|_{x_1 \notin C} = 0$ and $T_2|_{x_1 \notin C} = 0$. The lateral sides of the crystal are traction free and the bottom of the crystal is fixed $u_1|_{x_2=0} = 0$ and $u_2|_{x_2=0} = 0$.

3.3. SIZE EFFECT FOR SELF-SIMILAR ASPERITIES

Rectangular asperities provide an ideal tool to investigate size and shape effects on the shearing response, since the geometry is defined by only two parameters, i.e. the asperity width and height. Therefore, before investigating truncated sinusoidal asperities, discrete dislocation dynamics simulations are performed for rectangular asperities having a width between $w = 1$ μm and $w = 4$ μm at constant aspect ratio w/h_{asp}. The asperity is sheared at a constant rate up to a lateral displacement $u_1^{\mathrm{c}} = 0.04$ μm at the contact.

Plasticity size effects are most clearly shown when the elastic response is identical. To this end we introduce the asperity shear strain, defined for the two asperity shapes as follows:

$$\text{rectangular}: \qquad \gamma = \frac{u_1^{\mathrm{c}} - u_1^{\mathrm{b}}}{h_{\mathrm{asp}}}, \tag{3.3}$$

$$\text{sinusoidal}: \qquad \gamma = \frac{u_1^{\mathrm{c}} - u_1^{\mathrm{b}}}{A}. \tag{3.4}$$

Here u_1^b is the mean displacement along the asperity base, which is defined as the interface between asperity and crystal bulk (see Fig. 3.2). These definitions of asperity strain guarantee identical elastic response for self-similar asperities, and also limit the difference in elastic response between different asperity shapes used in this study. Figure 3.2b shows that for a few asperity geometries, both rectangular and truncated sinusoidal, the elastic response differs no more than 5 %. This allows for fair comparison of the shear strength of asperities with different geometries.

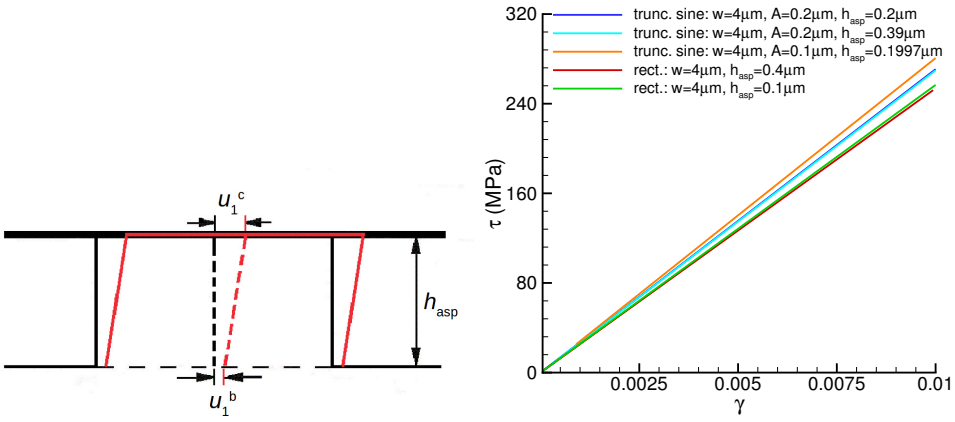

Figure 3.2: a) Schematic representation of the geometrical parameters used to calculate asperity shear strain, and b) the elastic response for a few asperity geometries used in this study.

Figure 3.3a shows the mean contact shear stress τ as a function of asperity shear strain for two groups of self-similar rectangular asperities with aspect ratio $w/h_{\text{asp}} = 10$ and $w/h_{\text{asp}} = 40$ given by the solid and dashed lines, respectively. An evident size effect is observed with small asperities giving a higher contact shear stress. Figure 3.3b shows the shear stress profiles along the contact for a small and a large asperity. A stochastic distribution of stress levels is observed, where the highest peaks in the contact shear stress profile are caused by dislocations piling up against the contact. The stress peaks are high, more than an order of magnitude larger than the nucleation strength of 50 MPa, which was also found in [24] for flattening of multiple asperity systems.

The lower mean contact shear stress in larger asperities observed in Fig. 3.3a reflects more plastic activity. This is exemplified by the dislocation structure and the shear stress (σ_{12}) distribution normalized by the average source strength (τ_s = 50 MPa) shown in Fig. 3.4 for two asperities at $\gamma = 0.015$. Figure 3.4a for $w = 1$ μm is scaled up to have the same size as Fig. 3.4b for $w = 4$ μm for better comparison.

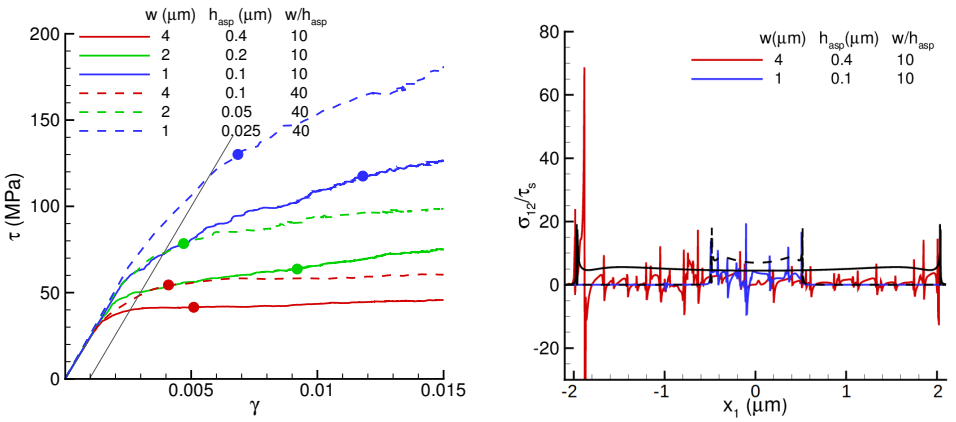

(a) (b)

Figure 3.3: a) Mean contact shear stress as a function of asperity shear strain for rectangular shaped asperities (the gray line indicates the 0.1% offset strain, while the colored dots indicate the data at 0.01 μm offset displacement as reported in Fig. 3.10). b) Comparison of the normalized shear stress profile for a large asperity and a small asperity with the same aspect ratio at shear strain $\gamma = 0.015$. The black curves indicate the corresponding elastic solution (dashed and solid for $w = 1$ and 4 μm, respectively).

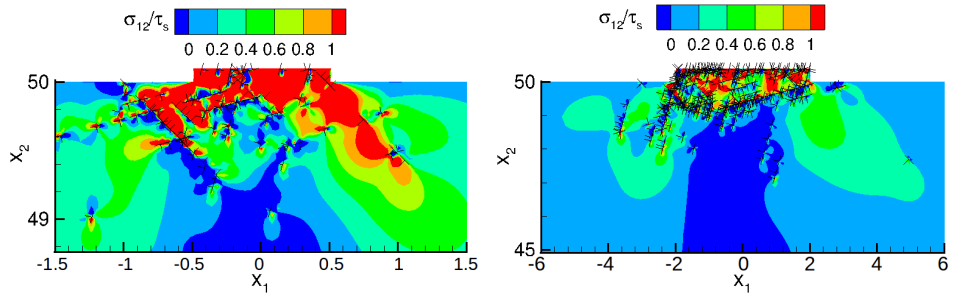

(a) (b)

Figure 3.4: Normalized shear stress distribution and dislocation structure at an asperity shear strain of 0.015 in a rectangular asperity a) of width $w = 1$ μm and height $h_{\text{asp}} = 0.1$ μm, and b) of width $w = 4$ μm and height $h_{\text{asp}} = 0.4$ μm.

The larger asperity in Fig. 3.4b is characterized by a lower stress, on average, both inside and below the asperity. Also it contains a visibly larger number of dislocations than the small asperity in Fig. 3.4a, consistent with the fact that there has been more plastic activity in the body with the largest asperity. Since the contact is impenetrable, the number of dislocations that can escape the asperity is small,

because they can leave the body only through free surfaces. Figure 3.4a and 3.4b also show that dislocations are present outside the area of the asperity itself, yet remain contained in a region that is small compared to the crystal. In the following we shall refer to the region underneath the asperity as the sub-asperity.

In conclusion of this section, it is found that the plastic shear response depends on the asperity size. This is firstly because the size of the asperity poses a constraint on the plastic activity in the asperity itself. Secondly, the size of the asperity also determines the size of the sub-asperity region affected by a strain gradient, and where dislocations can nucleate, provided that there are nucleation sources.

3.4. DEPENDENCE ON ASPECT RATIO FOR A RECTANGULAR ASPERITY

In this section the separate effects of asperity height and asperity width on the plastic response of the system are investigated. Figure 3.5 shows the contact shear strength taken at 0.1% offset strain as a function of asperity height for various values of the width. It becomes clear from these results that the size dependence observed in the previous section is mainly caused by the asperity width (=contact area); the dependence on asperity height is weaker. For large asperity width, the contact shear strength is about 45 MPa and insensitive to height. When the asperity width is small, i.e. $w = 0.5\ \mu$m, the mean contact shear stress is much larger, ranging from 149 MPa to 168 MPa depending slightly on height. Only for intermediate width, e.g. $w = 1\ \mu$m, the effect of height is significant, with the most shallow asperity ($h_{\text{asp}} = 0.025\mu$m) being more than a factor two stronger than the tallest ($h_{\text{asp}} = 0.4\mu$m).

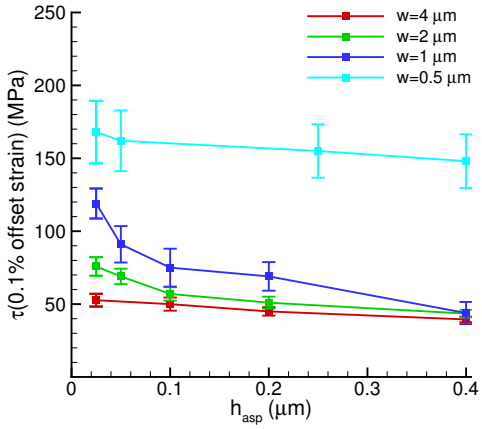

Figure 3.5: Effect of asperity height and width on the onset of plasticity.

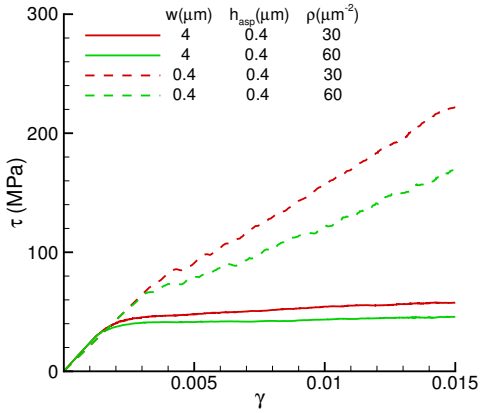

Figure 3.6: Effect of source density for two different rectangular asperity geometries.

The simulations performed so far used a dislocation source spacing corresponding to the default source density of $60\mu m^{-2}$. The average source spacing in these two-dimensional simulations is assumed to be a constant length, which is characteristic of the material, the processing and the loading history that the material has undergone. The ratio between source spacing and contact size determines how many sources are available to nucleate dislocations. It is therefore to be expected that the source spacing will affect the results. To investigate this, the mean contact shear stress is presented in Fig 3.6 for a relatively large ($w = 4$ μm) and relatively small ($w = 0.4$ μm) asperity each having two different source densities. For both asperities, a decrease of the source density by a factor two leads to an increase in the contact shear strength as well as to an increase in hardening slope. Reduction of the source density has a larger impact on the plastic behavior of the small asperity: the hardening slope increases by a factor of approximately 1.7, while it is negligible for the large asperity. This indicates that the plastic response becomes source limited for small asperities. For a small asperity, a low source density cannot guarantee on average the same amount of plastic deformation that is achieved with a higher source density.

To conclude this section, the asperity width, which coincides with the contact area, is the dominant length in the plastic shearing of rectangular asperities: it controls the contact shear stress and hardening. The height of the asperity, and therefore its volume is relevant only at intermediate values of the contact area, for the material parameters in this work around $w = 1$ μm. In a subsequent section, we will show that this is attributed to the relevance of asperity plasticity relative to sub-asperity plasticity.

3.5. ASPERITY GEOMETRY AND CONTACT AREA

To study the plastic shear response of a more realistic asperity geometry, we now consider a truncated sinusoidal shape (see Fig. 3.1b and Fig. 3.7a). The width of the asperities is varied from $w = 1$ μm to $w = 4$ μm, the amplitude from $A = 0.05$ μm to $A = 0.2$ μm and the contact area from $C = 0.1$ μm to $C = 2$ μm. The corresponding height of the asperity is given by

$$h_{\text{asp}} = A + A\cos\left(\frac{\pi C}{w}\right). \tag{3.5}$$

The ratios w/A and C/h_{asp} have to be constant in order to preserve asperity shape. Figure 3.7 shows the contact shear stress as a function of asperity shear strain for two scaled asperity geometries characterized by aspect ratios $C/h_{\text{asp}} = 1.025$ and 10, plotted by the solid and dashed lines, respectively. The curves with the same color represent sinusoidal asperities cut at different heights: the dashed curve is for a sinusoidal asperity with the same base width ($w = 4, 2$ and 1 μm) as that represented by the solid curve, but with smaller height and larger contact area. Similar to the response of rectangular shaped asperities, a size dependence

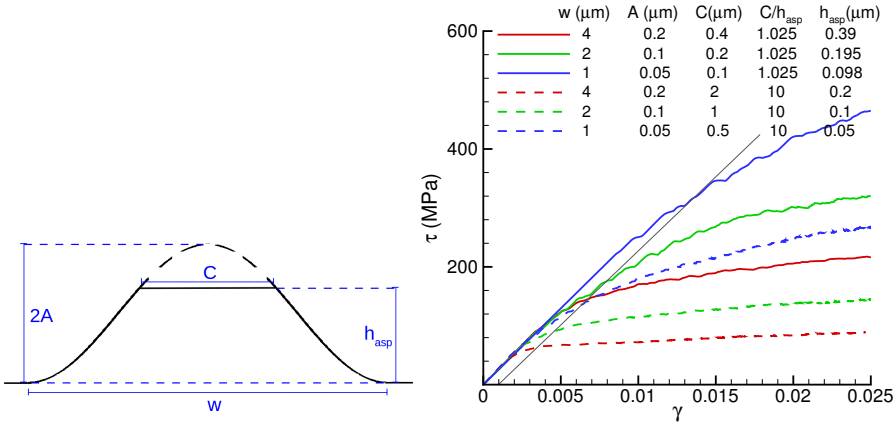

Figure 3.7: a) Schematic representation of the geometry of a truncated sinusoidal asperity, and b) size effect in the contact shear stress as a function of asperity strain for two different scaled truncated sinusoidal asperity geometries.

is found in Fig. 3.7b where smaller asperities show a harder response than self-similar larger asperities. However, by comparing each dashed line with the solid line with the same color, we also see a distinctly different feature of sinusoidal asperities in Fig. 3.7b. An increase in height, and thus in volume, leads to a larger

shear stress, in contrast to what was observed in Fig. 3.3a and Fig. 3.5 for rectangular asperities. The reason for this is that when a sinusoid is truncated at a smaller height, it has a larger contact area.

These observations hint that contact area plays a key role. This is investigated in Fig. 3.8 by plotting the shear strength of rectangular and truncated sinusoidal asperities (from Figs. 3.3a and 3.7b) versus asperity width w and versus contact area C. The error bars show the statistical variation among realizations. A significant variation in the shear strength is found in Fig. 3.8a for each width, and there is no correlation between shear strength and width. On the other hand, when the same data is presented as a function of contact area C in Fig. 3.8b, a consistent trend for both types of asperities is observed, showing a larger shear strength at smaller contact area. The reason is that the contact area determines

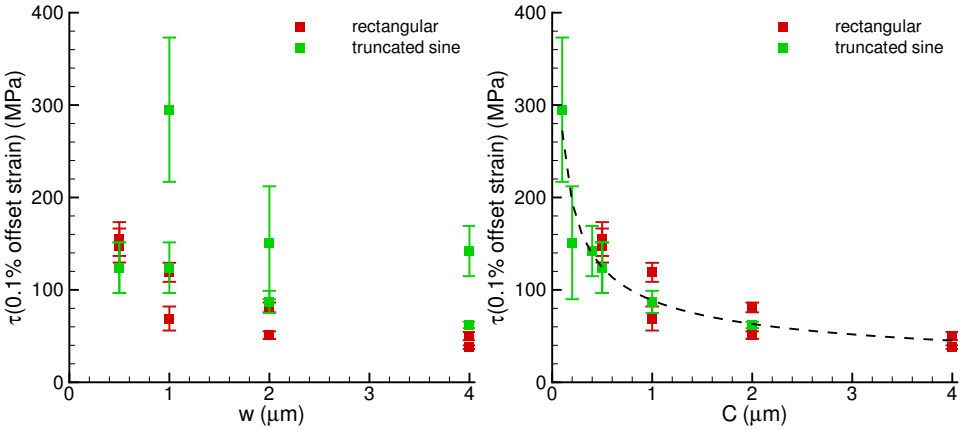

Figure 3.8: a) The shear strength as a function of width and, b) the shear strength as a function of contact area for rectangular and truncated sinusoidal shape.

the size of the stressed region in which dislocation nucleation occurs. Whether or not this region is confined to the asperity or resides mainly outside of the asperity is less relevant. Figure 3.9a and 3.9b show the shear stress (σ_{12}) distribution and the dislocation structure for a rectangular and a truncated sinusoidal asperity, respectively, both with a contact area $C = 1$ μm. The same contact area results in a shear stress distribution and a dislocation structure (average dislocation density) that are quite similar, although the width and the volume of the truncated sinusoidal asperity are respectively 4 and approximately 7.6 times larger than that of the rectangular asperity.

To further explore the importance of contact area, we compare the present

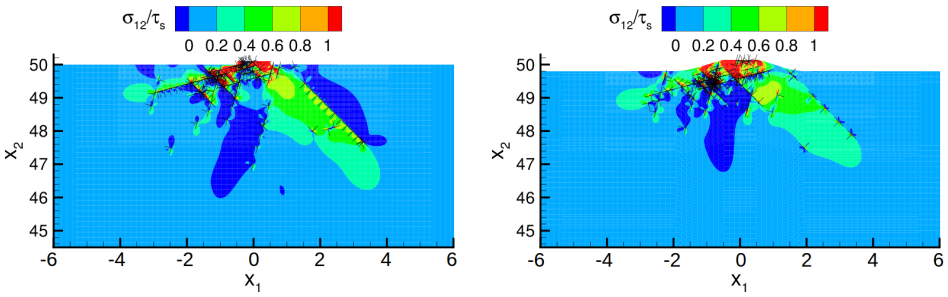

Figure 3.9: The shear stress (σ_{12}) distribution and the dislocation structure at 0.1% offset strain in a) a rectangular asperity ($w = 1$ μm, $h_{\text{asp}} = 0.1$ μm) and, b) a truncated sinusoidal asperity ($w = 4$ μm, $A = 0.2$ μm, $h_{\text{asp}} = 0.34$) having the same contact area $C = 1$ μm.

data for rectangular and truncated sinusoidal asperities with results for a zero-height asperity with contact area C, similar to Ref. [23], in Fig. 3.10. For a zero-

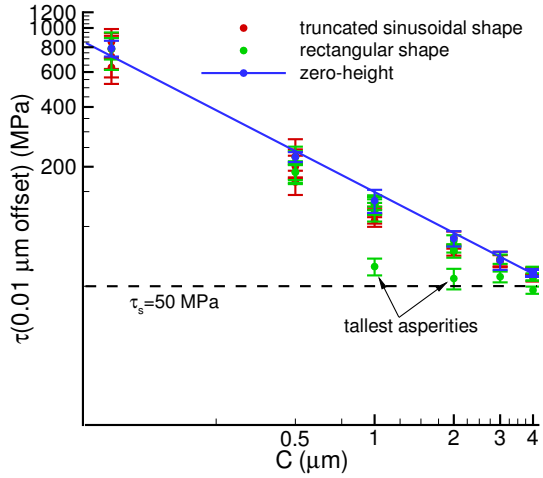

Figure 3.10: The contact shear stress at 0.01 μm offset displacement as a function of contact area C for rectangular and truncated sinusoidal asperities compared with results for zero-height asperities.

height asperity we cannot define asperity strain and therefore we here work with the asperity strength defined at an offset displacement of 0.01 μm (these data points are indicated with symbols in Fig. 3.3a). Error bars are included in Fig. 3.10 to show the variation among different realizations. As expected, both the geometry dependence (especially at intermediate contact size) and the statistical variations become increasingly important as contact size decreases. The strength

of the zero-height asperities depends on C following a power law with an exponent of roughly -0.7. The power law does not extend further to larger contact areas, since already for $C = 4$ μm the continuum limit (≈ 40 MPa) is almost approached. The powerfit of the shear stress of zero-height asperities is in good agreement with the shear stress of rectangular and truncated sinusoidal asperities for large and small values of C, i.e. approximately $C < 0.5\mu$m and $C > 3$ μm for the source density used in this study. This means that the geometry of the asperity barely affects the results at large and small contact area. This is because underneath large contacts the number of available sources is sufficient to ensure that the shear strength is reached. Therefore, an increase in height, even if accompanied by significant plasticity in the asperity, would not affect the shear strength. Underneath small contacts there are insufficient sources to sustain plastic deformation. Increasing the height would also not lead to much more plasticity, since the narrow asperity is source limited. The shape and size of the asperity are instead relevant for intermediate contact size, i.e. 0.5μm$< C < 3$ μm. In this range, taller asperities show a softer response due to significant asperity plasticity relative to the sub-asperity plasticity, as will be shown in the next section.

In conclusion, the problem of the shearing of a protruding asperity can be simplified to the problem of a zero-height asperity if the contact area is either larger than about 3 μm or smaller than 0.5 μm, for the specific source density used in these simulations.

3.6. ASPERITY VERSUS SUB-ASPERITY PLASTICITY

We have already observed that plastic activity takes place not only inside but also outside the asperity, in the sub-asperity. In the previous section we have postulated that plasticity inside the asperity can contribute significantly to the shearing response of asperities with intermediate contact size. Here, we will provide evidence for this. Furthermore, sub-asperity plasticity is not only important in determining the shearing behavior of single asperities, but is also likely to play an important role in surfaces with multiple asperities where the sub-asperity region is shared by neighboring asperities. Therefore, we here aim to give an estimate of the relative contribution of asperity plasticity compared to sub-asperity plasticity.

Slip in the material is a result of gliding dislocations and is therefore a measure of plastic activity. The slip is calculated by subtracting the elastic shear strain from the total shear strain resolved on each slip system. The total slip Γ_{tot} is then computed by integrating the sum of the magnitude of plastic slip on the three slip systems in the volume of the crystal as well as inside the asperity. The slip in the asperity Γ_{asp} as a fraction of the total slip in the crystal is given in Fig. 3.11a as a function of asperity height for all rectangular asperities presented in the work. Results are presented for the default source density $\rho_s = 60$ μm^{-2} as well as for a

lower source density, $\rho_s = 30\ \mu m^{-2}$, cf. Fig. 3.6. The size of the error bars indicates the variation in $\Gamma_{asp}/\Gamma_{tot}$ for different asperity width at the given height. For both source densities the relative slip in the asperity increases with increasing height. If the asperity is shallow, i.e. $h_{asp} < 0.125\ \mu m$, less than 25% of slip occurs in the asperity. When the asperity is taller, slip in the asperity becomes dominant, especially if the width of the asperity is also large. The lower source density results in a lower plastic activity in the asperity at all heights and thus, as expected, the plastic behavior of the asperity becomes less important as source density decreases.

Figure 3.11b shows the relative slip in the asperity as a function of contact area C. When the contact area is large, the slip in the asperity increases significantly with asperity height. However, when the contact area is significantly smaller than $1\ \mu m$, an increase in height gives rise to little additional slip in the asperity.

We know from the previous sections (see Fig. 3.5, Fig. 3.8b and Fig. 3.10) that the contact shear strength of a large contact is insensitive to height. Thus, for large contact areas, a larger asperity height gives more plasticity inside the asperity, but has no effect on the shear strength. On the contrary for small contact areas the shear strength is large, and neither the height nor the volume contribute to a reduction of the shear strength since plastic activity in thin and tall asperities is source limited. Only for intermediate contact areas an increase in asperity height leads to additional asperity plasticity and, as a consequence, to a softer shearing response.

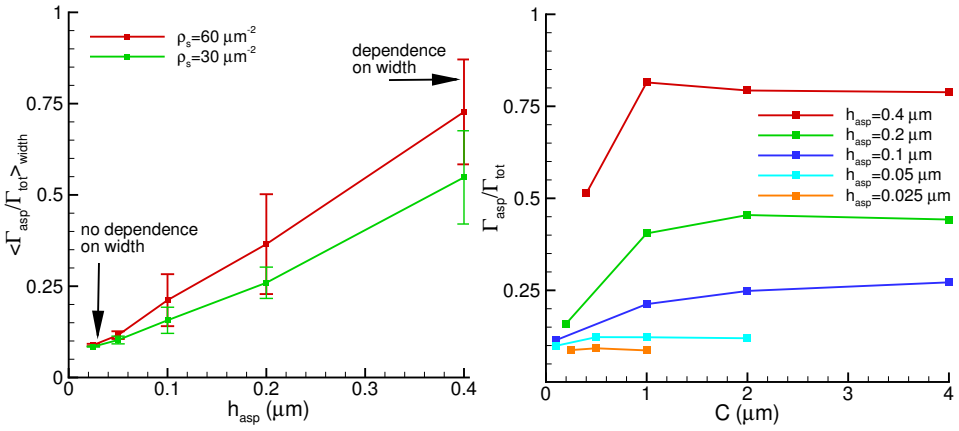

Figure 3.11: a) Relative slip in rectangular asperities for two source densities 0.01 μm offset displacement averaged over different width as a function of height. The dependence on asperity width is contained in the 'error bar' for each h_{asp}. b) Relative slip as a function of contact area for a source density of $\rho_s = 60\ \mu m^{-2}$.

3.7. CONCLUSIONS

In this work the plastic shear response of a single asperity protruding from a large metal crystal is investigated by means of discrete dislocation plasticity simulations. Three asperity shapes are considered: 1) rectangular shape, 2) truncated sinusoidal shape, and 3) zero-height. This study leads to the following conclusions.

- Self-similar asperities with reduced size have a higher contact shear strength than large asperities, even though the elastic behavior measured in terms of asperity shear strain is identical.
- Contact area and spacing between dislocation sources are the length scales that control the plastic behavior of the asperities: the contact area determines the size of the stressed region, inside and below the asperity, where dislocation nucleation can occur. Source spacing controls how many sources can be activated in the stressed region and thus give rise to plastic deformation.
- For small and large contact area, the asperity can be idealized to have zero-volume. Only for intermediate contact area, i.e. $0.5 < C < 3\mu$m for the dislocation source density used in this study, the shape and size of the asperity are relevant. The taller the asperity, the more plasticity inside of it, the softer its shearing response.

REFERENCES

[1] R. J. Dikken, E. Van der Giessen, and L. Nicola, *Plastic shear response of a single asperity: a discrete dislocation plasticity analysis,* Phil. Mag. **95(34)**, 3845 (2015).

[2] B. Bhushan, *Fundamentals of Tribology and Bridging the Gap Between the Macro - And Micro/Nanoscales* (Springer Netherlands, 2001).

[3] E. Gnecco and E. Meyer, *Fundamentals of Friction and Wear* (Springer Berlin Heidelberg, 2007).

[4] G. Amontons, *De la resistance caus'ee dans les machines,* Mem. de l'Academie Royale **A**, 257 (1699).

[5] F. P. Bowden and D. Tabor, *The Friction and Lubrication of Solids* (Oxford Univ. Press, New York, 1950).

[6] K. L. Johnson, *Adhesion and friction between a smooth elastic spherical asperity and a plane surface,* Proc. R. Soc. Lond. A **453**, 163 (1997).

[7] J. Gao, W. D. Luedtke, D. Gourdon, M. Ruths, J. N. Israelachvili, and U. Landman, *Frictional forces and amontons' law: from the molecular to the macroscopic scale,* J. Phys. Chem. B **108**, 3410 (2004).

[8] B. Luan and M. O. Robbins, *The breakdown of continuum models for mechanical contacts,* Nature **435**, 929 (2005).

[9] S. Sandfeld, T. Hochrainer, M. Zaiser, and P. Gumbsch, *Continuum modeling of dislocation plasticity: Theory, numerical implementation, and validation by discrete dislocation simulations,* J. Mater. Res. **26**, 623 (2011).

[10] A. Arsenlis and D. M. Parks, *Modeling the evolution of crystallographic dislocation density in crystal plasticity,* J. Mech. Phys. Solids **50**, 1979 (2002).

[11] S. Yefimov, E. Van der Giessen, and I. Groma, *Bending of a single crystal: discrete dislocation and nonlocal crystal plasticity simulations,* Modelling Simul. Mater. Sci. Eng. **12**, 1069 (2004).

[12] I. Groma, F. F. Csikor, and M. Zaiser, *Spatial correlations and higher-order gradient terms in a continuum description of dislocation dynamics,* Acta Mater. **51**, 1271 (2003).

[13] B. N. J. Persson, *Theory of rubber friction and contact mechanics,* J. Chem. Phys. **115**, 3840 (2001).

[14] M. H. Müser, *Rigorous field-theoretical approach to the contact mechanics of rough elastic solids,* Phys. Rev. Lett. **100**, 055504 (2008).

[15] Y. F. Gao and A. F. Bower, *Elastic-plastic contact of a rough surface with weierstrass profile,* Proc. R. Soc. Lond. A. **462**, 319 (2006).

[16] L. Nicola, A. F. Bower, K. S. Kim, A. Needleman, and E. Van der Giessen, *Multi-asperity contact: A comparison between discrete dislocation and crystal plasticity predictions,* Phil. Mag **88**, 3713 (2008).

[17] F. Sun, E. Van der Giessen, and L. Nicola, *Interaction between neighboring asperities during flattening: A discrete dislocation plasticity analysis,* Mech. Mater. **90**, 157 (2015).

[18] P. R. Cha, D. J. Srolovitz, and T. K. Vanderlick, *Molecular dynamics simulation of single asperity contact,* Acta Mater. **52**, 3983 (2004).

[19] J. Zhong, J. B. Adams, and L. G. Hector Jr., *Molecular dynamics simulations of asperity shear in aluminum,* J. Appl. Phys. **7**, 4306 (2003).

[20] Y. Choi, K. J. Van Vliet, J. Li, and S. Suresh, *Size effects on the onset of plastic deformation during nanoindentation of thin films and patterned lines,* J. Appl. Phys. **94**, 6050 (2003).

[21] J. A. Hurtado and K. S. Kim, *Scale effects in friction of single–asperity contacts. i. from concurrent slip to single–dislocation–assisted slip,* Proc. Roy. Soc. Lond. A mat. **455**, 3363 (1999).

[22] J. W. Hutchinson, *Plasticity at the micron scale,* Int. J. Solids Struct. **37**, 225 (2000).

[23] V. S. Deshpande, A. Needleman, and E. Van der Giessen, *Discrete dislocation plasticity analysis of static friction,* Acta Mater. **52**, 3135 (2001).

[24] F. Sun, E. Van der Giessen, and L. Nicola, *Plastic flattening of a sinusoidal metal surface: A discrete dislocation plasticity study,* Wear **296**, 672 (2012).

4

PLASTIC PLOUGHING VERSUS SHEARING

Parts of this chapter have been published in Ref. [1].

4.1. INTRODUCTION

Classically, the friction force is defined by Amontons law as being proportional to the normal load, $F_f = \mu L$. Tabor and Bowden realized that the reason for the relation between normal load and friction force was in the fact that the apparent contact area and the true contact area differ [2], and that upon increasing the normal load the real contact area also increases. They posed that the friction force should be given by a critical shear strength of the asperities of a rough surface and the true contact area: $F_f = \tau_{cs} A_c$. So to be able to predict the friction force, one has to know the evolving surface morphology to know the true contact area. Greenwood and Williamson developed a framework in which a rough surface is constructed as a collection of asperities with heights that are given by a Gaussian or exponential statistical distribution [3]. This means that also the contact between surfaces is given by a statistical distribution, as shown by [4, 5]. Studies on contact between rough surfaces have applied macroscopic plasticity models [6] [7]. However, plasticity is known to be size-dependent at the micron-scale, which in general entails that smaller systems are harder to plastically deform. Like already mentioned in the previous chapter, molecular dynamics contact studies [8] [9] are computationally expensive and therefore restricted to the nano-scale. Discrete dislocation (DD) plasticity is an intermediate method, that averages over atoms but accounts for the discreteness of dislocations by applying constitutive rules, and therefore is capable of capturing size-effects.

In the previous chapter the plastic shear response of rectangular and truncated sinusoidal single asperities with a perfectly adhesive contact is extensively analyzed. It is concluded that the contact area is dominant in controlling the plastic response. However, for real rough surfaces contact occurs not only by flat contact between asperities, but also by interlocking asperities as shown in Fig. 4.1. So the total friction force is a construct of the force caused by shearing adhesive contacts and interlocking asperities.

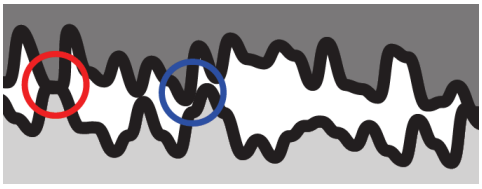

Figure 4.1: Example of contact between two rough surfaces. The red circle shows flat contact and the blue circle shows interlocking asperities.

When two bodies in contact are sheared, there is a critical shear strength at which the relative motion between the two surfaces occurs. For a flat contact

this can either be due to the breaking of adhesive bonds in the contact or due to plastic deformation of the asperity and sub-asperity, like in the previous chapter. The contact shear stress determines which mechanism is dominant in sliding. For ploughing, loss of adhesion is less likely to be the reason of sliding friction due to the interlocking of the asperities. This means that also for very high contact stress, plasticity is likely still the dominant relaxation mechanism.

In this chapter the plastic ploughing response of a single asperity is studied and compared to the plastic shearing response of a single asperity with a flat contact. Ploughing occurs by a rigid sinusoidal asperity in contact with a deformable asperity of similar shape. This chapter aims at obtaining an understanding on the possible differences between shearing and ploughing and whether the more complicated ploughing model can be replaced by simpler contact models in some cases.

4.2. PROBLEM FORMULATION

The computational method applied to study the plastic response of a single asperity, DD plasticity, is described in Chapter 2. The shearing model that forms the basis of Chapter 3 and is also used here is extensively discussed in Chapter 3. Here we focus mainly on the ploughing model. Figure 4.2 shows a schematic

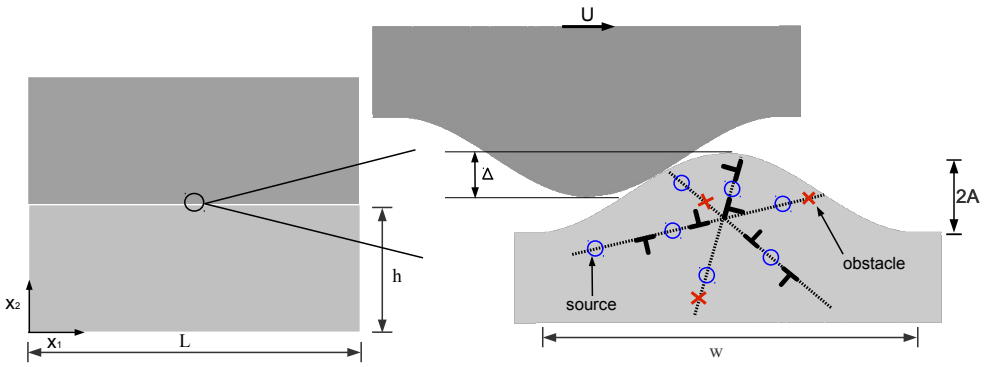

Figure 4.2: Schematic representation of the ploughing model.

representation of the ploughing model. A sinusoidal asperity of width w and amplitude A protrudes from a large single FCC metal crystal of height $h = 50$ μm and width $L = 1000$ μm. A rigid asperity of the same shape and size is responsible for the ploughing by lateral displacement. The contact between the two asperities can be formed at different depth and is defined by Δ as shown in Fig. 4.2. The initial contact area is zero and evolves depending on the size and shape of the

asperity. As for shearing, a perfectly sticking contact is assumed, so that no relative slip between the asperities occurs. The distribution of horizontal tractions $t_1 = \sigma_{1j} n_j$ in the contact C results in a ploughing force F_p. Since now the contact is not flat (i.e. aligned with the x_1-direction) anymore, as it was for shearing, the force becomes:

$$F_p = \int_{x_1, x_2 \in C} (\sigma_{11}\, \mathrm{d}\, x_2 + \sigma_{12}\, \mathrm{d}\, x_1) \tag{4.1}$$

For the non-contact parts of the systems the boundary conditions that are imposed are identical to the boundary conditions used for the shearing problem described in Chapter 3.

4.3. PLOUGHING DEPTH VERSUS SHEARING HEIGHT

Figure 4.3a shows the ploughing force as a function of applied displacement for an asperity of width $w = 4$ μm and amplitude $A = 0.4$ μm at a ploughing depth of $\Delta = 0.4$ μm for ten different realizations where the thick red curve represents the average ploughing force. A large variation is observed between the different real-

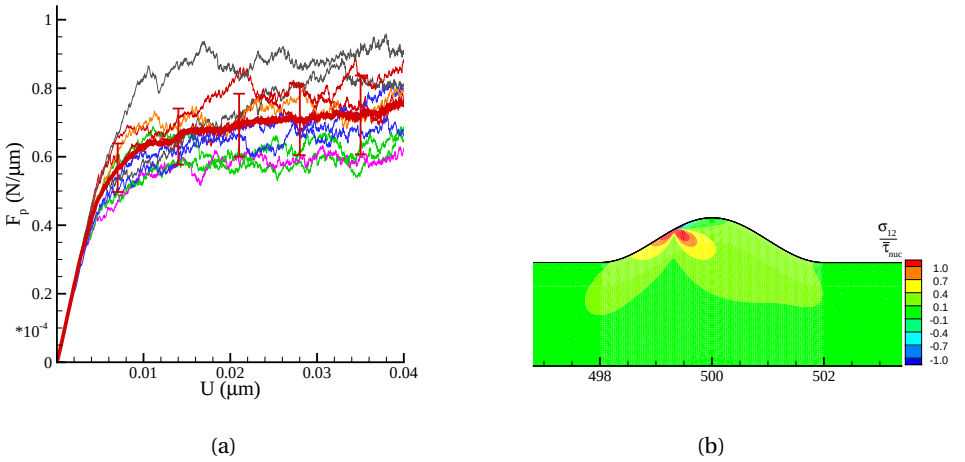

(a) (b)

Figure 4.3: a) Ploughing force as a function of applied displacement for an asperity of width $w = 4$ μm and amplitude $A = 0.4$ μm, and b) the normalized shear stress in the elastic regime.

izations. The reason for this large variation is found by looking at the shear stress in the elastic regime before the onset of plasticity shown in Fig. 4.3b. The shear stress is highly localized. Since the dislocation sources are randomly distributed throughout the material, the likelihood of finding a source in the local stress zone controls plasticity and thereby makes the plastic response highly probabilistic.

This is in line with the observation in Chapter 3 that a smaller contact area results in a larger variation in the contact shear strength.

Contact can be established at different ploughing depth. Figure 4.4a shows for an asperity of width $w = 4$ μm and amplitude $A = 0.4$ μm the ploughing force as a function of applied displacement at different ploughing depth including error bars showing the standard deviation. Although a difference is found in the average ploughing force where larger ploughing depth results in a slightly larger ploughing force, the standard deviation has such a large magnitude that the results overlap. This entails that the ploughing force is not significantly sensitive to the ploughing depth. The results can be converted into a statistical distribution that gives the probability of the ploughing force that is found during friction, shown in Fig. 4.4b. To show that the behavior shown in Fig. 4.4 is not specific for

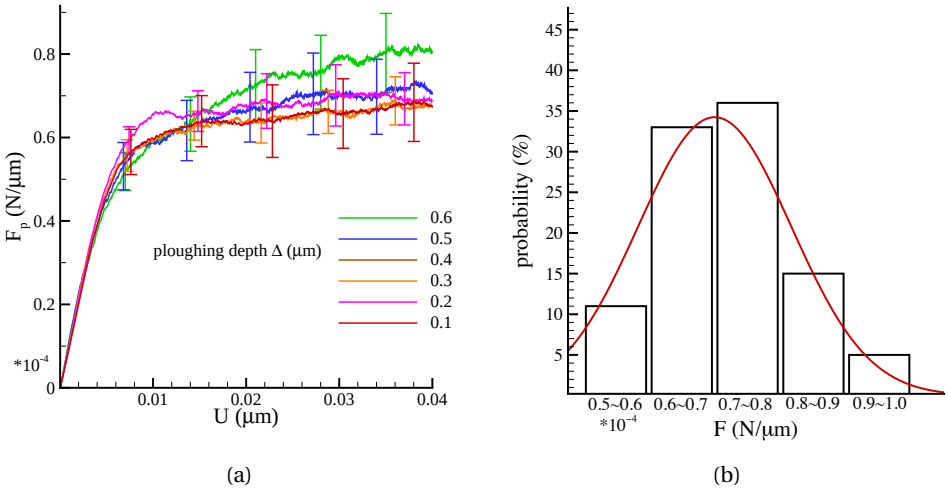

Figure 4.4: a) Ploughing force as a function of applied displacement at different ploughing depth, and b) the statistical distribution of ploughing force for an asperity of width $w = 4$ μm and amplitude $A = 0.4$ μm.

this particular asperity geometry, a similar analysis is performed for a less protruding asperity of width $w = 4$ μm and amplitude $A = 0.2$ μm. The ploughing force and the associated statistical distribution are shown in Fig. 4.5. For both asperity geometries it is found that the ploughing forces at different ploughing depth are statistically indistinguishable and the ploughing force is described by a Gaussian distribution. However, the parameters describing the statistics are not similar but dependent on the asperity geometry. The expected ploughing force for an asperity of width $w = 4$ μm and amplitude $A = 0.4$ μm is $0.75\text{x}10^{-4}$ N/μm,

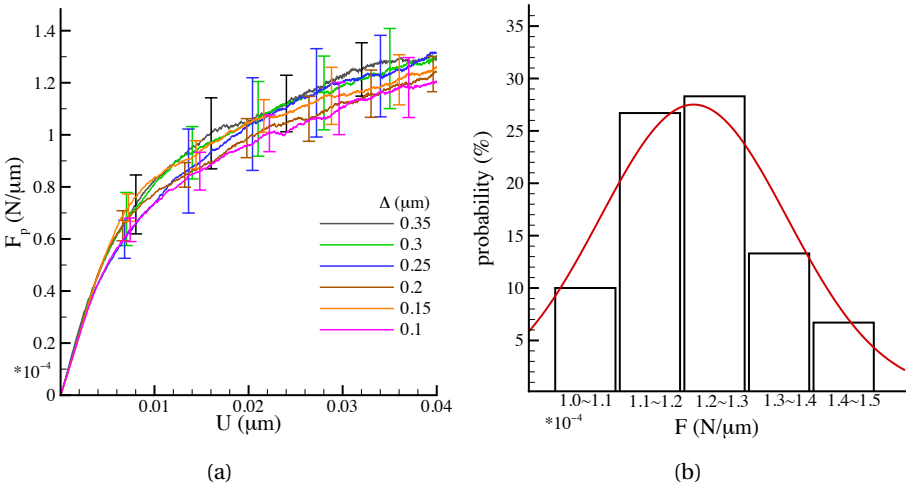

Figure 4.5: a) Ploughing force as a function of applied displacement at different ploughing depth, and b) the statistical distribution of ploughing force for an asperity of width $w = 4$ μm and amplitude $A = 0.2$ μm.

while the expected ploughing force for an asperity of width $w = 4$ μm and amplitude $A = 0.2$ μm is with 1.267x10^{-4} N/μm significantly larger because the relative contribution of plasticity in the asperity with smaller amplitude is smaller compared to the asperity with larger amplitude. The standard deviation however, is similar: 0.12x10^{-4} N/μm for width $w = 4$ μm and amplitude $A = 0.4$ μm and 0.145x10^{-4} N/μm for width $w = 4$ μm and amplitude $A = 0.2$ μm. Additional simulations with half the source and obstacle density show that the standard deviation increases to 0.26x10^{-4} N/μm, so that the standard deviation seems to scale approximately inversely with the source density in the range considered here[1].

Contrary to ploughing at different depth, shearing of a truncated sinusoidal asperity depends on asperity height. Figure 4.6a shows the shear force as a function of applied displacement for an asperity of width $w = 4$ μm, amplitude $A = 0.2$ μm and contact area $C = 2$ μm (resulting in an asperity height $h_{asp} = 0.2$ μm) for ten different realizations. Similar to the ploughing force a relative large variation is found in the shearing force. However, both the average shearing force and standard deviation of the shearing force depend heavily on the shearing height as shown in Fig. 4.6b, where the friction force at final displacement and the standard deviation are shown for two asperity geometries. Shearing at different asperity height entails different contact area. In Chapter 3 it is shown that the contact

[1] When increasing the source density towards the continuum limit, this relation is expected to break down at some point.

area is the controlling length scale of the plastic shear response of a single asperity. Figure 4.7a shows the friction force as a function of contact area for the same two asperity amplitudes. At small contact size the friction force is approximately constant, in agreement with the ploughing case for which the contact area is even smaller. Here we have to note that for small contact size, the contact shear stress is high, about 1 GPa, however the simulations do not account for the possibility of de-adhesion. At larger contact size, the friction force increases. However, the

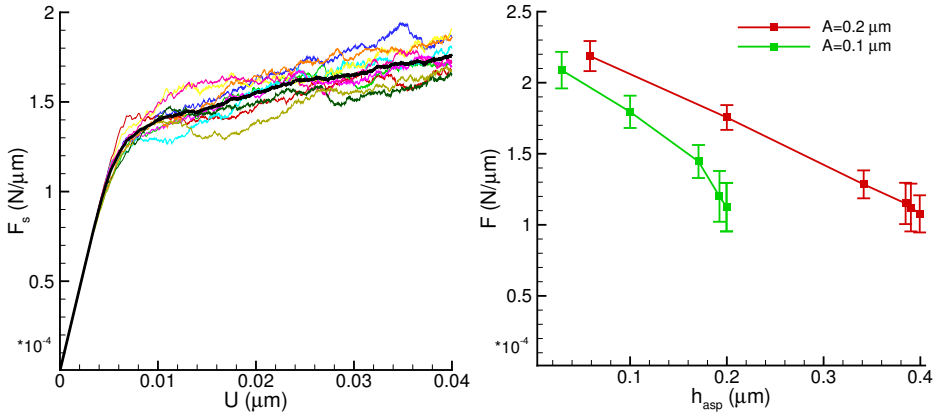

(a) (b)

Figure 4.6: a) The shear force as a function of applied displacement for an asperity of width $w = 4$ μm, amplitude $A = 0.2$ μm, $C = 2$ μm and height $h_{\text{asp}} = 0.2$ μm, and b) the friction force as a function of asperity height.

linear dependence is not a classical dependence (Amontons law) that states that if the contact area increases by a factor of 2 the friction force would also increase by a factor of two. Instead, the slope of the linear part at larger contact area is approximately $0.45\text{x}10^{-4}$ N/μm^2. Because the friction force is significantly different for different contact size, it is not fair to make a comparison of the standard deviation. Therefore we analyze the standard deviation relative to the average friction force. As shown in Fig. 4.7b the relative statistical uncertainty decreases with increasing contact area. At large contact size the statistical dependence in the friction force is only about 5% of the friction force, while at small contact size it can be up to 19%.

In conclusion, although the ploughing response is independent of ploughing depth, the shearing response is dependent on asperity height, due to the significant difference in contact area. Additionally, the variation in the response is clearly affected by the contact size, being significantly larger at small contact area, both for shearing and ploughing.

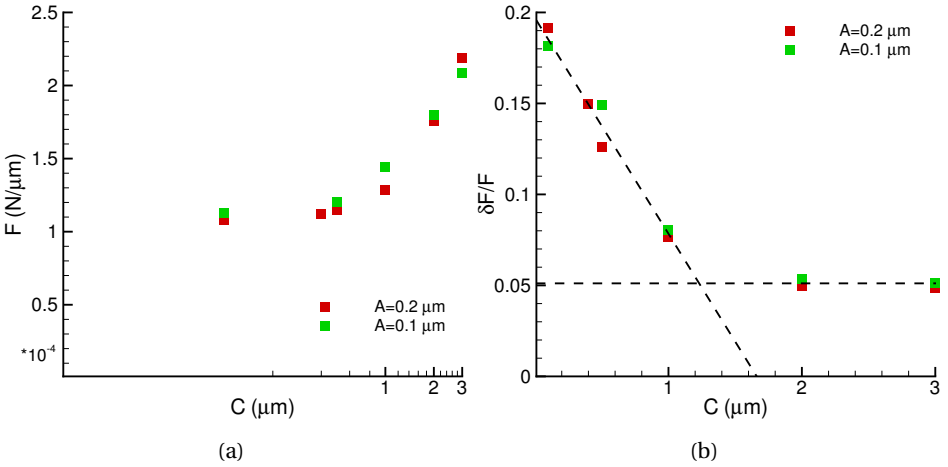

Figure 4.7: a) The friction force, and b) the relative standard deviation as a function of contact area for shearing of a truncated sinusoidal asperity.

4.4. SIZE-DEPENDENCE OF SELF-SIMILAR ASPERITIES

In this section the ploughing and shearing of asperities of the same shape ($A/w = 0.05$) but different size are investigated. For shearing two different cases are investigated. The first is where an asperity protrudes from the crystal and has a constant contact area. The second case has only a contact area: rigid asperity is sheared on top of a flat crystal. Figure 4.8 shows for clarity the three different models. The size-dependence is analyzed in terms of friction stress. For the two shearing models it is clear what to define as the friction stress, since it is simply the friction force divided by the contact area F/C. However, for the ploughing model there is no obvious definition of friction stress. The only geometrical length scale that the three models have in common is the asperity width. Therefore we define the friction stress for all cases as the friction force divided by the asperity width, F/w, which is shown in Fig. 4.9. It is found that for $w \leq 1$ μm, the is no significant difference in the response of the three models. However, for $w > 1$ μm the curves differ clearly. For ploughing an approximated slope of -1 is found. This entails that there is no size-dependence in the force, contrary to the behavior found for the two contact models, where a clear size-dependence is observed. The reason why the ploughing model does not show a size-dependence and the shear models do show a size-dependence is found in the contact area. For shearing it is already known from the previous chapter that the contact area is the dominant length scale controlling plasticity. However, for ploughing the contact area is very small, close to a point. Therefore the size of the asperity does not matter, since the contact stress field is like a point contact stress field. A similar behavior is

encountered in the indentation simulations using a circular indenter [10] where also a concentrated stress field is controlling the plastic response. To further ex-

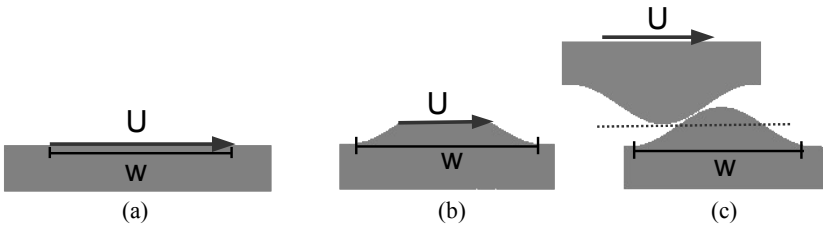

Figure 4.8: Different models: zero-height, shearing and ploughing.

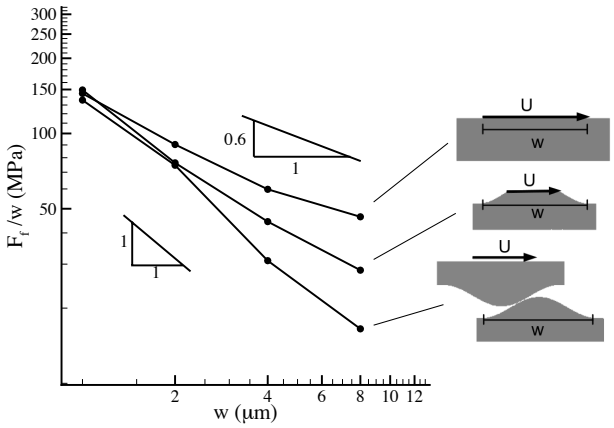

Figure 4.9: Friction stress as a function of asperity width for self-similar asperities for zero-height, shearing and ploughing.

plain the difference between the shearing and the ploughing asperity models we uncover three main differences:

- The displacement is for the shearing model prescribed along a relatively large contact. This leads to a larger force during elastic deformation and smaller fluctuations during plastic deformation.
- The ploughing model considers a larger asperity volume, since for shearing the asperity is truncated to be able to prescribe the displacement. This entails that the ploughing model has a larger amount of sources in the asperity.
- For shearing a perfectly adhesive contact is assumed. Therefore dislocation are prohibited to escape the material through the contact. To establish this

condition impenetrable obstacles are placed at the ends of the slip planes ending in the contact.

The second and third point are conditions that can be mimicked in the ploughing model. All sources in the ploughing model above the contact height in the shearing model are removed. As shown in Fig. 4.10 the ploughing response becomes closer to the shearing response. Now if also impenetrable obstacles are placed at the position where for shearing the contact would be, the results are even closer. Therefore it can be concluded that the kinematic constraints at the contact result in harder responses.

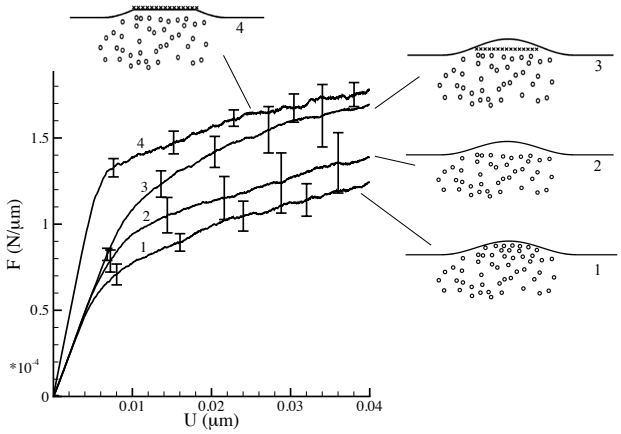

Figure 4.10: Applying constraints to the ploughing model make the ploughing response approach the shearing response.

4.5. CONTACT SIZE-DEPENDENCE IN PLOUGHING OF SELF-SIMILAR ASPERITIES

The previous section shows that for a contact area $C > 0.1$ μm the ploughing behavior is no longer size-independent, but clearly linearly dependent on contact area. In this section we make a comparison between ploughing with an evolving and a constant contact area. Fig. 4.11 shows the friction stress F/w as a function of the width w for three cases: 1) ploughing with evolving contact area (depending on size and shape) as in Section 4.4, 2) ploughing with constant contact area, $C = 25$ nm for all w, and 3) ploughing with contact area which scales with w. It is found in Fig. 4.11 that within statistical variation for all cases the friction strength scales with w^{-1}, and hence the behavior is similar irrespective on the contact definition itself, as long as the contact area is small.

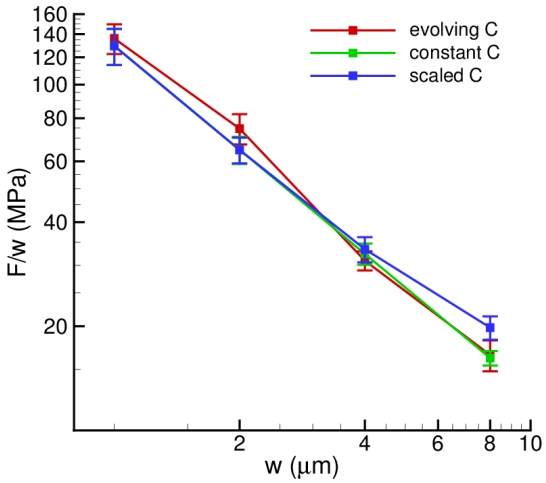

Figure 4.11: Comparison of the friction stress due to plastic ploughing for ploughing with evolving, constant and scaled contact area.

4.6. CONCLUSIONS

In this chapter the plastic ploughing response of a single asperity is studied and compared to the plastic shearing response of a single asperity with a flat contact. This leads to the following conclusions.

- The friction force, defined as the ploughing force at final displacement, is insensitive to the ploughing depth and follows a distribution that is almost Gaussian with a depth-independent standard deviation.
- Although ploughing is insensitive to the ploughing depth, shearing is very much sensitive to the shearing height, because of the associated change in contact area. It is found that a larger contact area results in a larger friction force. The relative standard deviation increases with decreasing contact area (or increasing height).
- For shearing of self-similar asperities and zero-height asperities a size-dependent response is found. However, the friction force for ploughing of self-similar asperities is size-independent.
- For small asperity size the friction strength measured in the asperity base is identical for ploughing and shearing, so that at small asperity size the more complex ploughing model can be replaced with the simpler flat contact shearing model.

REFERENCES

[1] H. Song, R. J. Dikken, L. Nicola, and E. Van der Giessen, *Plastic ploughing of a sinusoidal asperity on a rough surface,* J. Appl. Mech. **82(7)**, 071006 (2015).

[2] F. P. Bowden and D. Tabor, *The Friction and Lubrication of Solids* (Oxford Univ. Press, New York, 1950).

[3] J. A. Greenwood and J. B. P. Williamson, *Contact of nominally flat surfaces,* Proc. R. Soc. Lond. A. **295**, 300 (1966).

[4] B. N. J. Persson, *Theory of rubber friction and contact mechanics,* J. Chem. Phys. **115**, 3840 (2001).

[5] M. H. Müser, *Rigorous field-theoretical approach to the contact mechanics of rough elastic solids,* Phys. Rev. Lett. **100**, 055504 (2008).

[6] Y. F. Gao and A. F. Bower, *Elastic-plastic contact of a rough surface with weierstrass profile,* Proc. R. Soc. Lond. A. **462**, 319 (2006).

[7] L. Pei, S. Hyun, J. F. Molinari, and M. O. Robbins, *Finite element modeling of elasto-plastic contact between rough surfaces,* J. Mech. Phys. Solids. **53**, 2385 (2005).

[8] P. R. Cha, D. J. Srolovitz, and T. K. Vanderlick, *Molecular dynamics simulation of single asperity contact,* Acta Mater. **52**, 3983 (2004).

[9] J. Zhong, J. B. Adams, and L. G. Hector Jr., *Molecular dynamics simulations of asperity shear in aluminum,* J. Appl. Phys. **7**, 4306 (2003).

[10] A. Widjaja, A. Needleman, and E. Van der Giessen, *The effect of indenter-shape on sub-micron indentation according to discrete dislocation plasticity,* Model. Simul. Mat. Sci. Eng. **15**, 121 (2007).

5

IMPINGEMENT OF EDGE DISLOCATIONS ON ATOMICALLY ROUGH CONTACTS

... what statement would contain the most information in the fewest words? I believe it is the atomic hypothesis that all things are made of atoms—little particles that move around in perpetual motion, attracting each other when they are a little distance apart, but repelling upon being squeezed into one another. In that one sentence, you will see, there is an enormous amount of information about the world, if just a little imagination and thinking are applied.

Richard P. Feynman

Parts of this chapter have been published in Ref. [1].

5.1. INTRODUCTION

When dislocations impinge on two-dimensional defects like interfaces, grain boundaries (GBs), or contact areas between crystals, several mechanisms can occur, i.e. absorption, re-nucleation, transmission, or stagnation by pile-up [2–4]. Which of these mechanisms will prevail depends on a large number of variables, e.g. dislocation type, crystal structure, (relative) crystal orientations, loading and temperature. There is both experimental [5] and computational [6–10] evidence that a critical role is played by the atomic structure of the two-dimensional interface. While specific interfaces favor dislocation absorption through local atomic rearrangement [11], others favor dislocation nucleation into one of the two adjacent crystals [12]. Also, depending on the atomic interface structure, nucleation of new dislocations was measured to occur at a wide range of critical nucleation stresses [5].

The molecular dynamics studies that have been performed so far have focused on perfect interfaces [11–14]. However, real GBs are not perfect and contacts, formed by pressing two crystals together, are even less perfect, because of the presence of adatoms on each of the surfaces [15].

The main aim of this study is to identify, by means of molecular dynamics simulations, the effect of atomic scale roughness on the impingement behavior of dislocations on Al contacts between clean surfaces without native oxide layer. To this end, we characterize two dimensional contacts, also perfect ones (i.e. without adatoms), by their average atomic scale roughness. Interestingly, we find that there is a direct correlation between atomic scale roughness and the applied load required to nucleate a new dislocation from the contact after impingement. Notice that in previous studies, interfaces were characterized by their energy, but no universal correlation was found between interface energy and nucleation stress [14].

An additional question that we intend to answer is: what is the limit to the number of dislocations that can pile up on the same slip plane against an atomically rough contact? This is of interest to us because of the impact that pile-up length has on the plastic behavior of metal contacts at larger scales. Micro-scale models of the type of discrete dislocation plasticity are used to study the plastic behavior of micro-scale contacts [16–18], but details of the contact and of dislocation nucleation and absorption are below the resolution of the method. The contact is simply described as an impenetrable boundary for dislocations, where dislocations therefore form unbounded pile-ups. Interfaces can certainly be strong barriers for dislocation glide. It is shown, for instance, by Tsure *et al.* [19] that the interaction energy of an edge dislocation with an energetically stable Al grain boundary is 10^4 times higher than the Peierls potential. This could lead to dislocation pile-up, as for instance experimentally observed in Ref. [20]. Nevertheless,

absorption and re-nucleation are phenomena that limit the length of pile-ups on many interfaces, as supported by the experimental observations in Ref. [21] where at certain critical strain a sudden change in the dislocation distribution of the pile-up was found. Our goal in this respect is to extract information from the molecular dynamics simulations to determine what are the conditions that limit the length of a pile-up, and trigger re-nucleation. This information can be used in future discrete dislocation plasticity simulations of contact.

In this work two aluminum crystals with different orientation are pressed into contact. Dislocations are introduced in one of the crystals and their glide towards the contact is enforced by applying a normal load to the bi-crystal. The surface of each crystal is either perfect or contains adatoms.

The chapter is organized as follows: in Section 5.2 the method and problem formulation are presented. In Section 5.3 the contact is characterized and the atomic scale contact roughness is defined. In Section 5.4 the effect of atomic roughness on the impingement of single dislocations is investigated, while Section 5.5 is devoted to the impingement of multiple dislocations (up to 4) on contacts of various roughness. The roughening due to impingement and roughness dependent ability to absorb dislocations is studied in Section 5.6. Section 5.7 provides a discussion and guidelines for the implementation of constitutive rules in larger scale models.

5.2. COMPUTATIONAL APPROACH

The MD simulations are performed using LAMMPS [22] with a potential developed by Purja Pun and Mishin [23–25] which has shown to give accurate surface and stacking fault energies and is especially suitable for studying mechanical behavior of contacts, interfaces and dislocations.

Material choice and problem description

In the present study the impingement of edge dislocations on contacts is investigated. In FCC metals it is often energetically favorable for dislocations to exist as partial dislocations separated by a stacking fault ribbon. The width of the stacking fault ribbon d_{SF} is inversely related to the stacking fault energy γ

$$d_{\mathrm{SF}} \approx \frac{Gb^2}{4\pi\gamma}, \tag{5.1}$$

where G is the shear modulus and b is the magnitude of the Burgers vector [26]. The material chosen in this study is aluminum because it has a small stacking fault ribbon, and therefore allows for a relatively small simulation box. The stacking fault ribbon width that results from the potential used in this study is $d_{\mathrm{SF}} = 1.3$

nm, which is in close agreement with the experimental value, ranging from 1.1-1.6 nm [24].

The contact is established between two Al crystals with different orientation, constituting a bi-crystal. Figure 5.1 shows a schematic representation of the model. Two bi-crystals, A and B, are chosen with slip plane orientations that are either favorable or unfavorable for dislocation transmission. The difference between the two bi-crystals is only in the orientation of the upper crystal. The lower crystal is chosen such that the [110]-direction aligns with the x-axis, the $[\bar{1}10]$-direction aligns with y-axis and the [001]-direction aligns with the z-axis. For this orientation we have slip planes for which the dislocation line lies along the y-axis. The angle of the slip planes of two slip systems with the x-axis is $\pm 54.7^{o}$.

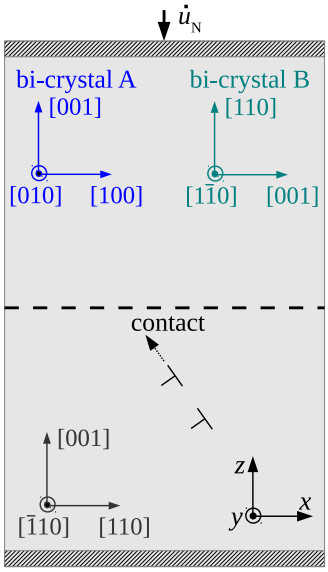

Figure 5.1: Schematic representation of the model showing bi-crystal A and B.

For the upper half of the bi-crystal, two orientations are used: for bi-crystal A, the [100]-direction aligns with the x-axis, the [010]-direction aligns with the y-axis and [001]-direction aligns with the z-axis. Dislocation transmission is not expected to occur, because this crystal has no slip planes for which the dislocation line lies along the y-axis.

For bi-crystal B, the [001]-direction aligns with the x-axis, the $[1\bar{1}0]$-directions aligns with the y-axis and the [110]-direction aligns with the z-axis. This crystal has, like the lower half of the bi-crystal, slip planes for which the dislocation line lies along the y-axis. The crystal is a 90^{o} rotation of the first crystal, which means that the angle of the slip planes of two slip systems with the x-axis is $\pm 35.3^{o}$. This

means that for bi-crystal B, dislocation transmission is possible.

The dimension in the y-direction is taken to be small, only five times the lattice constant, so that the dislocations are of edge character. Because the periodic box is small in this direction, the dislocation line can not bow out, so that spurious image forces due to line bowing are avoided [27].

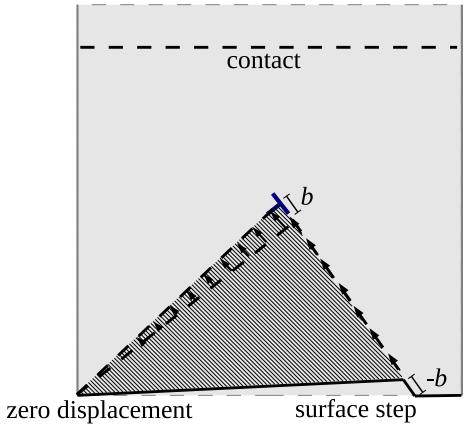

Figure 5.2: Schematic representation of the dislocation insertion in the lower part of the bi-crystal. Displacement is applied to the dark grey (hatched) domain, where the maximum displacement b is applied throughout the slip plane up to the location where the dislocation is inserted and zero displacement is applied at the opposite end of this location. After relaxation this results in a dislocation in the crystal and a surface step at the bottom.

The simulation box contains the bi-crystal and is periodic in the x- and y-direction. The box size is chosen large enough to not influence the dislocation behavior in terms of the onset of dislocation motion and the stress at which nucleation occurs from the contact. For the material studied here the size is $L_x = 445$ Å, $L_y = 20$ Å and $L_z = 810$ Å. Dislocations are inserted in the bottom crystal by prescribing displacement to the atoms in the dark grey (hatched) domain in Fig. 5.2, where the insertion of the dislocation is schematically depicted. The displacement applied ranges from zero for the atom at the bottom left hand side of the hatched region to b for the atoms at the right hand side of the hatched region. This creates a displacement step of size b at the bottom of the crystal. A relaxation run is then performed. During relaxation, a dislocation emerges at the top corner of the hatched region (see Fig. 5.3). If the dislocation is inserted close to the contact, the dislocation moves by itself into the contact during relaxation. This is referred to as 'directly inserting the dislocation into the contact' later in this work. Figure 5.4 shows the σ_{zz} stress state of the contacting crystals with the dislocation in the lower crystal, before loading is applied.

To induce motion of the dislocation towards the contact, eight atomic (x,y)

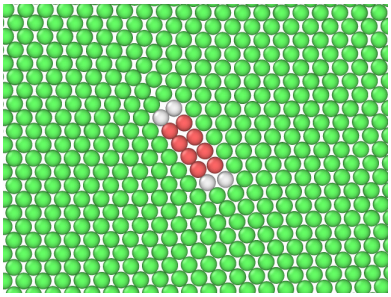

Figure 5.3: Two partial dislocation (grey) separated by a stacking fault (red) resulting from the procedure presented in Fig. 5.2. Atoms of FCC structure type are represented with green. The atomic structure is determined according to a Common Neighbor Analysis (CNA) [28].

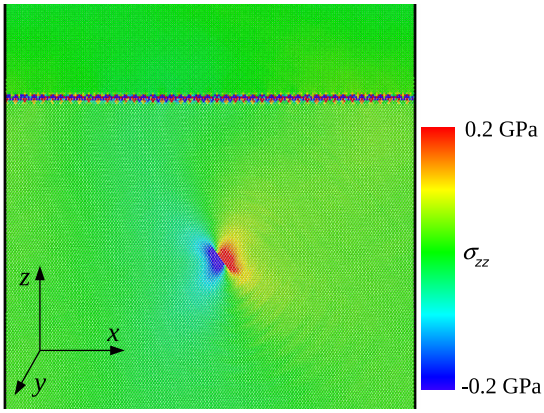

Figure 5.4: Normal stress, σ_{zz}, in the vicinity of the dislocation and the contact before the load is applied.

planes at the top of the upper crystal are displaced in the negative z-direction, while the positions of eight atomic (x,y) planes at the bottom of the lower crystal are fixed in the z-direction (see Fig. 5.1), but free in the periodic x- and y-direction. The number of (x,y) planes on which the load is applied is chosen such that load is uniform, not affected by the surface step at the bottom crystal. The displacement at the top is applied at a constant velocity $\dot{u}_N = 4$ m/s, three orders of magnitude lower than the speed of sound in Al, not only sufficiently low to avoid setting of shock waves, but also to model quasi-static loading at $5 \cdot 10^7$ s^{-1} strain rate[1].

An NPT ensemble in LAMMPS is used to maintain constant temperature and to keep the pressure on the periodic boundaries zero. The temperature is kept at 100 mK using a Nosé-Hoover thermostat.

[1] A strain rate of $1 \cdot 10^7$ s^{-1} shows identical results.

5.3. CHARACTERIZATION OF THE CONTACT

5.3.1. ATOMIC SCALE ROUGHNESS

Contacts between crystals with different orientation have different atomic structure and roughness. For the two bi-crystals considered here, Fig. 5.5 shows the atoms at the interface: these are atoms that do not have an FCC structure according to a Common Neighbor Analysis (CNA) [28]. To characterize the different contacts in this study we introduce a dimensionless atomic scale contact roughness R:

$$R = \begin{cases} 1 - \dfrac{N_c}{N_{int}}, & \text{if } N_c < N_{int} \\ 0, & \text{if } N_{int} = 0. \end{cases} \tag{5.2}$$

Here N_c is the number of contact atoms and N_{int} is the total number of interface atoms. An atom is defined as a contact atom if it belongs to the interface and is in compressive mode when a global infinitesimal compressive load is applied to the bi-crystal [29]. The interface atoms are all atoms that, based on a CNA do not have FCC structure, and therefore do not belong to either of the two perfect crystals in contact. The number of contact atoms relative to the interface atoms gives a measure of the freedom that the interface has for atomic rearrangement during impingement. Therefore this new definition of atomic scale contact roughness will prove to be pivotal in the description of the dislocation-interface interaction. The limit $R = 0$ is defined as the perfect contact between two single crystals with the same crystallographic structure and orientation, which in contact form nothing but a larger single crystal. With increasing R, the contact becomes progressively rougher and the stress state less uniform.

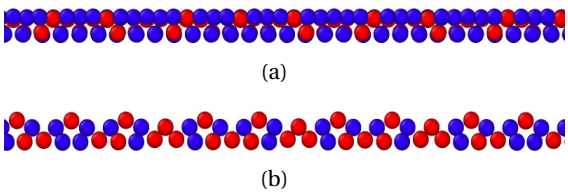

(a) (b)

Figure 5.5: Interface atoms, with contact atoms shown in blue, for perfect bi-crystals: a) bi-crystal A with low contact roughness ($R = 0.26$), and b) bi-crystal B with high contact roughness ($R = 0.45$). The atoms that have an FCC structure type, i.e. atoms that do not belong to the interface, are excluded. Only a part of the interface is shown.

The interfaces of the bi-crystals previously described are here called perfect contacts, as they are simply the interface between crystals with different orientation. In this study we will investigate both perfect contacts and contacts with N_{ad} adatoms. A total of N_{ad} atoms are randomly distributed on the two surfaces before they are put into contact. This is done as follows. The two surfaces are

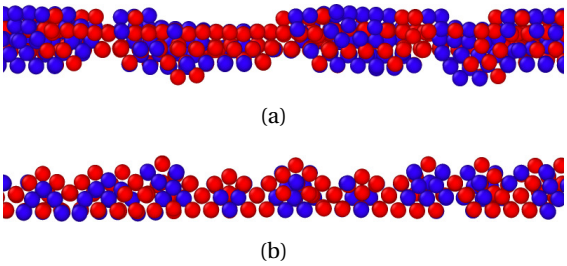

(a)

(b)

Figure 5.6: Interface atoms, with contact atoms shown in blue, for bi-crystals with 300 added adatoms: a) bi-crystal A with contact roughness $R = 0.55$, and b) bi-crystal B with contact roughness $R = 0.51$ if 300 adatoms are present. Only part of the interface is shown.

initially separated by $3a$. Adatom coordinates are randomly generated within the region between the two surfaces. After a relaxation run of 100 ps, necessary for the adatoms to find their equilibrium positions, the two crystals are brought together down to a separation distance of one lattice constant. Then in a second relaxation run, the contact is formed. Figure 5.6 shows two examples of contacts with 300 adsorbed atoms on the surfaces of the crystals shown in Fig. 5.5. Table 5.1 shows an overview of the atomic scale roughness of all the contacts studied in this work.

N_{ad}	0	50	100	200	300
R bi-crystal A	0.26	0.35	0.40	0.50	0.55
R bi-crystal B	0.45	0.46	0.48	0.49	0.51

Table 5.1: Atomic scale roughness R of the different contacts studied in this work. Contacts without adatoms are called perfect contacts.

5.3.2. ATOMIC SCALE ROUGHNESS COMPARED WITH CONTACT ENERGY

When a compressive load is applied to dislocation-free bi-crystals, the response is elastic up to a large applied load, until dislocation nucleation occurs from the contact. As an example of this, the stress-strain (σ_N–ϵ) response for three bi-crystals with different numbers of adatoms is shown in Fig. 5.7. The stress–strain curve of the crystals show a slight softening behavior at small strain, due to atomic rearrangement of the interface atoms, similarly to what is observed in [30, 31]. We will call the stress σ_N at which nucleation occurs nucleation stress and we will indicate it as σ_{nuc} also in the following. The three crystals in Fig. 5.7 differ by orientation (A or B), contact roughness and contact energy. The contact energy is defined as

$$\gamma = \frac{1}{S} \sum_{i \in V} (E_i - E_0), \tag{5.3}$$

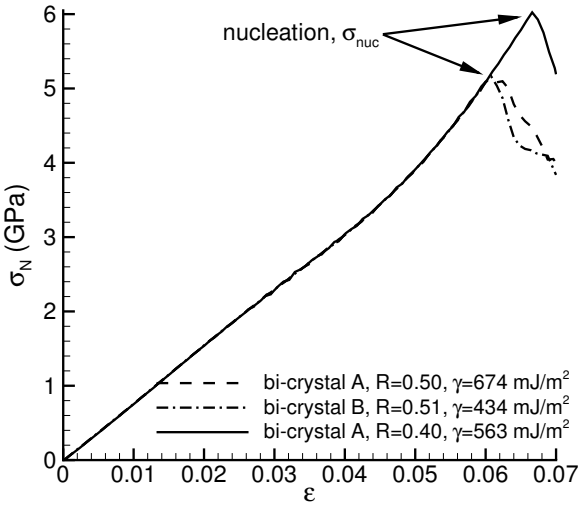

Figure 5.7: Stress-strain curves for bi-crystals with different interface energy γ and contact roughness R.

where S is the area of the contact interface ($S = L_x L_y$), E_i is the potential energy of atom i in the domain V, and E_0 is the atomic bulk potential energy. The domain V is chosen as 2/3 of the simulation box including the contact interface, such to exclude the free surfaces at the top and bottom of the bi-crystal. It is important to observe in Fig. 5.7 that the bi-crystals with the same contact roughness have the same nucleation stress, despite having different crystal orientations and different contact energy. This is not incidental, but a characteristic of all contacts studied in this work. This can be seen in Fig. 5.8, where the nucleation stress obtained for the bi-crystals with R given in Table 5.1, is presented as a function of roughness, R, and contact energy, γ. With increasing roughness the nucleation stress decreases linearly, since local stress concentrations become more pronounced. The increase is almost linear, as indicated by the red line, which intersects the vertical axis at about 11.2 GPa, in close agreement with the ideal strength of Al at zero-temperature of 11.7 GPa calculated in Ref. [32]. This is because a contact with zero contact roughness is a perfect crystal, made of two perfect single crystals with the same orientation being in contact. The stress state in such a crystal is uniform, and therefore the nucleation stress should correspond to the ideal strength of the material. The results demonstrate that the nucleation stress depends on the atomic scale roughness of the contact, while it is independent of its energy and of crystal orientation. A similar lack of universal correlation between the interface energy and the nucleation stress was already reported by Warner *et al.* [14].

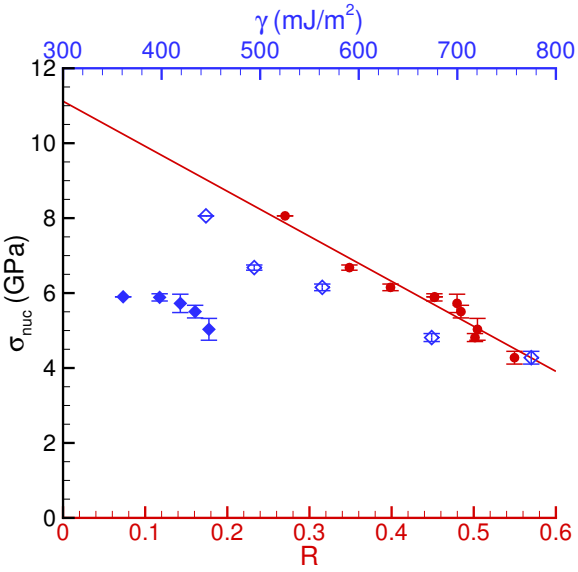

Figure 5.8: Stress at which nucleation occurs from the contact without impingement as functions of both interface energy γ (diamonds) and atomic scale contact roughness R (circles). The open and closed diamond symbols represent the interface energy for bi-crystal A and B, respectively.

5.4. IMPINGEMENT OF A SINGLE EDGE DISLOCATION

5.4.1. IMPINGEMENT ON PERFECT CONTACTS

A dislocation is introduced in bi-crystal A and, after relaxation, the bi-crystal is loaded in compression by normally displacing the top atoms of the upper crystal. The corresponding stress–strain (σ_N–ϵ) response is shown in Fig. 5.9 and compared to the response of a dislocation-free bi-crystal.

The applied displacement induces a shear stress on the dislocation which then glides towards the contact. The resolved shear stress at which the dislocation motion is initiated is 56 MPa (the point is indicated as 1 in Fig. 5.9), which is almost twice as large as the Peierls stress in aluminum (ca. 36 MPa). An overestimation of the Peierls stress is to be expected, since classical MD simulations conducted well below the Debye temperature do not account for zero-point fluctuations [33]. At $\sigma_N = 0.53$ GPa the dislocation is absorbed in the contact (point 2) and at $\sigma_N = 2.3$ GPa a new dislocation is nucleated from the interface. The stress-strain curve for the dislocation–free bi–crystal undergoes a sudden drop at a much larger loading, i.e. $\sigma_N \simeq 8$ GPa (not shown in the figure), when an avalanche of dislocations is nucleated, similarly to what is observed in [34]. Thus, impingement results in nucleation occurring at a significantly lower normal stress, almost 6 GPa lower than in a dislocation–free crystal.

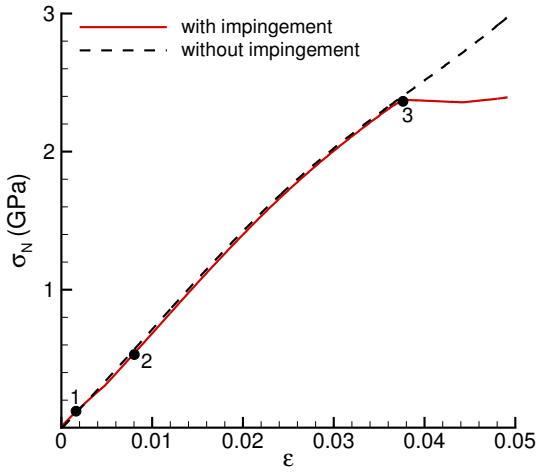

Figure 5.9: Stress-strain curve with and without impingement (initially dislocation-free) for bi-crystal A with contact roughness $R = 0.26$. Numbers indicate (1) the onset of dislocation motion, (2) dislocation absorption and (3) dislocation nucleation.

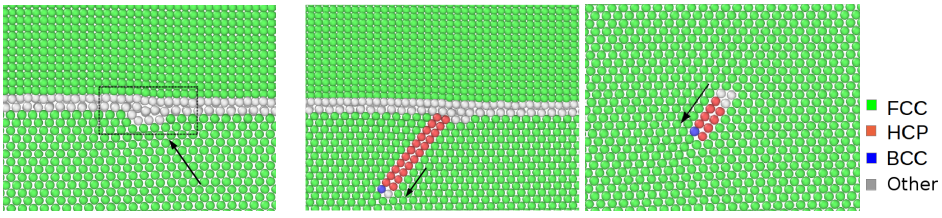

(a) (b) (c)

Figure 5.10: a) Surface step in the contact created by the impingement of a dislocation at a normal stress $\sigma_N = 0.53$ GPa, b) nucleation of a leading partial dislocation from the surface step, and c) the dislocation moving away from the contact (bi-crystal A, $R = 0.26$).

Since the contact is rather flat, the dislocation creates, upon absorption, a localized surface step with magnitude b, as shown in Fig. 5.10a. Even without applied load, a single dislocation would be absorbed during relaxation when placed close to the contact. It is this surface step that later on acts as dislocation nucleation site. As the leading partial dislocation is nucleated, it moves away from the contact, thereby increasing the stacking fault ribbon length, as shown in Fig. 5.10b. Once the trailing partial dislocation is nucleated the stacking fault ribbon length decreases as the dislocation moves away from the contact as shown in Fig. 5.10c.

Next we study impingement of a dislocation on the interface of bi-crystal B, which has a rougher interface than A, $R = 0.45$ (see Fig. 5.5b). There are three unique impingement sites as shown in Fig. 5.11, contrary to the previous case

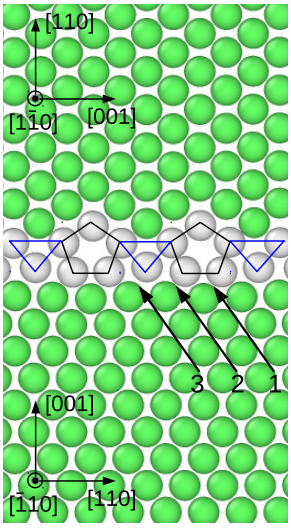

Figure 5.11: Interface of bi-crystal B ($R = 0.45$) with three different impingement sites.

where all impingement sites are equivalent.

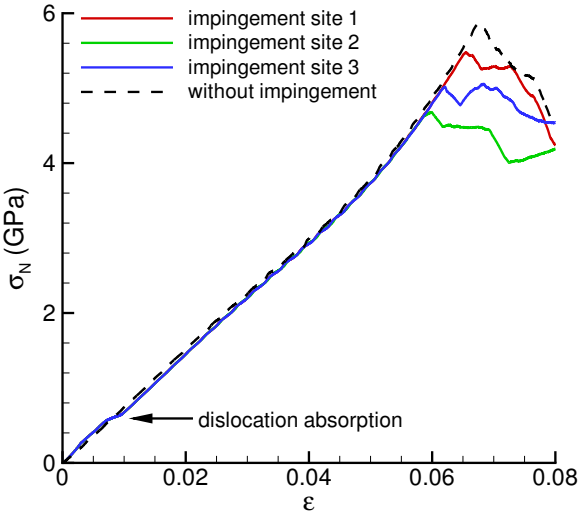

Figure 5.12: Stress-strain curves for dislocation impingement site 1, 2 and 3 (solid curves) in the interface of bi-crystal B and without dislocation impingement (dashed curve).

Figure 5.12 shows the normal stress-strain relation for the three impingement sites and for the dislocation-free bi-crystal shown by the black dashed curve. For a dislocation–free bi-crystal nucleation occurs at σ_N =5.9 GPa, a lower value than

for bi-crystal A (σ_N =8 GPa). As shown in Section 5.3, the reason for this is that the interface is rougher. The nucleation stress when there is dislocation impingement, is only moderately lower than the dislocation-free case, for all impingement sites, with σ_{nuc} ranging from 4.8 GPa to 5.5 GPa. It is found that, following the nucleation of the leading partial dislocation, twinning partial dislocations are nucleated in all cases, instead of a trailing partial dislocation (see Fig. 5.13). The nucleation of twinning partials occurs either into the lower or upper crystal. The absorption of a single dislocation in an intrinsically rough contact does not alter the local roughness significantly. Therefore, while the impingement site is sufficiently affected to act as nucleation site, nearby locations are also characterized by high stress concentrations. Once the leading partial dislocation is nucleated, it is followed by the nucleation of a twinning partial from an adjacent site, similarly to what has been observed by Dewald *et al.* [8] and Yamakov *et al.* [35].

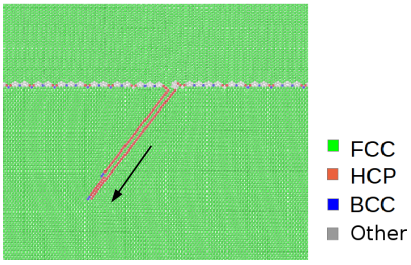

Figure 5.13: Nucleation of twinning partial dislocations from impingement site 3 of the interface of bi-crystal B with $R = 0.45$.

The nucleation stress after impingement for bi-crystal B is significantly larger than for bi-crystal A. This is rationalized considering that the effect of the induced roughness by the absorption of the dislocation on a flatter contact is significant, leading to high local stresses. For a contact that is already rather rough, as for bi-crystal B, the absorbed dislocation is accommodated more easily and gives rise to smaller local stress. This can be seen by contrasting Fig. 5.14a and b, where the stress state surrounding the impingement site after absorption is presented, after removal of the load.

5.4.2. IMPINGEMENT ON CONTACTS WITH ADATOMS

As mentioned earlier, rough contacts are constructed by placing randomly $0 < N_{ad} < 300$ aluminum atoms on the surfaces, which is up to approximately 20% of the number of atoms in one atomic plane. The bi-crystal is relaxed to ensure that the adatoms find their equilibrium positions.

We look at the effect of roughness R on the nucleation stress after dislocation

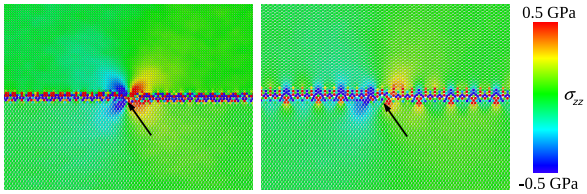

Figure 5.14: Normal σ_{zz} stress near the impingement site for a) bi-crystal A and, b) bi-crystal B.

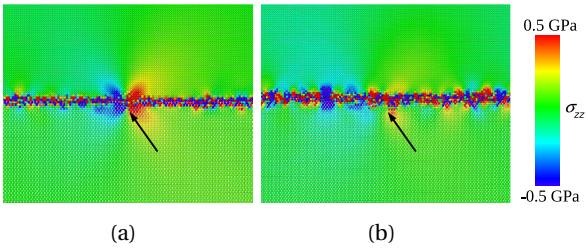

Figure 5.15: Normal σ_{zz} stress near the impingement site for bi-crystal A with contact roughness a) $R = 0.35$ and, b) $R = 0.55$, resulting from the adsorbed atoms in the contact.

impingement. Five different simulations are performed for each contact interface to collect statistics for different impingement locations in the contact. It is found that once the dislocation impinges, it is directly absorbed in the contact, similar to the behavior for impingement on perfect contacts. Figure 5.15 shows σ_{zz} around the impingement site for small and large roughness. The arrow indicates the impingement site. At low roughness, the stress concentration caused by the impinging dislocation is clearly visible. On the contrary, large roughness accommodates the dislocation Burgers vector easily and the location where the dislocation was absorbed is more difficult to detect, similar to what is observed for perfects contacts in Fig. 5.14.

For both bi-crystals with contact roughness $R \geq 0.35$, impingement can either result in nucleation of a dislocation or a twin, depending on the local roughness, i.e. local contact structure.

Figure 5.16 shows the average nucleation stress σ_{nuc} as a function of roughness R with and without impingement. As already shown in Fig. 5.8, if there is no dislocation impingement, the nucleation stress decreases approximately linearly with increasing contact roughness, irrespectively of crystal orientation (see red line). On the contrary, if there is dislocation impingement, for small R the nucleation stress is much lower than for dislocation-free crystals, and increases up to

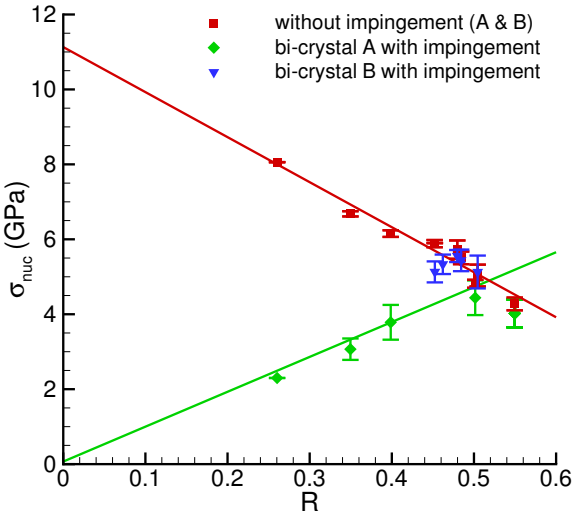

Figure 5.16: Nucleation stress as a function of roughness for bi-crystals A and B with varying numbers of adatoms at the interface. The data represented by square symbols is the same as in Fig. 5.8. The red and green lines are the linear fit of the red data point and green data points up to R=0.5, respectively.

$R \simeq 0.5$, because the stress concentration at the contact due to the absorbed dislocation is much more pronounced for low R (see Figs. 5.14 and 5.15). Above $R \simeq 0.5$ dislocation-free crystals have the same σ_{nuc} as crystals with impingement. This is because above a certain contact roughness, an impinging dislocation does not additionally contribute to the the contact roughness, which is by itself sufficient to trigger dislocation nucleation.

5.5. IMPINGEMENT OF MULTIPLE DISLOCATIONS

In this section the impingement of a train of dislocations (up to four) on various contacts is investigated. First we focus on perfect contacts, i.e. without adatoms. The dislocations are inserted consecutively at approximately 13 nm distance from each other. After each insertion a relaxation run is performed. To reduce the required size of the simulation box, the first dislocation is inserted directly in the contact, see Fig. 5.17.

If multiple dislocations impinge, we find that the first nucleation event is always a dislocation, never a twin. As previously discussed, the absorption of a single dislocation in an intrinsically rough contact does not alter the local roughness significantly, so that nucleation can also occur from adjacent sites, leading to the nucleation of a twin. However, when a dislocation impinges at a site where a dislocation is already absorbed, the local roughness caused by the impingement

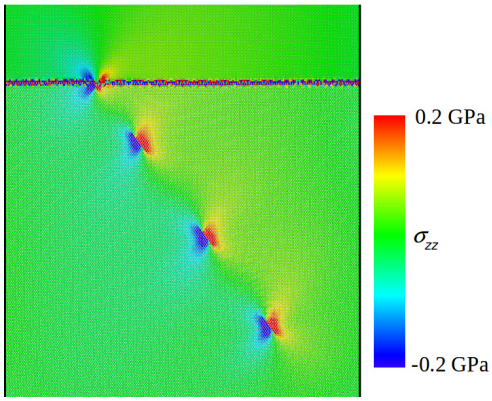

Figure 5.17: Initial state of bi-crystal A with $N_d = 4$, three dislocation in the lower crystal and one inserted directly in the contact.

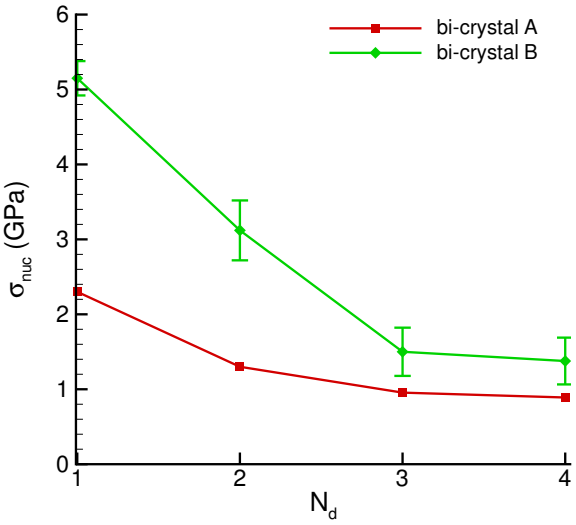

Figure 5.18: Nucleation stress as a function of the number of dislocations in a pile-up for both bi-crystals A and B without adatoms.

is noticeably different with respect to the rest of the contact. The large stress concentration at the site facilitates nucleation of a dislocation. Since dislocations in the pile-up push onto the dislocation step in the contact and for the next dislocation to be absorbed in the contact, a dislocation has to be re-nucleated from the impingement site. Figure 5.18 shows σ_{nuc} as a function of the number of dislocations in the pile-up N_d for bi-crystal A and B. It is shown that initially σ_{nuc} decreases fast with increasing N_d, since the local stress at the impingement site is significantly higher due to the second dislocation in the pile-up. For $N_d \geq 3$ the

nucleation stress becomes approximately constant, at about 0.9 and 1.4 GPa for bi-crystal A and B, respectively, since the dislocations further away from the contact do not contribute much to the contact stress field. The error bar for the curve of bi-crystal B gives the variation between the different impingement sites and is about 0.31 GPa. So for a relative small pile-up of only three dislocations, the behavior is already negligibly affected by increasing the number of dislocations further.

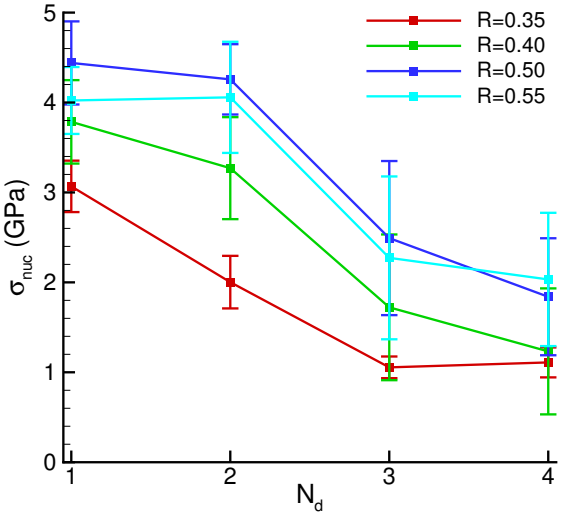

Figure 5.19: Nucleation stress as a function of the number of dislocations in the pile-up for bi-crystal A with different number of adatoms and therefore different R.

Next we study the impingement of multiple dislocations on a contact containing adsorbed atoms. We choose to focus on bi-crystal A with adatoms, since for this bi-crystal the addition of adatoms on the surfaces changes R significantly as shown in Table 5.1. Figure 5.19 shows σ_{nuc} as a function of N_{d} for contacts with different roughness. Consistently with the results in Fig. 5.16, the nucleation stress with dislocation impingement for all N_{d} increases with increasing roughness up to approximately $R = 0.5$, where the influence of R appears to vanish. Also, the nucleation stress decreases with increasing number of dislocations in the pile-up up to $N_{\text{d}} = 3$. Note that, for all R, σ_{nuc} at $N_{\text{d}} = 4$ is significantly lower than the stress at nucleation without impingement in Fig. 5.8.

5.6. CONTACT ROUGHENING DUE TO IMPINGEMENT

In this section we study the effect that the impingement of a train of four dislocations has on local roughness. We take as example the case of bi-crystal A.

Figure 5.20 shows the number of dislocations in the pile-up n_{d} (excluding the dislocation initially in the contact) in red, the number of absorbed dislocations n_{abs} in blue and the number of nucleated dislocations n_{nuc} in green as a function of normal stress. The simulation starts with three dislocations in the pile-up and one absorbed in the contact. At $\sigma_{\mathrm{N}} = 0.35$ GPa, the second dislocation of the pile-up is absorbed in the contact. For a third dislocation from the pile-up to be absorbed, a dislocation has to be nucleated from the impingement site back into the crystal. The process of absorption and nucleation continues until all four dislocations initially present have caused the nucleation of four dislocations. Note that the total number of absorbed dislocations in the contact n_{abs} does not grow beyond two.

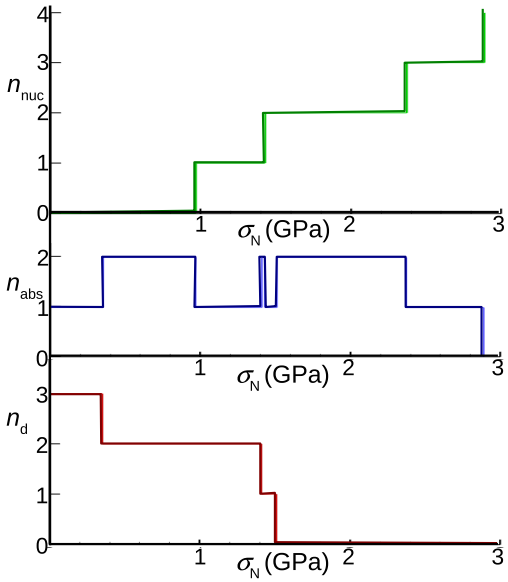

Figure 5.20: Number of dislocations in the pile-up n_{d}, the number of nucleated dislocations n_{nuc}, and the number of absorbed dislocations n_{abs} as a function of normal stress for bi-crystal A.

As mentioned earlier, the dislocations in the initial pile-up are all on the same slip plane. However, the four nucleated dislocations are all found to be on different slip planes, spanning in total a distance of seven slip planes. The reason for this is found in the way in which dislocations are absorbed in the contact. For the absorption of two consecutive dislocations, the atoms in the contact rearrange to accommodate the dislocations, causing the total Burgers vector of the two dislocations to spread out in the contact. Therefore, nucleation back into the lower crystal is very likely to occur at different slip planes. This process of absorption and re-nucleation results in local roughening of the contact (see Fig. 5.21). This

causes the last nucleation event in Fig. 5.20 to occur at a larger stress, about 0.6 GPa larger, than would be expected based on single dislocation impingement (see Fig. 5.16).

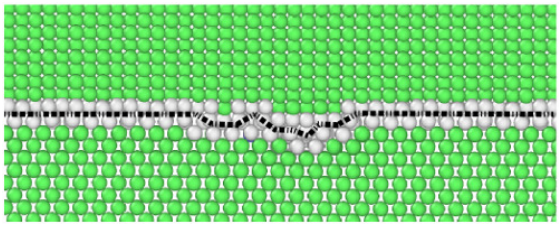

Figure 5.21: Local contact structure of bi-crystal A after nucleation of four dislocations following the impingement of four dislocations. The initial roughness is $R = 0.26$, the final local roughness, calculated in a 5 nm window, is $R_{\mathrm{loc}} = 0.35$.

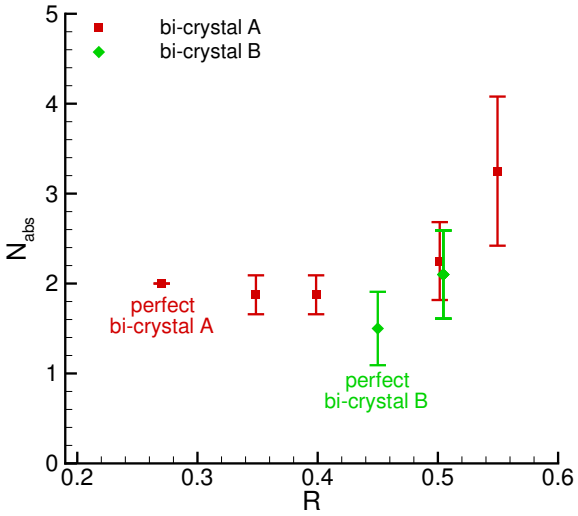

Figure 5.22: Number of dislocations that can be absorbed by a contact as a function of roughness when four dislocations impinge.

Figure 5.22 shows the number of absorbed dislocations N_{abs} that the contact can accommodate as a function of R. It appears that for $R < 0.5$ no more than two dislocations can be absorbed in the contact. For $R > 0.5$ the number of dislocations that can be absorbed is found to increase. Although the roughness also gives rise to stress concentrations, a larger roughness also entails more freedom for local atomic rearrangement and hence more dislocations can be absorbed at increased R.

5.7. DISCUSSION

In this work it has been shown for the first time that the atomic scale roughness of the contact interface plays a key role in the impingement behavior of single and multiple dislocations. The atomic scale roughness is critical in predicting the nucleation stress, while for instance GB energy does not seem to hold predictive power, similar to what is reported in Ref. [14]. The varying local roughness results in a variation in nucleation stress and absorption stress, similar to the results in [9] where it is concluded that the local structure determines the nature of the interaction between dislocation and GB.

In this atomic-scale work, the nucleation stress is measured globally. However, in micron-scale models this stress can be interpreted as a local stress, since the length scale in these models is orders of magnitude larger. Therefore, the results of this work can be incorporated in larger scale dislocation dynamics models in which stress relaxation in the material occurs by the collective behavior of dislocations (nucleation, annihilation, glide, (de-)pinning), as [16–18], to more accurately describe dislocation impingement at contacts. At present such models do not incorporate absorption of dislocations and nucleation from contacts. Interfaces are generally treated as impenetrable barriers for dislocations, on which dislocation pile-ups grow unbounded. The fact that pile-ups can have a significant effect on the plastic response is for instance shown in Ref. [17], where pile-ups on single asperity contacts result in a hardened response. The present work shows at which local normal stress state, the pile-up will no longer grow, because the dislocations are absorbed at the impingement site and/or re-nucleated from the it, controlled by the atomic contact roughness. The nucleation stresses for pile-ups beyond four dislocations on Al nano-scale contacts found in this study range from 0.9 GPa to 2.1 GPa depending on the roughness. Such rather large stresses are not likely to be reached at the contact when a material at the micron-scale deforms plastically under contact loading. For this reason we do not expect that the results of micron-scale dislocation dynamics simulations of contact will be significantly affected by modifying the constitutive laws in the light of the results of this work.

5.8. CONCLUSIONS

Molecular dynamics simulations have been performed to study the impingement behavior of edge dislocations on aluminum contacts.

- Atomic scale contact roughness, as described by the simple, novel definition proposed in this work, is found to control dislocation absorption and re-nucleation from the impingement site, since the contact roughness is a measure of the freedom for atomic rearrangement during impingement.

On the other hand no universal correlation is found between contact energy and the nucleation stress.

- The normal stress at which re-nucleation occurs increases with increasing atomic scale roughness until a certain threshold, $R \approx 0.5$. Above this threshold, the effect of a single absorbed dislocation on roughness is insignificant. Therefore, above this threshold the nucleation stress is unaffected by impinging dislocations.
- When multiple dislocations impinge on the same site, the nucleation stress decreases with the number of dislocations. However, when the number of impinging dislocations is larger than 3, the normal nucleation stress becomes constant. This is because the dislocations at the tail of the pile-up contribute less to the stress field in the area surrounding the impingement site.
- The repeated process of absorption and re-nucleation of multiple dislocations leads to local contact roughening.
- Impingement of a single dislocation on a rough contact can result in the nucleation of a twin, given the large stress concentration at points close to the impingement site. When multiple dislocations impinge, twins are no longer observed, since in these cases the stress concentration is much stronger at the impingement site itself than in the rest of the contact.
- The contact pressure at which nucleation occurs is rather large, in the order of 1 GPa. Only when this large pressure is exceeded, dislocations from a pile-up are expected to be absorbed and re-nucleated, decreasing the pile-up length. Therefore, for moderate applied loading it is expected that long dislocation pile-ups can form.

An important implication of this study is that the large pile-ups that are found in micron-scale contact models are indeed realistic features of the plastic contact response. This conclusion is strengthened by our observation that the repeated process of dislocation absorption and re-nucleation locally roughens the contact, thereby increasing locally the nucleation stress.

REFERENCES

[1] R. J. Dikken, B. J. Thijsse, and L. Nicola, *Impingement of edge dislocations on atomically rough contacts,* Comput. Mater. Sci. **128**, 310 (2017).

[2] T. C. Lee, I. M. Robertson, and H. K. Birnbaum, *Prediction of slip transfer mechanisms across grain boundaries,* Scr. Metall. **23**, 799 (1989).

[3] T. C. Lee, I. M. Robertson, and H. K. Birnbaum, *Tem in situ deformation study of the interaction of lattice dislocations with grain boundaries in metals,* Phil. Mag. A **62**, 131 (1990).

[4] T. C. Lee, I. M. Robertson, and H. K. Birnbaum, *An in situ transmission electron microscope deformation study of the slip transfer mechanisms in metals,* Metall. Trans. A **21A**, 2437 (1990).

[5] Z. Shen, R. H. Wagoner, and W. A. T. Clark, *Dislocation and grain boundary interactions in metals,* Acta metall. **36**, 3231 (1987).

[6] M. Dewald and W. A. Curtin, *Multiscale modelling of dislocation/grain-boundary interactions: I. edge dislocations impinging on σ11 (1 1 3) tilt boundary in al,* Modelling Simul. Mater. Sci. Eng. **15**, S193 (2007).

[7] M. Dewald and W. A. Curtin, *Multiscale modelling of dislocation/grain boundary interactions. ii. screw dislocations impinging on tilt boundaries in al,* Phil Mag **87(30)**, 4615 (2007).

[8] M. Dewald and W. A. Curtin, *Multiscale modeling of dislocation/grain-boundary interactions: Iii. 60^o dislocations impinging on σ3, σ9 and σ11 tilt boundaries in al,* Modelling Simul. Mater. Sci. Eng. **19**, 055002 (2011).

[9] M. de Koning, R. J. Kurtz, V. V. Bulatov, C. H. Henager, R. G. Hoagland, W. Cai, and M. Nomura, *Modeling of dislocation–grain boundary interactions in fcc metals,* J. Nucl. Mater. **323**, 281 (2003).

[10] M. de Koning, R. Miller, V. V. Bulatov, and F. F. Abrahams, *Modelling grain-boundary resistance in intergranular dislocation slip transmission,* Phil. Mag. A **82**, 2511 (2003).

[11] T. Shimokawa, T. Kinari, and S. Shintaku, *Interaction mechanism between edge dislocations and asymmetrical tilt grain boundaries investigated via quasicontinuum simulations,* Phys. Rev. B **75**, 144108 (2007).

[12] T. Shimokawa, *Asymmetric ability of grain boundaries to generate dislocations under tensile or compressive loadings,* Phys. Rev. B **82**, 174122 (2010).

[13] H. Van Swygenhoven, P. M. Derlet, and A. Hasnaoui, *Atomic mechanism for dislocation emission from nanosized grain boundaries,* Phys. Rev. B **66**, 024101 (2002).

[14] D. H. Warner, F. Sansoz, and J. F. Molinari, *Atomistic based continuum investigation of plastic deformation in nanocrystalline copper,* Int. J. Plasticity **22**, 754 (2006).

[15] F. Besenbacher, *Scanning tunnelling microscopy studies of metal surfaces,* Rep. Prog. Phys. **59**, 1737 (1996).

[16] R. J. Dikken, E. Van der Giessen, and L. Nicola, *Plastic shear response of a single asperity: a discrete dislocation plasticity analysis,* Phil. Mag. **95(34)**, 3845 (2015).

[17] H. Song, R. J. Dikken, L. Nicola, and E. Van der Giessen, *Plastic ploughing of a sinusoidal asperity on a rough surface,* J. Appl. Mech. **82(7)**, 071006 (2015).

[18] K. Ng Wei Siang and L. Nicola, *Discrete dislocation plasticity analysis of contact between deformable bodies of simple geometry,* Modelling Simul. Mater. Sci. Eng. **24**, 045008 (2016).

[19] T. Tsuru, Y. Shibutani, and Y. Kaji, *Fundamental interaction process between pure edge dislocation and energetically stablegrain boundary,* Phys. Rev. B **79**, 012104 (2009).

[20] W. A. Soer and J. T. M. De Hosson, *Detection of grain-boundary resistance to slip transfer using nanoindentation,* Mater. Lett. **59**, 3192 (2005).

[21] S. Sun, B. L. Adams, and W. E. King, *Observations of lattice curvature near the interface of a deformed aluminium bicrystal,* Phil. Mag. **80**, 9 (2000).

[22] S. J. Plimpton, *Fast parallel algorithms for short-range molecular dynamics,* J. Comp. Phys. **117**, 1 (1995).

[23] G. P. Purja Pun and Y. Mishin, *Development of an interatomic potential for the ni-al system,* Phil. Mag. **89**, 3245 (2009).

[24] Y. Mishin, D. Farkas, M. J. Mehl, and D. A. Papaconstantopoulos, *Interatomic potentials for monoatomic metals from experimental data and ab initio calculations,* Phys. Rev. B **59**, 3393 (1999).

[25] Y. Mishin, *Atomistic modeling of the γ and γ'-phases of the ni–al system,* Acta Mater. **52**, 1451 (2004).

[26] D. Hull and D. J. Bacon, *Introduction to Dislocations*, 4th ed. (Butterworth-Heineman, Oxford, 2001).

[27] B. A. Szajewski and W. A. Curtin, *Analysis of spurious image forces in atomistic simulations of dislocations,* Modelling Simul. Mater. Sci. Eng. **23**, 025008 (2015).

[28] A. Stukowski, *Structure identification methods for atomistic simulations of crystalline materials,* Modelling Simul. Mater. Sci. Eng. **20**, 045021 (2012).

[29] Y. Mo, K. T. Turner, and I. Szlufarska, *Friction laws at the nanoscale,* Nature **457**, 1116 (2009).

[30] J. Schiotz, F. D. Di Tolla, and K. W. Jacobsen, *Softening of nanocrystalline metals at very small grain sizes,* Nature **391**, 561 (1998).

[31] J. Schiotz, T. Vegge, F. D. Di Tolla, and K. W. Jacobsen, *Atomic-scale simulations of the mechanical deformation of nanocrystalline metals,* Phys. Rev. B **60(17)**, 11971 (1999).

[32] G. Sin'ko and N. A. Smirnov, *Ab initio calculations of the equation of state and elastic constants of aluminum in the region of negative pressures,* JETP Lett. **75**, 184 (2002).

[33] L. Proville, D. Rodney, and M. C. Marinica, *Quantum effect on thermally activated glide of dislocations,* Nature Materials **11**, 845 (2012).

[34] A. Cao and E. Ma, *Sample shape and temperature strongly influence the yield strength of metallic nanopillars,* Acta Mater. **56(17)**, 4816 (2008).

[35] V. Yamakov, D. Wolf, S. R. Phillpot, A. K. Mukherjee, and H. Gleiter, *Dislocation processes in the deformation of nanocrystalline aluminium by molecular-dynamics simulation,* Nature Materials **1**, 45 (2002).

6

FRICTION OF ATOMICALLY STEPPED SURFACES

Self-organized criticality is a new way of viewing nature... perpetually out-of-balance, but organized in a poised state.

Per Bak

Parts of this chapter have been published in Ref. [1]

6.1. INTRODUCTION

Friction of rough surfaces is the outcome of multiple asperities of different size being flattened and sheared. However, even contacts at the nano-scale can exhibit roughness in the form of atomic scale steps. Such steps are essentially the smallest scale of roughness and can originate for example from crystal growth [2, 3] or the escape of dislocations through surfaces [4–6] and are known to affect friction [7]. Several experimental studies [8–10] have revealed that the friction stress of a tip dragged along a stepped surface is larger compared to the friction stress of a tip dragged on an atomically flat surface. The reason for this increase has been attributed to the surface potential landscape [8, 10] associated to stepped surfaces, where an additional barrier to motion, the Ehrlich-Schwoebel barrier [11, 12], has to be overcome in the direction perpendicular to the step. Consistently with these findings, interface imperfections, of the type of steps and ledges, have been found to increase the shear strength of various interfaces, as those of metallic multi-layers [13]. Furthermore, it has been hypothesized that static friction increases due to defects like vacancies and impurities at the interface that allow surfaces to sink into their pinning potentials despite the elastic energy that this costs [14].

The aim of this study is to understand the role of atomic scale steps on the frictional behavior of metal contacts. The size of the steps considered here is in the order of the dislocation Burgers vector (up to $7b$). We are interested in understanding whether these steps will maintain their size during contact sliding, or evolve towards a flatter surface, and through which atomic processes this would occur. Another question we intend to answer is whether the stress concentration associated with the step is sufficient to nucleate dislocations under moderate contact loading, and how dislocation nucleation would contribute to frictional sliding. Molecular dynamics simulations of the deformation of poly-crystalline metals has shown a competition between stress relaxation by dislocation glide and by grain boundary slip [15]. Since in a molecular dynamics simulation grain boundaries and dry nano-contacts do not differ much, we are interested in verifying whether a similar competition between dislocation nucleation and slip can be found also for the stepped contacts. If dislocations would play a role during frictional sliding of stepped contacts, their behavior would be markedly different than that of flat contacts.

Whether or not the frictional behavior of flat and stepped contacts is intrinsically different might have implications also in relation to the self-organized criticality of friction. In the past three decades, the concept of self-organized criticality has been introduced to explain physical processes involving dissipation [16, 17]. In one of the first works on self-organized criticality (SOC), it has been hypothesized that this concept is underlying for spatial and temporal scaling in dis-

sipative non-equilibrium systems [17]. This is certainly interesting in the context of friction, where the length scales involved differ by orders of magnitude. Several experimental and theoretical studies have confirmed the existence of SOC in sliding friction [18–21].

In this work it is found that both flat and stepped surfaces present self-organized criticality. However, the atomic mechanisms that come into play are very different for stepped and flat contacts. Stress relaxation of flat contacts occurs purely by contact slip, while for stepped contacts the steps can move along the contact plane but also normally to the plane. Despite the mechanisms are different the power law statistics are affected rather minorly.

The chapter is organized as follows: in Section 6.2 the computational approach and problem formulation are presented. In Section 6.3 the friction behavior of single step surfaces in contact is analyzed. In Section 6.4.1 this is continued for step pair surfaces in contact. Section 6.4.2 is devoted to the study of step pair surfaces of larger height, i.e. nano-scale asperities. Finally, the conclusions are presented in Section 6.5.

6.2. COMPUTATIONAL APPROACH AND PROBLEM FORMULATION

The molecular dynamics (MD) simulations are performed using LAMMPS [22] with an EAM potential [23] developed by Purja Pun and Mishin [24–26]. This potential has shown to give accurate surface and stacking fault energies, making it especially suitable for studying the mechanical behavior of contacts and interfaces.

In this work we focus on fcc metals. Aluminum has a large stacking fault energy, which entails that the separation of the two partials, by which a dislocation exists in an fcc metal, is small. This limits the necessary dimensions of the simulation box, and hence the simulation time. Some of the simulations were repeated with nickel and we could indeed verify that the results obtained in this study are qualitatively similar for different fcc metals. It is therefore expected that the qualitative results in general apply to ultra-clean, oxide-free fcc metal surfaces. Although we are aware that aluminum has a high oxidation rate, and that such ultra-clean, oxide-free metal surfaces are less realistic, this is convenient for the aim of this study, which is to fundamentally understand the effect of steps on friction.

The contact is formed between two crystals with the same height (in the z-direction, perpendicular to the contact plane) $h/2 = 45$ nm, so that the total height is $h = 90$ nm. The width w in the periodic x-direction is varied between 15 and 45 nm. The periodic y-direction is taken short, $d = 2$ nm, so that the steps are straight line-defects in the contact (see Fig. 6.1). The two crystal orientations that are chosen both have symmetric slip systems for which the (dislocation) slip line

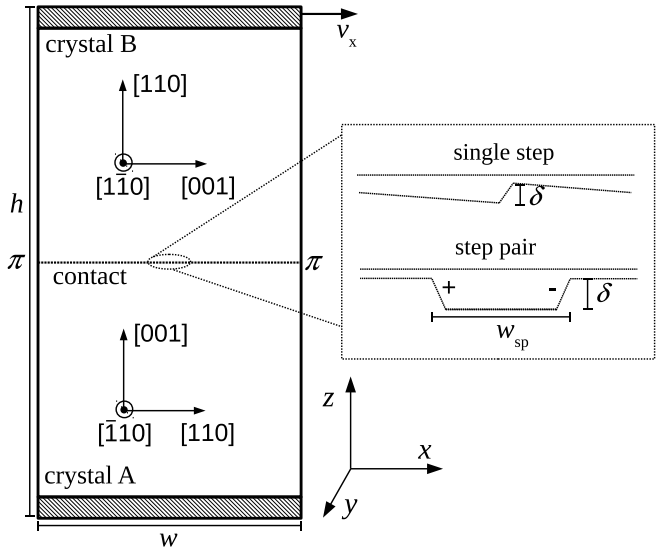

Figure 6.1: Schematic representation of the model. The step height δ varies and relates to the lattice constant a, i.e. the Burgers vector $b = a/\sqrt{2}$.

lies along the short y-axis and are shown in Fig. 6.1.

Both periodic steps and step pairs (see Fig. 6.1) are studied. Periodic steps are created by applying vertical displacements to atoms in the lower crystal, such that at the periodic boundary the applied vertical displacement is zero and in the middle of the simulation cell it is δ (see Fig. 6.1). The periodic boundary conditions in the x-direction effectively let us investigate a periodic array of steps. We here assume that the steps can emerge due to the absorption of impinging dislocations from the crystal. In Ref. [4] it is found that maximum two dislocations can be absorbed at the same impingement site. Therefore the height of the step δ (in the z-direction) is taken to be $a/2$ or a, which represents 1 or 2 escaped dislocations, respectively.

The step pairs are created by removing atomic planes parallel to the crystal surfaces (see Fig. 6.1). This creates two steps of opposite sign.

The distance between the two crystals is initially a. The contact forms during a relaxation run. Depending on the step height, a closed contact or a contact with a gap (free surfaces) forms. In this work a vertical atomic separation smaller than one lattice parameter a is defined as a 'closed' contact, otherwise as a gap.

After the system is relaxed, 10 atomic planes at the top of the upper crystal are displaced in the x-direction over a distance of 40 nm with a constant velocity $v_T = 2$ m/s, while keeping 10 atomic planes at the bottom of the lower crystal fixed in the x-direction. This gives an applied strain rate of approximately $2 \cdot 10^7$ s^{-1}. In

this work, we focus on understanding the effect of different step geometries. No normal load is applied, and the contact interaction between the surfaces is purely by atomic interactions. To this end atoms are unconstrained in the z-direction, unless otherwise specified.

For a single step, the problem is not symmetric, and both loading directions are studied, indicated by step-up and step-down as shown in Fig. 6.2. For a step pair, the geometry is symmetric, therefore only loading in the positive x-direction is studied.

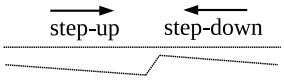

Figure 6.2: Schematic representation of the two loading directions for periodic (single) step contacts.

An NPT ensemble is applied to mimic the material response at the nano-scale. Heat conduction in a metal is in reality dominated by free electrons. However, classical MD simulation can not account for this. To compensate for the much too low heat conduction, the system is thermalized to the desired temperature [27], 300 K, using a Nosé-Hoover thermostat.

6.3. CONTACTS WITH PERIODIC STEPS

6.3.1. SELF-ORGANIZED CRITICALITY OF ATOMIC SCALE FRICTION

We study the effect of a periodic array of single steps of small height, $\delta_0 = a/2$ and $\delta_0 = a$, on the friction behavior of a contact for both loading directions and compare the results with an atomically flat contact. The small step height results always in a closed contact. Figure 6.3 shows the σ_{xz} shear stress for step height $\delta_0 = a = 0.405$ nm. The stress concentration at the step arises due to closure of the contact. In order to eliminate the effect of thermal fluctuations, the system has been cooled to 1K to visualize the stress.

The applied displacement first results in elastic shearing ($u_x < 2$ nm), as seen in Fig. 6.4, where results for various step spacings are shown, together with the response of a flat contact. The shear stress is defined as $\tau = F_x/(wd)$, where the total force F_x measured at the top of the upper crystal in the x-direction is divided by the constant area wd. Contacts with different step density have the same elastic shearing response. At about $u_x = 2$ nm ($\gamma \approx 0.022$) sliding sets in resulting in a fluctuating friction stress ranging from about 400 MPa to 900 MPa. In this work 'sliding' indicates the total displacement of one crystal with respect to the other, while 'slip' indicates each discrete displacement jump occurring after a sticking period, as shown in Fig. 6.4. Decreasing the step spacing results in

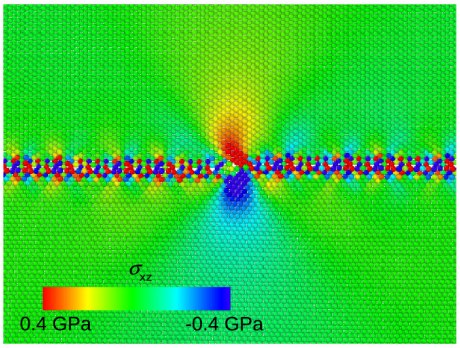

Figure 6.3: Shear stress σ_{xz} in the vicinity of a single step (height $\delta = 0.405$ nm).

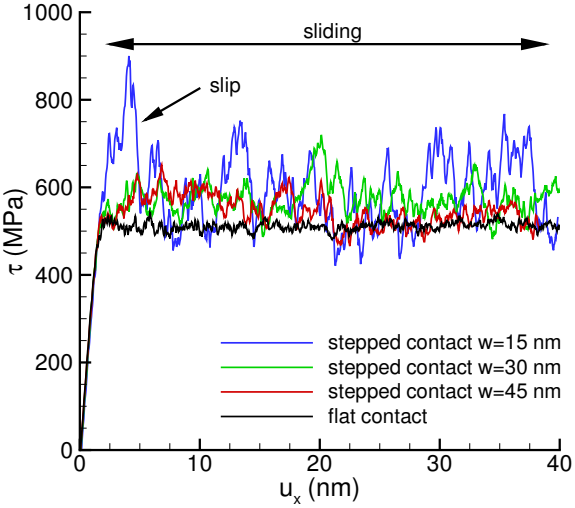

Figure 6.4: Shear stress τ as a function of applied displacement u_x for different step spacing and for a flat contact, with the definition of sliding and slip depicted.

increased fluctuations in the friction stress, while the average friction stress increases only moderately. Every simulation is repeated four times with different initial atomic velocities (different realizations), to find the average behavior. The average friction stress τ_{fr} and the root mean square fluctuation are determined from the shear stress curves of the different realizations during sliding and shown in Fig. 6.5, for both loading directions. The average friction stress τ_{fr} of stepped contacts is slightly higher than for a flat contact. More pronounced are the differences in terms of rms fluctuations of the friction stress. The difference is more pronounced for smaller step spacing, i.e. for rougher surfaces; while there are no visible differences in the loading direction.

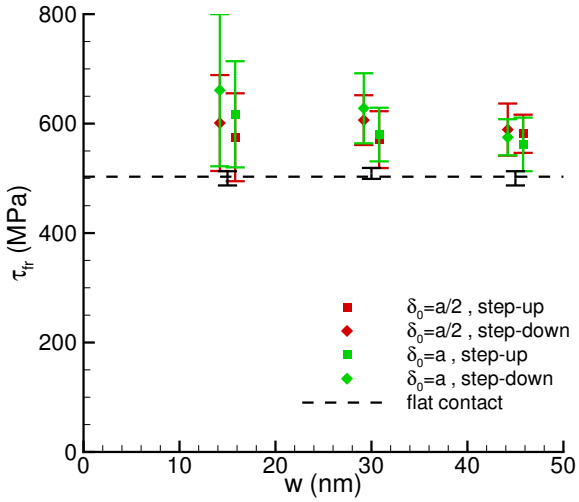

Figure 6.5: Average and rms variation of friction stress τ_{fr} during sliding as a function of step spacing w for both sliding directions. For clarity the data points have been shifted by 0.8 nm.

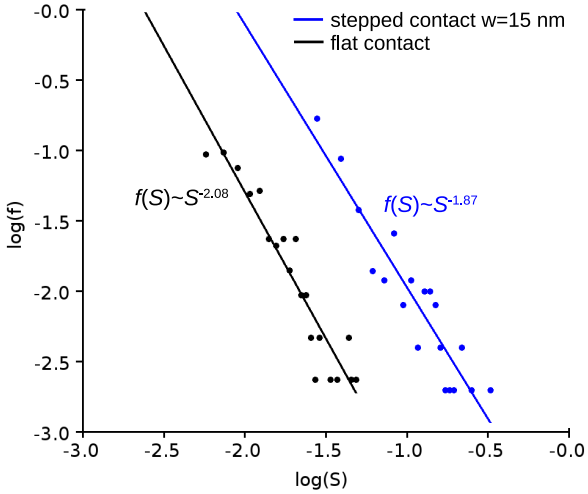

Figure 6.6: Distribution $f(S)$ of the stress drops $S = \Delta\tau_{\mathrm{d}}/\bar{\tau}$, where $\Delta\tau_{\mathrm{d}}$ is the size of the stress drop and $\bar{\tau}$ is the average friction stress during sliding. The two limiting cases of Fig. 6.4 are shown, the stepped contact with spacing $w = 15$ nm and a flat contact. The intermediate cases $w = 30$ nm and $w = 45$ nm are between the two limits.

The most important features of self-organized criticality are [28, 29]: 1) an abundance of meta-stable states, 2) the energy continuously put into the system is partly released in recognizable relaxation events, 3) the system is slowly driven

away from the ground state so that the average waiting time between events and the event duration time are clearly separated, 4) the size of the relaxation events follows a power law distribution, 5) all statistical properties should be stationary in the large-time limit, indicating that the attractor of the self-organized state is found. The subject of this work also includes these features: 1) the contact involves a large ensemble of atoms that during sliding are in meta-stable states, 2) the energy put into the system during 'stick' is released in recognizable relaxation events during 'slip', i.e. there are stress drops in the friction stress, 3) in Fig. 6.4 it is clearly seen that the event duration time (slip) is much faster than the waiting time between events and hence the system is driven slowly, 4) the size of the stress drops S is given by power-law statistics $f(S) \propto S^{\beta}$ as shown in Fig. 8.1, 5) sliding occurs in the attractor state, which means that the stress drop statistics do not change over time. The attractor associated with the self-organized critical state depends on the step density. Therefore, also the stress drop statistics are different for stepped or flat surfaces in contact (Fig. 8.1). For flat contacts, stress drops of smaller magnitude occur more often than for stepped contacts. For stepped contacts, stress drops with larger magnitude are more frequent. Hence, the power-law exponent for a stepped contact is $\beta_{\text{stepped}} = -1.87$ larger than for a flat contact $\beta_{\text{stepped}} = -2.08$, i.e. the stress that can build up and is released is larger for smaller step spacing (larger step density). The atomistic mechanisms that govern the stress drop-statistics for stepped contacts are various: not only local slip across the step, but also step motion and contact migration, as will be discussed in the following section.

6.3.2. NORMAL CONTACT MIGRATION

A closer look at the sliding process of the stepped contacts reveals that additional to slip at the contact, another mechanisms occurs: motion of the step along the contact resulting in normal migration of the entire contact. Migration of the contact is a stress relaxation mechanism that competes with contact slip. The direction of migration depends on the loading direction as shown in Fig. 6.7. The contact migration is a consequence of the motion of the step similar to the mechanism for grain boundary migration discussed in Refs. [30–32]. In Refs. [30, 31] it is explained how local atomic rearrangement leads to step motion from which the migration results. In Ref. [32] it is found that grain boundaries that are intrinsically immobile become mobile through additional line-defects like steps. The phenomenon is analogous to re-crystallization (see Fig. 6.7). A unit displacement of the step in the horizontal direction induces a unit displacement in the vertical direction. Inverting the loading direction inverts the stress state and hence results in step motion and contact migration in the opposite direction.

Figure 6.8 shows the absolute normal migration distance $|u_{\text{n}}|$ per unit applied

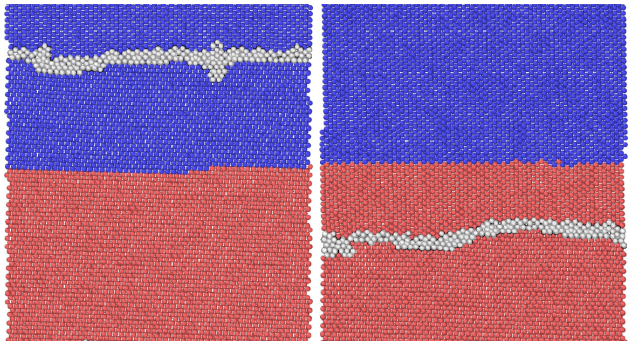

(a) (b)

Figure 6.7: Contact migration at u_x = 40 nm for a) the step-up loading direction and b) the step-down loading direction. Atoms that originally belong to crystal A (B) are indicated with the color red (blue). The grey atoms indicate the new position of the contact, based on CNA.

displacement as a function of step spacing. As to be expected with increasing step density, the normal migration increases. Figure 6.8 shows that for $\delta_0 = a/2$

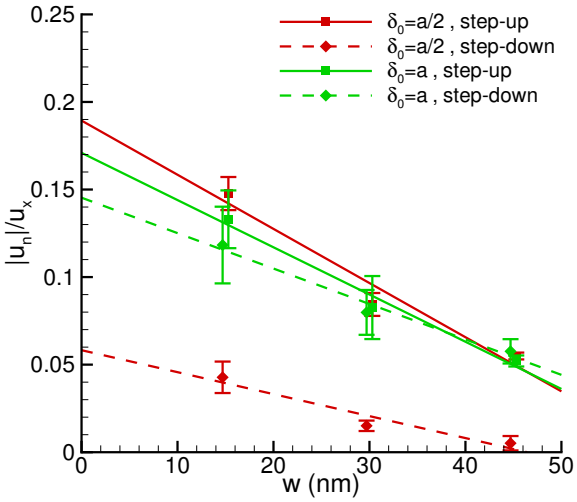

Figure 6.8: Normal migration distance $|u_n|$ per unit applied displacement as a function of step spacing (i.e. box width). For clarity the data points have been shifted ±0.3 nm for the positive and negative x-direction, respectively. The error bars denote the rms variation in the normal migration.

in the step-down direction, the migration distance is significantly lower than in the other cases, and thus contact slip prevails over contact migration since during sliding the total sliding displacement equals the applied displacement. The cause for the prevailing local slip across the step in the step-down loading direc-

tion is due to the asymmetry of the Ehrlich-Schwoebel barrier [11, 12] as shown in Fig. 6.9. For slipping across the step in the step-up direction, atoms have to come out of a low energy well and be pushed over a high energy barrier. For slipping across the step in the step-down direction, atoms have to cross a lower energy barrier towards lower energy level and hence slipping across the step is facilitated. With increasing step height, also the barrier height increases and hence only when the step height is large enough ($\delta_0 = a$), the barrier height becomes so large that slipping across the step is unfavorable so that for both sliding directions step motion is promoted. Interestingly, for steps of height $a_0/2$ slip over the

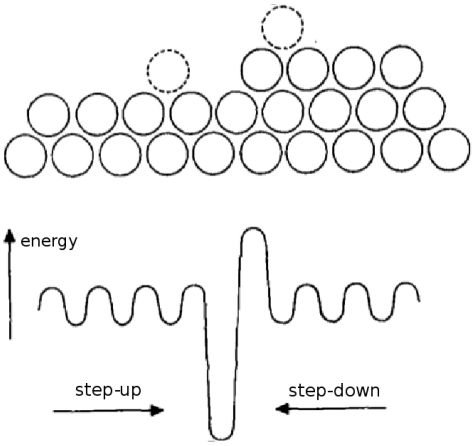

Figure 6.9: Ehrlich-Schwoebel barrier [11, 12] showing the asymmetry of the potential landscape near the step.

step and step motion involve energy barriers that have similar height, so that the friction stress is independent of loading direction (see Fig. 6.5), although in one direction local slip across the step dominates over step motion and in the other direction step motion dominates over local slip across the step.

Rare migration reversal

In most cases normal migration occurs in one particular direction, related to the loading direction. However, there are cases where the direction of migration is reversed, as can be seen in Fig. 6.10 where the average z-coordinate of the contact is presented. Reversal occurs at about $u_x = 10$ nm. This is caused by the nucleation of dislocations, which cause a change in the sign of the step. In an FCC metal it is often energetically favorable for a dislocation to split into two partial dislocations separated by a stacking fault, and this is also the case for Al. The atoms in the stacking fault ribbon have a local HCP structure, so that the number of atoms with HCP structure is a measure of the number of dislocations in the ma-

terial. In Fig. 6.10 it is shown that initially there are no atoms with HCP structure in the system (based on a Common Neighbor Analysis, CNA [33], excluding the contact), i.e. there are no dislocations. Only at an applied displacement of about 10 nm, significantly beyond the onset of sliding as seen in Fig. 6.4, dislocation nucleation occurs. The number of HCP atoms, on average approximately 65, and the separation of the partials, indicates that two dislocations (four partial dislocations) are nucleated. It is the nucleation of these two dislocations that changes the sign of the step in the contact and causes the reversal of the migration direction. Migration reversal by dislocation nucleation is a rare event in simulations

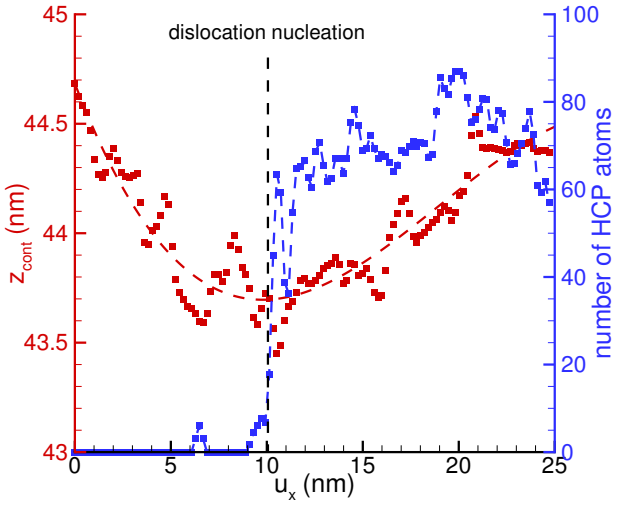

Figure 6.10: Average z-coordinate of the contact (red) and the number of atoms with HCP structure (blue) as a function of applied displacement.

with a negligible normal loading, as it was only found in 1 out of 24 cases studied.

6.3.3. VACANCY GENERATION

A contact, flat or stepped, between two crystals with different orientation entails a certain excess free volume compared with the perfect crystal, so that the contact can be thought of as a potential reservoir of vacancies. It has been reported that curvature driven grain boundary migration can result in the generation of vacancies to accommodate the excess free volume [34] associated with the decrease in the grain boundary volume. For a flat contact in this study it has been found that upon applied tangential displacement, pure slip at the contact occurs, and the excess free volume at the contact is unchanged. However, as just shown, a stepped contact migrates in the normal direction, which is similar to a re-crystallization process. It is found that this re-crystallization can result in the generation of va-

cancies, which are found in the re-crystallized part of the bi-crystal. This is shown in Fig. 6.11, where only atoms that do not have a perfect local FCC structure are represented.

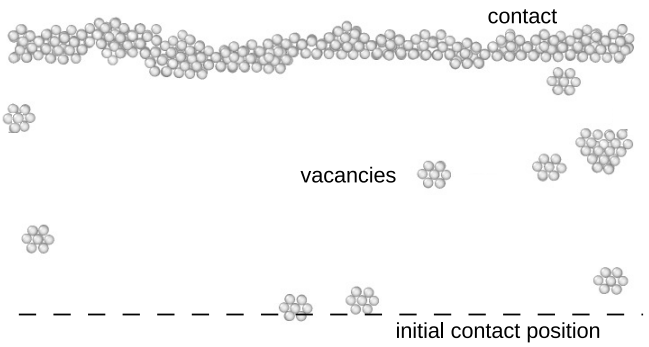

Figure 6.11: Contact after 40 nm applied displacement in the positive x-direction, clearly showing vacancies generated between the initial and the current position of the contact. Only atoms that do not have a perfect local FCC structure are shown.

It is important to realize that this vacancy generation is found to take place at room temperature. The local vacancy concentration near the contact that results from the normal migration is more than two orders of magnitude higher than the equilibrium vacancy concentration at room temperature. We expect that in cases when both plastic deformation and contact migration occur together, dislocation climb might even occur at room temperature. Experimental observations of dislocation climb in Al/Nb multi-layers indicates that dislocation climb can indeed occur at room temperature due to high vacancy concentration in the interfaces [35].

6.4. CONTACTS WITH PERIODIC STEP PAIRS

6.4.1. SMALL STEP HEIGHT

In this section we will study the friction behavior of step pairs and compare it to that of periodic single steps and atomically flat contacts. The step pairs introduce an additional parameter, the width between the opposite steps w_{sp0}. To study the effect of w_{sp0} we choose one specific box width $w = 30$ nm and vary the pair width. For each case four simulations with different initial atomic velocities are performed. Figure 6.12 shows the average friction stress and its rms variation during sliding as a function of the step pair width to spacing ratio, w_{sp0}/w, for three different step heights and for the flat contact. We find that the average friction stress is not significantly affected by the width of the step pair. This might seem surprising at first sight, but the absence of a clear trend is due to the fact that the

steps move independently in a stochastic manner, so that the initial configuration is soon lost during sliding.

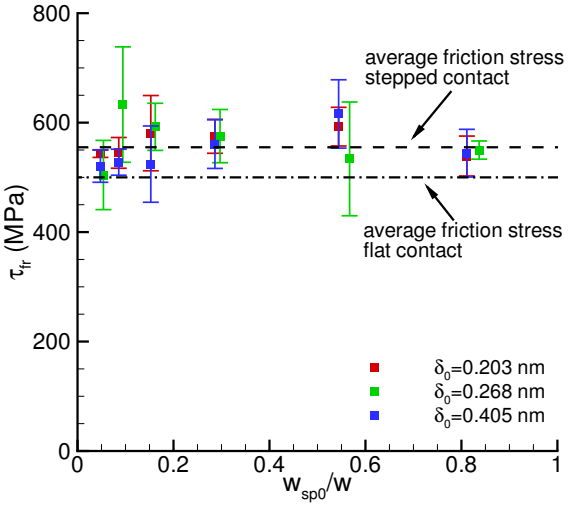

Figure 6.12: Average and rms variation of the friction stress as a function of normalized pair spacing w_{sp0}/w for several step heights. The line for the flat contact is the same as in Fig. 6.4.

In the previous section it was shown that a self-organized critical state is involved in sliding friction and that the fluctuations in the friction stress are larger at smaller step spacing. Interestingly, for the periodic step pair contacts it is found that there exist two sliding states: one being 'jerky' with large stress fluctuations, the second one being 'smooth' with small fluctuations (Fig. 6.13). The smooth sliding state is associated with the attractor: sliding can transit through self-organization from the jerky state into the smooth state. This self-organization is carried by the atomic rearrangement of the contact. Figure 6.13 shows an example for which the transition between jerky sliding and smooth sliding occurs at about $u_x = 20$ nm. Also the fractional change in the number of interface atoms (non-FCC atoms) N_{int}, $(N_{int} - N_{int,0})/N_{int,0}$, as a measure of the interface roughness is shown. It is seen that the decrease in interface roughness coincides with the jerky-smooth sliding transition. From start the steps are separated, and hence the contact has a jagged roughness. The components of the steps are observed to move individually, thereby initially maintaining the jagged roughness (Fig. 6.14a). Although the steps are opposite, they do not annihilate, since there is still an excess volume with respect to a flat contact. In the process of sliding, atomic rearrangement (self-organization) through step motion results in an evolving contact topology, i.e. lower roughness. Eventually the self-organization results in a flatter contact, since the constituents of the step pair organize in a low-energy config-

uration, which results in a 'wave' that travels through the contact during sliding opposite to the loading direction, as shown in Fig. 6.14b.

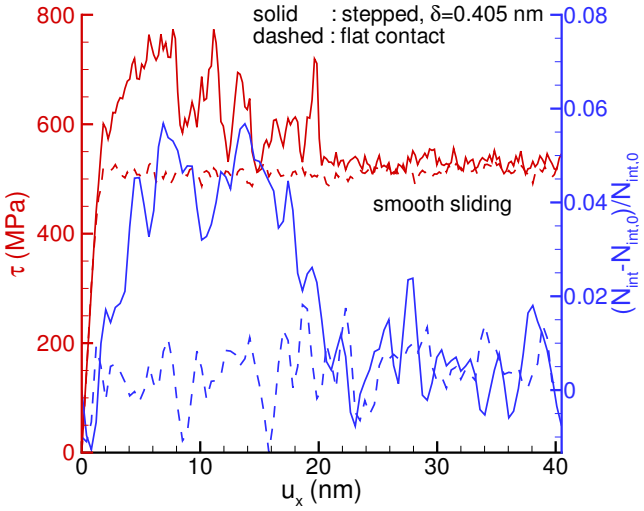

Figure 6.13: Example of shear stress τ (red) and fractional interface roughness $(N_{\text{int}} - N_{\text{int},0})/N_{\text{int},0}$ (blue) as function of applied displacement u_x. A comparison of the two graphs shows that the large fluctuations in the friction stress coincide with the roughened contact.

Recently a combined computational and experimental study of wear of metal surfaces scratched with a tip pointed towards an analogy with laminar and turbulent flow [27, 36]. However, in Refs. [27, 36] laminar plastic flow developed into turbulent plastic flow. The transition found in the present work is from a "turbulent" state into a "laminar" state. Processes at the atomic scale control energy dissipation at the nano- or even micro-scale. Obviously, the stress drop statistics are significantly different in the jerky state compared to the smooth sliding state. The jerky state is similar to sliding friction of a contact with large step density, while the smooth sliding state is similar to sliding of a flat contact.

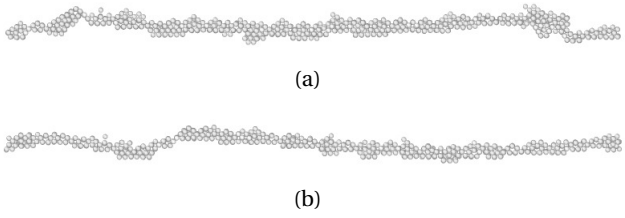

Figure 6.14: The contact structure showing a) jagged roughness in the jerky sliding stage at $u_x \approx 8$ nm, and b) a smooth 'wave' in the contact during the smooth sliding stage at $u_x \approx 30$ nm. Atoms that do not belong to the interface, i.e. that have FCC structure type, are excluded.

The sliding displacement u_{smooth} at which the transition to smooth sliding occurs, defined as the displacement between the onset of sliding and the transition, is shown in Fig. 6.15 as a function of w_{sp0}/w. For the smallest step height the transition is almost immediate once sliding is initiated. For larger step height, significant atomic rearrangement is involved (Fig. 6.14) and the transition is found to take place at greatly varying displacements for different initial conditions (realizations).

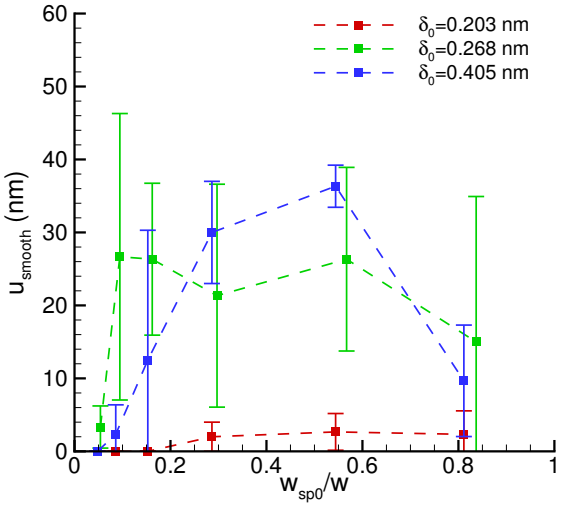

Figure 6.15: Average sliding displacement and rms variation (between different realizations) at which the transition to smooth sliding occurs as a function of the relative pair width.

One final note on the possibility of contact migration of step pair surfaces in contact. Because the steps are initially opposite, there is no net migration, since one of the steps causes migration upwards, while the other causes migration downwards, effectively canceling each other. However, as found in the previous section, dislocation nucleation from the contact can statistically occur. This leads to a net step height in the contact, which undoes the cancellation, and therefore leads to migration of the contact. Since this is found to occur in only about 10 % of the cases, without correlation with pair spacing or step height, we consider it of only minor significance in the friction behavior of stepped surfaces in spite of its fundamental interest.

A note on shearing with a normal load applied

The simulations of the step pair contacts, where repeated after applying a normal load to the contact, to highlight the effect of dislocation nucleation. With the

application of normal load it is indeed expected that dislocation and twin nucleation from the steps becomes relevant. It is found that up to an applied normal load of 3 GPa no dislocation and/or nucleation during normal loading occurs. However, as shearing sets in, the higher the normal load, the more likely the nucleation of dislocations and/or twins becomes. Above a normal load of 1.5 GPa, we always observe dislocation and/or twin nucleation. When dislocation/twin nucleation occurs the transition between jerky and smooth sliding is no longer observed. This is because the nucleation of a dislocation/twin affects the net step height of the contact which from zero becomes b. The presence of a net step height leads to contact migration and smooth sliding is never achieved. Below a normal load of 1.5 GPa the likelihood of observing jerky-smooth sliding transition decreases with increasing normal load.

6.4.2. LARGE STEP HEIGHT: NANO-SCALE ASPERITIES

In this section we will study the friction behavior of contacts with step pairs of large height, $\delta \approx 1.5$ nm. After relaxation the contact does not close, resulting in a gap. The contact can be thought of as being made by a surface consisting of a periodic array of nano-scale asperities of various widths w_{sp0} touching an atomically flat surface. The normalized contact area is then given by:

$$\frac{A_{\mathrm{r}}}{wd} = \frac{w - w_{\mathrm{sp}}}{w}. \tag{6.1}$$

Here A_{r} is the contact area, d is the periodicity in the small y-direction. The contact area is not always constant during shearing, therefore for characterization we will use A_{r0}, w_{sp0} and δ_0 for the initial contact area, step pair width and step height, respectively. Without subscript $_0$, the variables refer to evolving quantities. Figure 6.16 shows an example of the initial contact structure with a clear gap. Two

Figure 6.16: Contact with nano-scale asperities for case AB. Atoms that do not belong to the interface, i.e. that have FCC structure type, are excluded.

cases are studied: case AB, crystal A has a stepped surface and crystal B a flat surface, and case BA, for which the situation is reversed. Figure 6.17 shows the shear stress as a function of applied displacement for different w_{sp0}/w. Larger w_{sp0}/w entails smaller initial contact area leading to larger contact stress and hence an earlier onset of sliding as seen in Fig. 6.17. Figure 6.18 shows the static friction stress τ_{s} (taken at 1 nm offset displacement) as a function of the normalized initial contact area $A_{\mathrm{r0}}/(wd)$ for the two different cases. Both cases show a linear

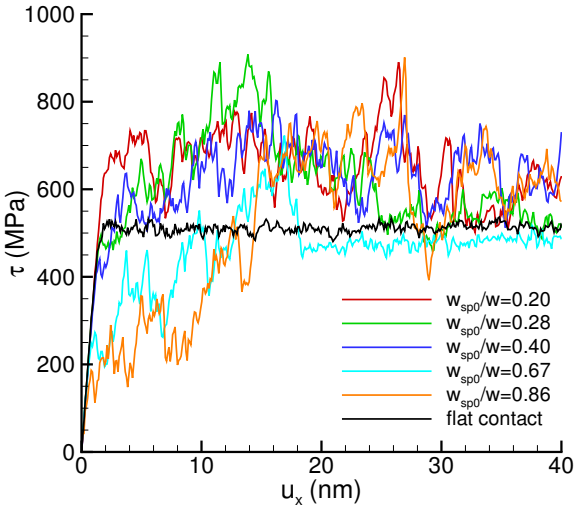

Figure 6.17: Shear stress as a function of applied displacement for different step pair widths (for large step height). One curve (light blue) shows the statistical transition to smooth sliding similar to the transition found for small height step pairs.

relation in τ_s with contact area. Stepped surfaces give clearly a larger static friction stress than a flat contact.

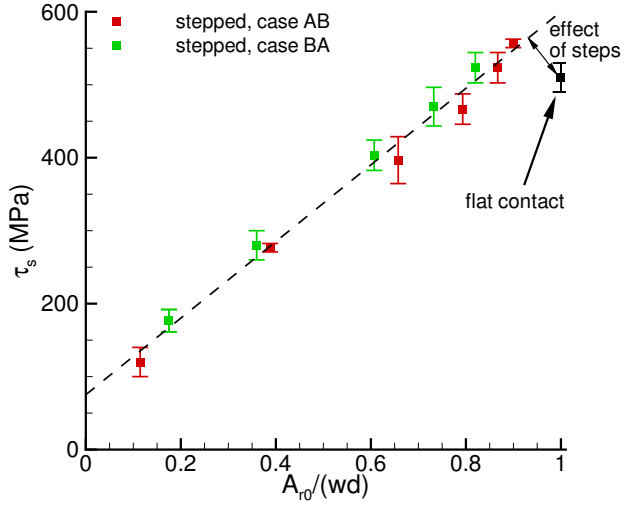

Figure 6.18: Static friction stress as a function of the normalized contact area. Error bars give the rms variation between different realizations.

In Fig. 6.19 it can be seen that during sliding, material is transferred from one

surface to the other. This is similar to the re-crystallization process observed previously for single periodic steps, except for the fact that here the contact topology changes drastically by material transfer, and hence it is appropriate to refer to it as a wear process [37]. The other difference is that the contact does not migrate, unless dislocation nucleation occurs, and therefore the vacancies that are generated are re-absorbed during sliding. Due to atomic wear the contact area increases, i.e. the gap decreases, until full contact is reached. This increase in contact area is the cause for the increase in τ at small shearing displacement in Fig. 6.17.

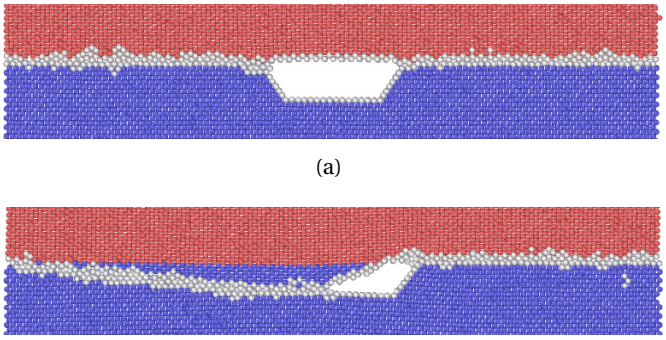

(a)

(b)

Figure 6.19: a) The initial contact (case AB), atoms that originally belong to crystal A(B) are indicated with the color blue(red). The grey atoms indicate the position of the contact, based on CNA. b) Developing wear at $u_x \approx 5$ nm.

Figure 6.20 shows the sliding displacement u_c needed for the gap to completely close. For large step pair width, i.e. small contact area, lesser material of the small asperity is available to be transferred until full contact is reached, and therefore the gap closes at rather low sliding displacement. At small step pair width, i.e. large contact area, only a small amount of material is needed to be transferred from one surface to the other to close the gap, so that also in this case the gap closes at rather low sliding displacement. At intermediate step pair width the sliding displacement to closure is larger. The maximum does not occur at $A_{r0}/(wd) = 0.5$, since the closure is a non-linear process in which the interaction between the free surfaces is involved, leading to sudden gap closure when the distance between the free surfaces becomes small enough. The wear process is especially important when the initial contact area is small, when the largest difference is found between the static friction stress and the sliding friction stress in the large u_x limit.

As the gap closes, the free surface area decreases, together with the potential energy (change in the order of 1 meV/atom). The dissipated energy in this process is in reality absorbed by a large heat bath. Since our simulations consider

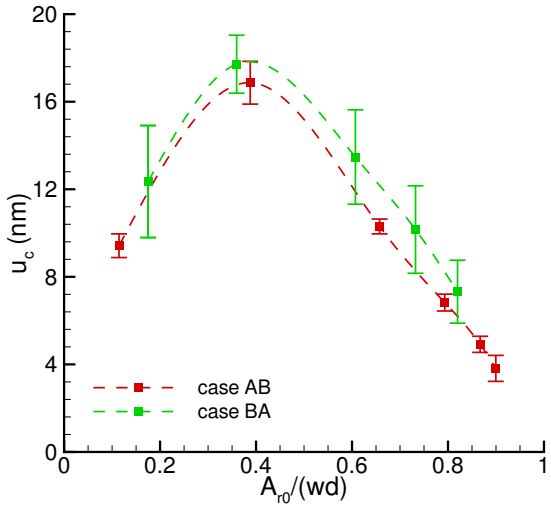

Figure 6.20: Sliding displacement to closure u_c as a function of normalized contact area. This is the difference in applied displacement between the onset of sliding and full closure of the gap. The error bars indicate the rms variation between different realizations.

a rather limited systems size, the thermostat takes care of the absorption of the generated heat. Once the gap is completely closed, the friction stress is statistically independent of w_{sp0}/w, i.e. the behavior becomes like the behavior of step pair contacts with small contact height, as discussed in the previous section.

6.5. CONCLUSIONS

Room-temperature molecular dynamics simulations of contact friction between two differently oriented Al crystals have yielded the following results:

- Sliding friction of stepped surfaces has all the properties of self-organized criticality. The power law slip statistics depend on the step spacing: large slip events are much more probable for contacts with small step spacing than for contacts in the large spacing limit, i.e. atomically flat contacts.

- Apart from slipping, atomic steps can move along the contact and concurrently migrate perpendicular to the contact. Contact migration occurs only when there is a net step height, it is a re-crystallization phenomenon and results in vacancy generation near the contact.

- When the steps are in pairs, there is no net step height and overall migration of the contact does not take place. The stick-slip behavior of these contacts occurs in two clearly distinguishable stages, first jerky with large stick and

slip events, then smooth and similar to a flat surface. The two stages are separated by a marked transition. The friction behavior is statistically independent of step pair width.

- Step pair contacts of large height, where there is a gap between the surface, suffer from wear, which results in a growing contact area, eventually making the friction behavior similar to that of small height step pair contacts.

REFERENCES

[1] R. J. Dikken, B. J. Thijsse, and L. Nicola, *Friction of atomically stepped surfaces,* Phys. Rev. B (2016).

[2] E. Vlieg, A. W. Denier van der Gon, and J. F. van der Veen, *Surface x-ray scattering during crystal growth: Ge on ge(111),* Phys. Rev. Lett. **61(19)**, 2241 (1988).

[3] J. F. Lutsko, A. E. S. Van Driessche, M. A. Durán-Olivencia, D. Maes, and M. Sleutel, *Step crowding effects dampen the stochasticity of crystal growth kinetics,* Phys. Rev. Lett. **116**, 015501 (2016).

[4] R. J. Dikken, B. J. Thijsse, and L. Nicola, *Impingement of edge dislocations on atomically rough contacts,* Comput. Mater. Sci. **128**, 310 (2017).

[5] T. Shimokawa, T. Kinari, and S. Shintaku, *Interaction mechanism between edge dislocations and asymmetrical tilt grain boundaries investigated via quasicontinuum simulations,* Phys. Rev. B **75**, 144108 (2007).

[6] S. H. Oh, M. Legros, D. Kiener, and G. Dehm, *In situ observation of dislocation nucleation and escape in a submicrometre aluminium single crystal,* Nature Materials **8(2)**, 95 (2009).

[7] B. Luan and M. O. Robbins, *The breakdown of continuum models for mechanical contacts,* Nature **435**, 929 (2005).

[8] T. Müller, M. Lohrmann, T. Kässer, O. Marti, J. Mlynek, and G. Krausch, *Frictional force between a sharp asperity and a surface step,* Phys. Rev. Lett. **79**, 5066 (1997).

[9] K. Meine, T. Schneider, D. Spaltmann, and E. Santner, *The influence of roughness on friction - part i: The influence of a single step,* Wear **253**, 725 (2002).

[10] H. Hölscher, D. Ebeling, and U. D. Schwarz, *Friction at atomic-scale surface steps: Experiment and theory,* Phys. Rev. Lett. **101**, 246105 (2008).

[11] G. Ehrlich and E. J. Shipsey, *Step motion on crystal surfaces,* J. Appl. Phys. **37(10)**, 3682 (1966).

[12] R. L. Schwoebel and F. G. Hudda, *Atomic view of surface self-diffusion: Tungsten on tungsten,* J. Chem. Phys. **44(3)**, 1039 (1965).

[13] N. Abdolrahim, I. N. Mastorakos, S. Shao, D. F. Bahr, and H. M. Zbib, *The effect of interfacial imperfections on plastic deformation in nanoscale metallic multilayer composites,* Comput. Mater. Sci. **86**, 118 (2014).

[14] J. B. Sokoloff, *Possible microscopic explanation of the virtually universal occurrence of static friction,* Phys. Rev. B **65**, 115415 (2001).

[15] N. Q. Vo, R. S. Averback, P. Bellon, S. Odunuga, and A. Caro, *Quantitative description of plastic deformation in nanocrystalline cu: Dislocation glide versus grain boundary sliding,* Phys. Rev. B **77**, 134108 (2008).

[16] P. Bak, C. Tang, and K. Wiesenfeld, *Self-organized criticality: An explanation of the 1/f noise,* Phys. Rev. Lett. **59(4)**, 381 (1987).

[17] P. Bak, C. Tang, and K. Wiesenfeld, *Self-organized criticality,* Phys. Rev. A **38(1)**, 364 (1988).

[18] H. J. Feder and J. Feder, *Self-organized criticality in a stick-slip process,* Phys. Rev. Lett. **66(20)**, 2669 (1991).

[19] F. R. Zypman, J. Ferrante, M. Jansen, K. Scanlon, and P. Abel, *Evidence of self-organized criticality in dry sliding friction,* J. Phys.: Condens. Matter **15**, L191 (2003).

[20] S. V. Buldyrev, J. Ferrante, and F. R. Zypman, *Dry friction avalanches: Experiment and theory,* Phys. Rev. E **74**, 066110 (2006).

[21] P. Creeger and F. R. Zypman, *Entropy content during nanometric stick-slip motion,* Entropy **16(6)**, 3062 (2014).

[22] S. J. Plimpton, *Fast parallel algorithms for short-range molecular dynamics,* J. Comp. Phys. **117**, 1 (1995).

[23] M. S. Daw and M. I. Baskes, *Embedded-atom method: Derivation and application to impurities, surfaces, and other defects in metals,* Phys. Rev. B **29**, 6443 (1984).

[24] Y. Mishin, D. Farkas, M. J. Mehl, and D. A. Papaconstantopoulos, *Interatomic potentials for monoatomic metals from experimental data and ab initio calculations,* Phys. Rev. B **59**, 3393 (1999).

[25] Y. Mishin, *Atomistic modeling of the γ and γ'-phases of the ni–al system,* Acta Mater. **52**, 1451 (2004).

[26] G. P. Purja Pun and Y. Mishin, *Development of an interatomic potential for the ni-al system,* Phil. Mag. **89**, 3245 (2009).

[27] N. Beckmann, P. A. Romero, D. Linsler, M. Dienwiebel, U. Stolz, M. Moseler, and P. Gumbsch, *Origins of folding instabilities on polycrystalline metal surfaces,* Phys. Rev. Appl. **2**, 064004 (2014).

[28] B. Persson and E. Tosatti, *Physics of Sliding Friction* (Kluwer Academic Publishers, 1996).

[29] B. Bhushan, *Fundamentals of Tribology and Bridging the Gap Between the Macro - And Micro/Nanoscales* (Springer Netherlands, 2001).

[30] A. Rajabzadeh, F. Mompiou, M. Legros, and N. Combe, *Elementary mechanisms of shear-coupled grain boundary migration,* Phys. Rev. Lett. **110**, 265507 (2013).

[31] N. Combe, F. Mompiou, and M. Legros, *Disconnections kinks and competing modes in shear-coupled grain boundary migration,* Phys. Rev. B **93**, 024109 (2016).

[32] C. P. Race, R. Hadian, J. von Pezold, B. Grabowski, and J. Neugebauer, *Mechanisms and kinetics of the migration of grain boundaries containing extended defects,* Phys. Rev. B **92**, 174115 (2015).

[33] A. Stukowski, *Structure identification methods for atomistic simulations of crystalline materials,* Modelling Simul. Mater. Sci. Eng. **20**, 045021 (2012).

[34] M. Upmanyu, D. J. Srolovitz, L. S. Shvindlerman, and G. Gottstein, *Vacancy generation during grain boundary migration,* Interface Science **6(4)**, 289 (1998).

[35] N. Li, J. Wang, J. Y. Huang, A. Misra, and X. Zhang, *In situ tem observations of room temperature dislocation climb at interfaces in nanolayered al/nb composites,* Scr. Mater. **63**, 363 (2010).

[36] N. K. Sundaram, Y. Guo, and S. Chandrasekar, *Mesoscale folding, instability, and disruption of laminar flow in metal surfaces,* Phys. Rev. Lett. **109**, 106001 (2012).

[37] T. D. B. Jacobs and R. W. Carpick, *Nanoscale wear as a stress-assisted chemical reaction,* Nature Nanotechnology **8**, 108 (2013).

7

UNEXPECTED SENSITIVITIES IN LOW TEMPERATURE MOLECULAR DYNAMICS SIMULATIONS

Perturbations may even make the system more robust, by helping it to discover a more stable organization.

Francis Heylighen

Parts of this chapter are intended to be published in Ref. [1].

7.1. INTRODUCTION

Results of molecular dynamics (MD) simulations can vary between different calculations. Firstly because of thermal noise inherent to physical problems at finite temperature. Secondly, MD simulations involve solving coupled differential equations [2], so that changes in the initial atomic velocities/positions or different implementation of a parallel processing scheme can result in different outcomes. Hence, at finite temperature, simulations have to be repeated with different initial atomic velocities, randomly generated from a Maxwell-Boltzmann distribution, to obtain a reliable average response, especially those simulations in which effects of interest depend strongly on rare events at the atomic level. In contrast, it is often assumed that low temperature MD simulations or molecular statics (MS) simulations, where the temperature is effectively 0 K, are insensitive to different initial atomic velocities, since the spread in atomic velocities is negligible and thermal noise is suppressed. However, in this chapter we shall show that this assumption does not hold for all problems and depends on the topology of the problem. Hence, one has to be very cautious in doing low temperature MD and interpreting the results.

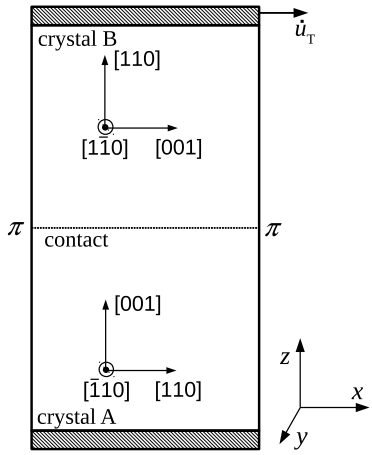

Figure 7.1: Schematic representation of the two crystals in contact with a shear load applied at the top.

As benchmark problem the atomic scale friction of aluminum nano-scale contacts is studied under shear loading using an EAM potential [3] at two temperatures: room temperature, T = 300 K, and near-zero temperature, T = 0.1 K. A schematic representation of the model is shown in Fig. 7.1. The simulation box size is 30 nm x 2 nm x 90 nm. A schematic representation of the different contact topologies, before and after relaxation, is shown in Fig. 7.2. The contact between

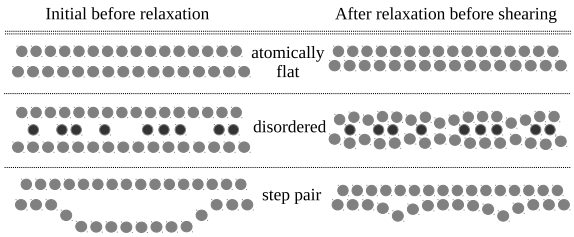

Figure 7.2: Schematic representation of the different contact topologies before and after relaxation. Note that the character of steps is one-dimensional, while the character of adatoms is zero-dimensional.

two crystals is chosen either atomically flat, disordered by randomly placed adsorbed atoms (20 % of one atomic plane) or stepped, i.e. one surface contains a step pair of which the constituents are of opposite sign, so that there is no net step height. The height of the step is only one lattice parameter, so that almost full contact is formed upon relaxation. Only at the location of the steps, stress concentrations arise due to strongly local symmetry breaking, shown in Fig 7.3. Since

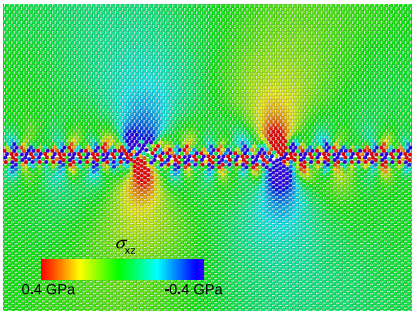

Figure 7.3: Stress concentration near the step pair shown in Fig. 7.2, related to strongly local symmetry breaking in the topology of stepped contacts.

periodic boundary conditions are used, the stepped surface can also be viewed as a surface containing a periodic array of small height asperities. Such surface roughness can emerge due to crystal growth or dislocation escape. Additionally, friction simulations are performed of stepped contacts with additional structural disorder by randomly placed adatoms at the surfaces (20 % of one atomic plane). Sliding friction is established by applying a tangential displacement u_T at constant velocity at the top boundary of the upper crystal, while keeping the bottom boundary of the lower crystal fixed. The whole system is thermalized to the desired temperature using a Nosé-Hoover thermostat, avoiding local heating during sliding. The study in this chapter is an extension of the more elaborate study on

the frictional behavior of stepped surfaces in contact at room temperature presented in Chapter 6.

7.2. RESULTS

The shear stress for stepped, disordered and flat contacts at room temperature, $T = 300$ K, is shown as a function of applied displacement in Fig. 7.4 for different initial atomic velocities and/or different numbers of processors used for parallelization. Parallelization entails that the physical space of the system is parti-

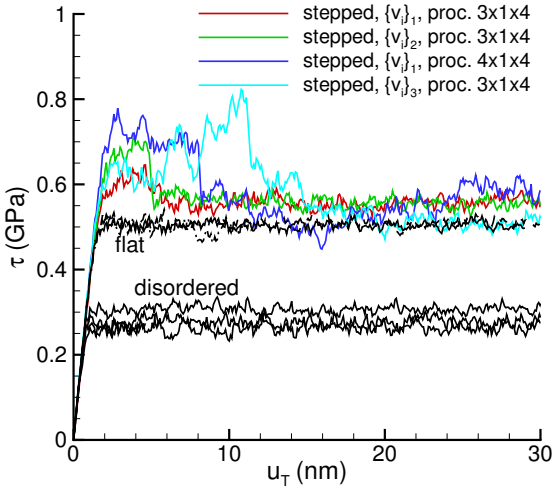

Figure 7.4: Shear stress τ as a function of applied displacement u_T for friction simulations of stepped, flat and disordered contacts at room temperature, $T = 300$ K. Different initial atomic velocities are used or different number of processors are used for parallelization. The colored and black curves represent the stepped and flat/disordered contacts, respectively. Similar conditions are used for the black curves as represented by the legend for the colored curves.

tioned into sub-systems to decrease computational time. Given the finite floating point precision, a different number of processors can lead to small differences in velocities, positions and forces due to rounding. The room temperature simulations do not provide unexpected results. As expected, the elastic part is identical for all cases. At an applied displacement of $u_T \approx 2$ nm, sliding sets in. For both atomically flat and disordered contacts there is no significant effect of initial velocities or different numbers of processors. For a disordered contact, the friction stress is lower than for a flat contact, since atoms at the interface are out of registry compared to a flat contact, so that it takes lesser applied mechanical energy to overcome the barrier for sliding. For stepped contacts, however, there is a clear effect on the onset of sliding for different initial atomic velocities or different numbers of processors. This is caused by the fact that the steps with the

local stress concentrations act as additional barriers for sliding and to overcome this barrier preferably the vectors of the atomic velocities have to align, which occurs by chance. As sliding develops, it is found that the friction stress converges to (near-) smooth sliding with approximately the same friction stress. In Chapter 6 it is shown that this transition to smooth sliding of stepped contacts occurs due atomic rearrangement, i.e. self-organization of the steps, which decreases the contact roughness caused by the local symmetry breaking at the steps. Note that the dark blue curve in Fig. 7.4 is slightly more fluctuating than the other curves. In this case a single dislocation is nucleated from the contact, giving the contact a net step height and making it slightly rougher, which explains the fluctuations in friction stress.

For room temperature simulations we can therefore conclude that the initial velocities, or numbers of processors, are irrelevant for the onset of sliding of an atomically flat or disordered contact, but are very important for a stepped contact, i.e. local behavior. For large u_T, the initial differences average out and the behavior becomes statistically independent of the small differences caused by different initial atomic velocities or different parallelization.

Studying the mechanical response of materials with MS/MD simulations at zero or near-zero temperature is thought of to have the advantage that the spread in atomic velocities/positions/forces that exists at room temperature, is completely or nearly absent. Secondly, thermal activation is negligible at low temperature, so that if the strain rate is low enough, the simulations are quasi-static and the results are rate-independent. One would therefore expect that if we repeat the previous simulations at near-zero temperature, $T = 0.1$ K, the results, especially for the stepped contacts, would be insensitive to different initial conditions or different number of processors for parallelization, and one could suffice with only a single simulation.

The shear stress as a function of applied displacement at $T = 0.1$ K for stepped, atomically flat and disordered contacts with different initial velocities and/or different numbers of processors is shown in Fig. 7.5. The stress levels are higher compared to the room temperature simulations, since the thermal activation present at room temperature, is suppressed at 0.1 K. Similarly to the room temperature simulations, it is found that both the onset of sliding and the friction stress in the developed sliding stage of the flat and disordered contacts is independent of initial velocities or numbers of processors used. However, for the stepped contact, the behavior is significantly different from the behavior at room temperature. Interestingly, in contrast with the room temperature simulations, it is now the onset of sliding that is insensitive to initial atomic velocities or number of processors, as shown in the inset in Fig. 7.5. The spread in velocities is near-zero, so that all atomic velocity vectors at the contact have the same direction to overcome

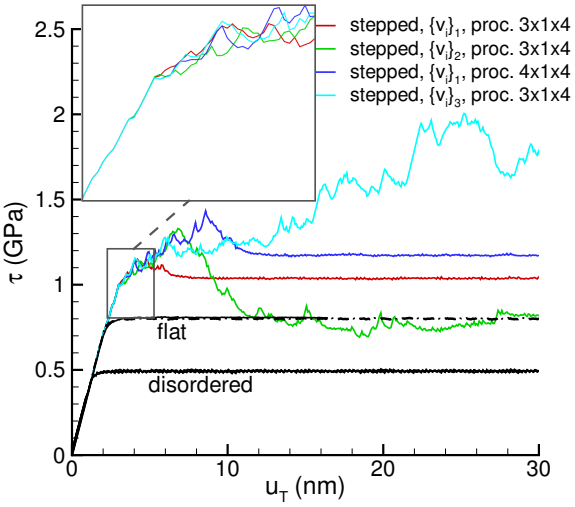

Figure 7.5: Shear stress τ as a function of applied displacement u_T for friction simulations of stepped, flat and disordered contacts at near-zero temperature $T = 0.1$ K. Different initial atomic velocities are used or different number of processors are used for parallelization. The colored and black curves represent the stepped and flat/disordered contacts, respectively. Similar conditions are used for the black curves as represented by the legend for the colored curves.

7

the barriers caused by the steps. However, as sliding develops, the results start to diverge, which eventually develops into very different friction stress in the later sliding stage for different initial velocities or different numbers of processors. The green curve in Fig. 7.5 shows the lowest friction stress for stepped contacts and the behavior still shows some stochasticity due to local roughness. The reason is found to be similar to what was discussed previously for the dark blue curve in Fig. 7.4, i.e. in this case a single dislocation is nucleated from the contact leading to a net step height in the contact and a rougher contact. The light blue curve

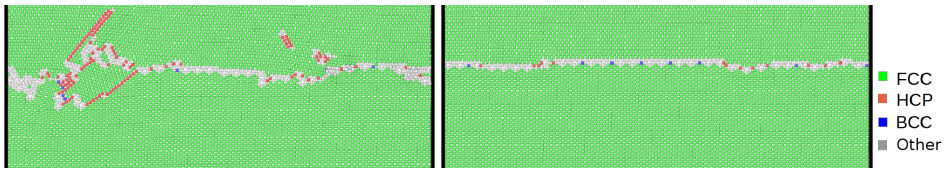

(a) (b)

Figure 7.6: Very different contact structures that have developed for an applied displacement $u_T = 20$ nm at $T = 0.1$ K. Different initial atomic velocities can result in (a) the nucleation of dislocations and twins from the contact or (b) a highly smooth contact structure with steps. Coloring is according to a Common Neighbor Analysis (CNA) [5].

in Fig. 7.5 shows significantly increasing friction stress. In this case dislocations and twins are nucleated from the contact, which increases the roughness of the contact as shown in Fig. 7.6a. However, there are also two cases (red and blue in Fig. 7.5) that show smooth sliding due to the atomic rearrangement, leading to a rather smooth contact shown in Fig. 7.6b, which contains steps (zero net step height) that can move in the contact plane.

We can conclude that, surprisingly, small changes in the initial or processing conditions at low temperature lead to very different results when atomic rearrangement from an initial state with strongly local symmetry breaking (like stepped contacts) is involved. Unexpectedly, the results are very sensitive to different initial or processing conditions.

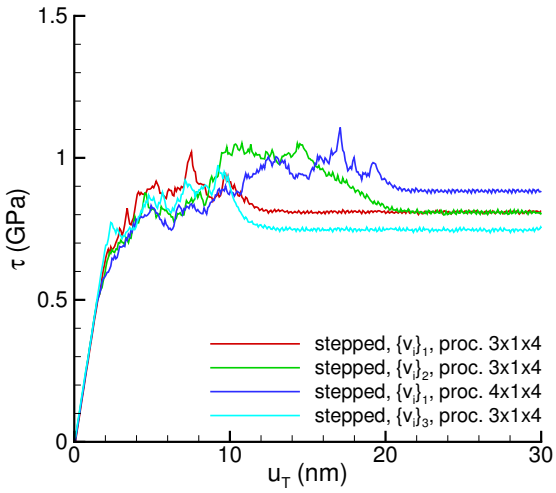

Figure 7.7: Shear stress τ as a function of the applied displacement u_T for friction simulations of stepped contacts at a temperature $T = 0.1$ K with additionally randomly placed adatoms (20 % of one atomic plane) at the surfaces.

Instead of increasing the temperature to induce noise/disorder, we can also randomly place adatoms (20 % of one atomic plane) on the surfaces for a stepped contact at $T = 0.1$ K, leading to increased disorder. Figure 7.7 shows that the large variation in the shear stress during sliding for low temperature simulations of a stepped contact (Fig. 7.5), although not zero, is significantly decreased. The variation in shear stress during sliding relative to the average value is $\Delta\tau/\bar{\tau} = 0.07$ for the case of a stepped contact with adatoms, where for the case of a purely stepped contact it is $\Delta\tau/\bar{\tau} = 0.36$. In comparison, the relative variation at room temperature in the developed sliding stage is $\Delta\tau/\bar{\tau} = 0.06$, close to the relative variation in the friction stress at 0.1 K with additional structural disorder. So the sensitivity to different initial or processing conditions in the developing friction stress re-

lated to the initial strongly local symmetry breaking at the contact is suppressed by either additional structural or thermal disorder.

7.3. CONCLUSIONS

In conclusion, when performing low temperature MD simulations on a problem that involves significant atomic rearrangements related to a state of initial strongly local symmetry breaking, small differences in initial or processing conditions in absence of thermal noise or structural disorder can lead to a large variation in the obtained results. The initial response related to dissipation, i.e. stress relaxation, is identical at low temperature. However, the system evolves through a landscape of local instabilities for which continuously new minimal energy states are found, which makes it sensitive to small changes in initial velocities or rounding errors in using a different parallelization scheme. This can therefore lead to a large variation in the results. Finite temperature or structural disorder washes out the irregular low temperature events sequence and leads to a stable and robust average behavior [6]. Obviously this does not mean that low temperature MD without additional structural disorder is useless. For problems where the interest is in the onset of deviation from elastic behavior, only a low number of dissipation events are involved and the results are still reliable with rather small variation.

REFERENCES

[1] R. J. Dikken, A. Elzas, and B. J. Thijsse, *Unexpected sensitivities in low temperature molecular dynamics simulations,* Comput. Mater. Sci. (2016).

[2] S. J. Plimpton, *Fast parallel algorithms for short-range molecular dynamics,* J. Comp. Phys. **117**, 1 (1995).

[3] G. P. Purja Pun and Y. Mishin, *Development of an interatomic potential for the ni-al system,* Phil. Mag. **89**, 3245 (2009).

[4] R. J. Dikken, B. J. Thijsse, and L. Nicola, *Friction of atomically stepped surfaces,* Phys. Rev. B (2016).

[5] A. Stukowski, *Structure identification methods for atomistic simulations of crystalline materials,* Modelling Simul. Mater. Sci. Eng. **20**, 045021 (2012).

[6] H. Von Foerster, *"On self-organizing systems and their environments" in Self-organizing systems*, m.C. Yovits and S. Cameron (eds.).

8

Concluding remarks

Reason, or the ratio of all we have already known, is not the same that it shall be when we know more.

William Blake

8.1. CONCLUSIONS

The objective of this work has been to obtain a better understanding of contact and friction. To this end, a computational study of a fundamental nature has been performed, focussing on micro-scale metal single asperities and nano-scale metal contacts. In the following, the main conclusions of each chapter shall be presented.

In Chapter 3, a discrete dislocation plasticity analysis of the plastic shear response of micro-scale single asperities of rectangular and truncated sinusoidal shape is presented. The advantage of these shapes is that the real contact area is equal to the apparent contact area and is constant during deformation. This study leads to the following conclusions:

- Self-similar asperities with small size have a higher contact shear strength than large asperities, even though the elastic behavior measured in terms of asperity shear strain is identical.
- Contact area and spacing between dislocation sources are the length scales that control the plastic behavior of the asperities: the contact area determines the size of the stressed region, inside and below the asperity, where dislocation nucleation can occur. Source spacing controls how many sources can be activated in the stressed region and thus gives rise to plastic deformation.
- For small and large contact area, the asperity can be idealized to have zero volume. Only for intermediate contact area, i.e. $0.5\ \mu\text{m} < C < 3\ \mu\text{m}$ for the dislocation source density used in this study, the shape and size of the asperity are relevant. The taller the asperity, the more plasticity inside it, the softer its shearing response.

In Chapter 4 a discrete dislocation plasticity analysis of the ploughing response of sinusoidal asperities and the comparison with the shear response of asperities is presented. This leads to the following conclusions:

- The friction force, defined as the ploughing force at final displacement, is insensitive to the ploughing depth and follows a distribution that is almost Gaussian with a depth-independent standard deviation.
- Although ploughing is insensitive to the ploughing depth, shearing is very much sensitive to the shearing height, because of the associated change in contact area. It is found that a larger contact area results in a larger friction force. The relative standard deviation increases with decreasing contact area (or increasing height).

- For shearing of self-similar asperities and zero-height asperities a size-dependent response is found. However, the friction force for ploughing of self-similar asperities is size-independent.

- For small asperity size the friction strength measured in the asperity base is identical for ploughing and shearing, so that at small asperity size the more complex ploughing model can be replaced with the simpler flat contact shearing model.

Since dislocation pile-ups on the contact can significantly affect the plastic response of asperities, we have studied with atomistic simulations the impingement behavior of edge dislocations on contacts under quasi-static loading conditions in Chapter 5. This study has led to the following conclusions:

- Atomic scale roughness, a simple, novel definition proposed in this work, is found to control dislocation absorption and re-nucleation from the impingement site.

- The normal stress at which re-nucleation occurs increases with increasing atomic scale roughness until a certain threshold. Above this roughness, the effect of a single absorbed dislocation is insignificant compared to the contact roughness.

- When multiple dislocations impinge, the nucleation stress decreases with the number of dislocations. For more than three dislocations in a pile-up, the normal stress at nucleation becomes constant.

- The repeated process of absorption and re-nucleation of multiple dislocations leads to local contact roughening.

- Impingement of a single dislocation on a contact can result for large roughness in the nucleation of a twin. When multiple dislocations impinge, twins are no longer observed.

- The contact pressures at which nucleation occurs are rather large, in the order of one GPa. Only when this is exceeded, dislocations from a pile-up are expected to be absorbed and re-nucleated, decreasing the pile-up length. Therefore, for moderate applied loading it is expected that long dislocation pile-ups can form.

Roughness does not only exist at the asperity level (micro-scale contacts) but also at the atomic level (nano-scale contacts). Atomic scale steps formed for instance by the escape of dislocations through surfaces or through crystal growth,

make nano-scale contacts atomically rough. In Chapter 6 we have studied the effect of atomic scale steps on the friction behavior of nano-scale Al contacts, leading to the following conclusions:

- Sliding friction has all the properties of a self-organized critical state. The power law slip statistics depend on the step spacing: large slip events are much more probable for contacts with small step spacing than for contacts in the large spacing limit, i.e. atomically flat contacts.

- A small net step height (order of magnitude of one lattice constant) in the contact results in contact migration perpendicular to the contact plane, due to the motion of the step along the contact plane. Contact migration results in vacancy generation in the re-crystallized part near the contact.

- Step pair contacts of small height, have two clearly distinguishable sliding stages, jerky and smooth, separated by a marked transition. While the contact is initially rough, the steps organize in such way that a smooth contact topology is obtained, leading to smooth sliding. The friction behavior is statistically independent of step pair width.

- Step pair contacts of large height, where there is a free gap between the surface, suffer from wear, which results in a growing contact area, eventually making the friction behavior similar to that of small height step pair contacts. The onset of sliding is clearly affected by the step pair width, i.e. smaller initial real contact area entails lower static friction stress.

In Chapter 7 the unexpected observation is done that sliding friction for stepped contacts is very sensitive to initial or processing conditions for MD simulations at low temperature. Since it is commonly assumed that MD simulations at low temperature do not show significant variation in the results, due to the (near) absence of thermal noise, this observation urges for very careful considerations when performing low temperature MD simulations involving dissipation-processes.

8.2. OUTLOOK

This work is motivated by the need for a deeper understanding of friction of rough metal surfaces in contact. However, since this fundamental study focusses on specific length scales, it does not provide for answers on the interplay between different relaxation mechanism, like dislocation nucleation and glide and contact slip. One of the major recommendations is therefore to construct a multi-scale model in which both atomistic and dislocation processes are incorporated. This will certainly become relevant when considering real rough surfaces in contact.

It is expected that certain contact regions in such rough contacts will show plastic deformation of asperities, while other contact regions, where the local shear stress is high, will show sliding through local slip and step motion.

In this study it is observed that friction of nano-scale contacts involves a self-organized critical state. This means that the statistics of the stress drops during sliding is described by a power-law distribution. A closer look at the friction stress versus applied displacement curves for zero-height asperities has revealed a similar feature. Figure 8.1 shows the power-law statistics of the stress drops during sliding for both nano- and micro-scale Al contacts. Of course we can only make such a comparison if the stress-curves does not show significant hardening, since self-organized criticality (SOC) requires a steady-state. For smaller contact area the stress-curves show more hardening, and therefore do not comply to the criteria of SOC. This means that SOC does not simply apply to all length-scales. However, in this work we have already observed that SOC can occur also when multiple relaxation mechanisms occurring simultaneously (local slip and step motion at the nano-scale). It would be interesting to study whether sliding friction of real rough surfaces, entailing multiple length scales and hence multiple relaxation mechanisms, has the properties of a self-organized critical state.

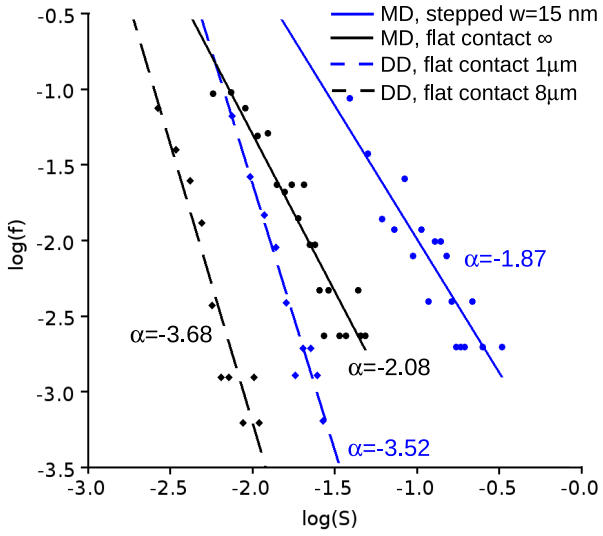

Figure 8.1: Power-law statistics of the stress drops in friction simulations of micro-scale contacts using discrete dislocation dynamics and nano-scale contacts using molecular dynamics.

Lastly, in this study we have applied small-strain discrete dislocation dynamics for the analysis of the plastic shear response of single asperities. However, since this involves a problem with large strain gradient, it is hypothesized that

the finite strain method described in Ref. [1] is more appropriate to accurately incorporate lattice rotation. It has yet to be shown to which extent finite strain dislocation dynamics will give different results or not, but a finite strain study will definitely give a relevant extension to the gained knowledge of the shear response of single asperities in this work.

REFERENCES

[1] N. Irani, J. J. C. Remmers, and V. S. Deshpande, *Finite strain discrete dislocation plasticity in a total lagrangian setting,* J. Mech. Phys. Solid **83**, 160 (2015).

ACKNOWLEDGEMENT

The road of doing PhD research is one mainly travelled in solitude. It certainly has been an enriching experience for me in many ways. There are a few people that I like to thank for their support. First of all my promotors Barend Thijsse and Lucia Nicola for their guidance and critical comments on this work.

I would like to thank the people from the fourth floor, and more in general from the Materials Science department, for providing a friendly environment. Specifically, I would like to mention Kelvin, Casper, Mohsen, Nilgoon, Astrid, Ann-Sophie, Fengwei and Yunhe, for their pleasant company at the university and by times for stimulating discussions. I would also like to thank Marcel Sluiter for useful discussions during group meetings.

Finally, I would like to thank my family and friends for supporting me and listening to me talking about my research, although it might have been a bit abstract sometimes.

The experiences of the last five years and interactions with a lot of different people will have a lasting effect on the rest of my life. I have learned more in various areas than I could have imagined when I started on this road. The last five years have broadened and strengthened the foundation on which I will continue to build in the rest of my life and career. I am thankful to everyone who has contributed to this.

CURRICULUM VITÆ

Robbert-Jan DIKKEN

10-01-1986 Born in Wateringen, the Netherlands.

Sept. 2004– July 2008	B.Eng. in Applied Physics Applied Physics, TH Rijswijk, the Netherlands *Thesis:* Fourier Transform Spectrometer for THz frequency response measurements of SIS tuning circuits
Febr. 2007– Oct. 2011	Project employee, Peutz, Zoetermeer, the Netherlands
Sept. 2008– Febr. 2011	M.Sc. in Applied Physics Applied Sciences, TU Delft, the Netherlands *Thesis:* AC quantum transport: Non-equilibrium in mesoscopic wires due to time-dependent fields
Dec. 2011– Febr. 2017	Ph.D. in Computational Materials Science Materials Science and Engineering, TU Delft, the Netherlands *Thesis:* Friction and plasticity of micro- and nano-scale metal contacts
March. 2017–	Aspirant project leader, Peutz, Zoetermeer, the Netherlands

List of Publications of this Work

1. **R.J. Dikken, E. Van der Giessen, L. Nicola**, *Plastic shear response of a single asperity: a discrete dislocation plasticity analysis*, Philosophical Magezine **95**(34), 3845 (2015).

2. **H. Song, R.J. Dikken, L. Nicola, E. Van der Giessen**, *Plastic ploughing of a sinusoidal asperity on a rough Surface*, Journal of Applied Mechanics **82**(7), 071006 (2015).

3. **R.J. Dikken, B.J. Thijsse, L. Nicola**, *Impingement of edge dislocations on atomically rough contacts*, Computational Materials Science **128**, 310 (2017).

4. **R.J. Dikken, A. Elzas, B.J. Thijsse**, *Unexpected sensitivities in low temperature molecular dynamics simulations*, submitted to Computational Materials Science (2016).

5. **R.J. Dikken, B.J. Thijsse, L. Nicola**, *Friction of atomically stepped surfaces*, submitted to Physical Review B (2016).